

Editor Decision: Publish subject to minor revisions (review by Editor) (04 Dec 2015) by Luke Skinner

Comments to the Author:

Dear I. Neugebauer,

thank you for your response to the review comments, which were generally positive and supportive of publication in *Climate of the Past*.

I invite you to submit a final revised manuscript for acceptance subject to editorial review. However, I would encourage you to reconsider your discussion section, and in particular the speculative additions that might be made in light of the review comments. In particular, I would suggest that the discussion of 'phasing' of aridity/lake levels versus North Atlantic climate might be slightly confused in that 'in phase/anti-phase' behaviour has no clear meaning in this context, where we are comparing 'cold' with 'dry'. A cold North Atlantic coincides with either dry or wet conditions in the Levant, but why should one of these be seen as representing 'out of phase' behaviour?

Furthermore, I wonder if there is perhaps some confusion between 'interstadials' in the terrestrial glacial-interglacial stratigraphy (lasting ~10,000 years, and being clearly linked to astronomical forcing) and interstadials of the Greenland event stratigraphy (which are truly millennial, and have no demonstrable link to insolation forcing per se). I would encourage you to include some 'constrained' speculation as suggested by the review comments (e.g. there may have been 'glacial/interglacial' or 'short/long term' regimes in Levantine hydroclimate variability, as driven by North Atlantic climate changes, which may have been activated by changes in ice sheet volume/height, affecting the response of Levantine hydroclimate to cold conditions in the North Atlantic etc...); however, please be careful in your description of these propositions and in your reference to terms like 'phasing', 'millennial' etc...

I look forward to receiving your revised manuscript.

Yours sincerely,
Luke Skinner

Response to the Editor's comments (17 Dec 2015):

Dear Luke Skinner,

thank you very much for considering our manuscript and for your helpful comments. We agree with your concerns and follow your suggestion to avoid terms like 'phasing' or 'millennial' in the discussion chapter 5.4 and the conclusions. Regarding your comment about the Greenland interstadials, we like to point out that the last glacial inception does not show a typical millennial-scale behavior, but interstadials were longer in Greenland during that time (please see our Figure 5 of the manuscript) compared to MIS 4-2. However, we followed your and the reviewer's #2 advice and included some 'constrained speculation' about the influence of ice sheet volume/height on the Levantine hydroclimate in the manuscript, lines 512-525.

For completeness, please find below the original responses to the reviewers' comments, followed by the revised manuscript, where all changes are marked via 'track changes'. We hope that you find our manuscript now acceptable for publication in *Climate of the Past*.

On behalf of the authors,
Yours sincerely,
Ina Neugebauer

Response to Referee #1:

This review of the anonymous referee #1 is in general very positive and we would like to thank the reviewer for these encouraging words.

Four minor suggestions/ technical comments were given by the referee that we addressed in the revised manuscript; please see also below:

1. Page 3641/lines 16-19: It would be good for the non-expert readership to provide some additional information on how the geochemistry of the brine and the geometry of the basin do not allow a complete drying of the Dead Sea.

Reply: We fully agree to this point and have added in the revised manuscript (pages 13-14/lines 377-383): “... First, the specific chemical composition of the Dead Sea brine (mainly Mg, Na, Ca and Cl) allows reaching a very high salinity with a low water activity and vapour pressure. Therefore, the rate of evaporation decreases with increasing salinity. Second, the low surface area to volume ratio of the lake basin limits the amount of evaporated water. In addition, the relative humidity of the air above the brine has to be close to zero in order to further evaporate a highly concentrated brine which, however, was never observed (Katz and Starinsky, 2015) and is considered unlikely especially at very low lake levels due to the wind-protected topography of the deep Dead Sea basin.”

2. Page 3644/line 25: You may also see Rohling et al. (2015) for a recent review on the sapropel formation in the Mediterranean Sea (including sapropels S3 and S4).

Reply: We have added this reference in the revised manuscript (page 16/line 464).

3. Please check the Fig. 2 call outs. I think they should be ‘Fig. 2d’ and ‘Fig. 2e’ in page 3633/ line 26 and page 3633/line 3, respectively.

Reply: This has been corrected.

4. Please spell out MIS and XRF when they first appear in the text; add XRD after ‘... diffraction’ in page 3632/line 11.

Reply: This has been corrected.

Additional references in the revised manuscript:

Katz, A. and Starinsky, A., 2015. No drawdown and no hyperaridity in the ancient Dead Sea: (Comments to Torfstein's et al. (2015) paper, EPSL 412, 235–244). *Earth and Planetary Science Letters* 427, 303-305.

Rohling, E.J., Marino, G. and Grant, K.M., 2015. Mediterranean climate and oceanography, and the periodic development of anoxic events (sapropels). *Earth-Science Reviews* 143, 62-97.

Response to Referee #2:

We would like to thank the referee #2 for his/her positive comment on our manuscript. The reviewer raised some intriguing questions that we addressed partly in the manuscript and in more detail in the following:

'The point that, in my opinion, could benefit from further or more explicit comment is the interesting finding that during the studied time interval, lake level changes are in phase with Greenland and European climatic and environmental changes. This is in contrast to the well-known prevailing opposition, as expressed in this introduction to the paper: "The lakes expanded during glacial intervals... whereas interglacials are generally characterised by lake contraction". This switching of phasing across the glacial inception period is not explicitly stated (although it may be implicit in discussion of forcing factors in section 5.4 and also in the final conclusion point in section 6). In general, the long interstadial episodes of the early last glacial share many characteristics with interglacials (for example, with forest development in long southern European pollen records), but here the hydrological pattern is opposed.

Can the authors comment further on why this switching may occur (i.e. expand further on the global boundary conditions under which the Dead Sea experiences dominant Atlantic-Mediterranean climate impacts), ...?'

Reply: This is a very good point that we missed to discuss because at first we considered that a bit too speculative. However, the reviewer comment encouraged us to change our opinion and revise the discussion in the last paragraph of section 5.4 by pointing out more clearly the shift from an 'in-phase behaviour' (cold North Atlantic, dry Levant) during the early last glacial (millennial time scales) to an 'out-of-phase behaviour' (cold North Atlantic, wet Levant with high Lake Lisan levels) during the Pleniglacial (longer time scales of ten thousands of years).

In our opinion the Dead Sea always experienced dominant Atlantic-Mediterranean climate impacts, however, in different ways. We agree to the reviewer that the shift in climate response in the Levant at the onset of MIS 4 is related to changes in climate boundary conditions. The biggest change that occurred during that time is the build-up of the Northern hemisphere ice sheets, which may have crossed a certain threshold in elevation to trigger a major change in northern hemisphere atmospheric circulation by splitting up the Jetstream, as already shown by Webb III et al. (1993). This should have forced the Westerlies sufficiently far south that Mediterranean cyclones were funnelled towards the central Levant, which led to doubling of annual rainfall in this region (Enzel et al., 2003, 2008; Rohling, 2013).

In contrast, during the early last glacial period winter rains increased in the eastern Mediterranean during periods of maximum insolation and seasonality (see e.g. Kutzbach et al. 2014), i.e. broadly coinciding with the warmer interstadials. On the other hand, during periods with lower insolation and seasonality winter rains decreased and the climate became dryer in the Levant during cold periods. This in-phase response function of the hydroclimate in the Levant to northern hemisphere orbital forcing collapsed only when the atmospheric circulation got re-organised and shifted towards the south at the time when the ice sheets became a morphological barrier for large-scale wind systems. As aforementioned, we consider this a hypothesis of which some parts are supported by data and

modelling, which as a whole should be further tested by both further modelling and more high-resolution proxy records from this region.

'... what the wider implications are for pan-Mediterranean climate gradients, ...?'

Reply: Climate gradients in the Mediterranean are complex, different on different time scales and determined by different boundary conditions. As we mainly focus on millennial-scale changes, this question is beyond the scope of this paper, but we like to share some ideas within the frame of an open discussion:

On Holocene decadal to centennial timescales, a seesaw pattern in the Mediterranean with climatic gradients from West to East and Northeast to Southeast has been observed (e.g. Roberts et al. 2012; Neugebauer et al. 2015). These gradients are likely related to complex and not yet fully understood teleconnections between the North Atlantic Oscillation, the Siberian High Pressure System and the eastern Mediterranean Cyprus Lows. The superimposed, long-term millennial- and multi-millennial-scale climate fluctuations, however, seem to be similar across the Mediterranean and forced by orbital insolation, although the responses in the different regions of the Mediterranean may be delayed or different in intensity (e.g. Roberts et al. 2011). On a glacial-interglacial time scale it is the change in boundary conditions causing a southward shift and funnelling of the Mediterranean cyclones particularly to the Levant during glacial times that results in the observed difference to other parts of the Mediterranean.

Besides different boundary conditions and forcing factors, i.e. the complex climatic mechanisms, another equally important factor further complicates the reconstruction of Mediterranean climate gradients. This is the use of different proxies and different climate archives, which often exhibit different responses to climate, challenging a regional comparison of these records. Last but not least, chronological synchronisation is another crucial issue that still requires improvements.

'... and whether it may be a predictable feature of glacial inceptions during earlier climatic cycles?'

Reply: This is also an interesting idea, but it leads us even more into a speculative discussion. Since earlier glacial inceptions have experienced similar boundary conditions, one should assume that the Dead Sea level has reacted similarly as during the last early glacial period. However, one should also keep in mind that, even if glacial-interglacial cycles are broadly similar, there are also clear differences in the characteristics of individual interglacials and glacials. For example, the southward extent, and probably even the height of the Fennoscandian ice sheet during the last three glaciations exhibits significant differences. If this might have influenced the boundary conditions of the atmospheric circulation is unknown. Therefore, and since we do not have any confidence for predictable features of earlier glacial inceptions, we do not include this discussion in the paper. Instead, we consider this as an intriguing problem for further research.

References:

Enzel, Y., Bookman, R., Sharon, D., Gvirtzman, H., Dayan, U., Ziv, B., and Stein, M.: Late Holocene climates of the Near East deduced from Dead Sea level variations and modern regional winter rainfall, *Quaternary Research*, 60, 263-273, DOI: 10.1016/j.yqres.2003.07.011, 2003.

- Enzel, Y., Amit, R., Dayan, U., Crouvi, O., Kahana, R., Ziv, B., and Sharon, D.: The climatic and physiographic controls of the eastern Mediterranean over the late Pleistocene climates in the southern Levant and its neighboring deserts, *Global Planet. Change*, 60, 165-192, 10.1016/j.gloplacha.2007.02.003, 2008.
- Kutzbach, J. E., Chen, G., Cheng, H., Edwards, R. L., and Liu, Z.: Potential role of winter rainfall in explaining increased moisture in the Mediterranean and Middle East during periods of maximum orbitally-forced insolation seasonality, *Clim. Dyn.*, 42, 1079-1095, 10.1007/s00382-013-1692-1, 2014.
- Neugebauer, I., Brauer, A., Schwab, M. J., Dulski, P., Frank, U., Hadzhiivanova, E., Kitagawa, H., Litt, T., Schiebel, V., Taha, N., Waldmann, N. D., and Party, D. S.: Evidences for centennial dry periods at ~3300 and ~2800 cal. yr BP from micro-facies analyses of the Dead Sea sediments, *Holocene*, 25, 1358-1371, 10.1177/0959683615584208, 2015.
- Roberts, N., Brayshaw, D., Kuzucuoğlu, C., Perez, R., and Sadori, L.: The mid-Holocene climatic transition in the Mediterranean: Causes and consequences, *The Holocene*, 21, 3-13, 10.1177/0959683610388058, 2011.
- Roberts, N., Moreno, A., Valero-Garcés, B. L., Corella, J. P., Jones, M., Allcock, S., Woodbridge, J., Morellón, M., Luterbacher, J., Xoplaki, E., and Türkeş, M.: Palaeolimnological evidence for an east-west climate see-saw in the Mediterranean since AD 900, *Global Planet. Change*, 84-85, 23-34, <http://dx.doi.org/10.1016/j.gloplacha.2011.11.002>, 2012.
- Rohling, E. J.: Quantitative assessment of glacial fluctuations in the level of Lake Lisan, Dead Sea rift, *Quaternary Science Reviews*, 70, 63-72, <http://dx.doi.org/10.1016/j.quascirev.2013.03.013>, 2013.
- Webb III, T., Ruddiman, W. F., Street-Perrott, F. A., Markgraf, V., Kutzbach, J. E., Bartlein, P. J., Wright Jr., H. E., and Prell, W. L.: Climatic changes during the past 18,000 years: regional syntheses, mechanisms, and causes, in: *Global Climates since the Last Glacial Maximum*, edited by: Wright Jr., H. E., Kutzbach, J. E., and Webb III, T., 514-535, 1993.

1 **Hydroclimatic variability in the Levant during the early last**
2 **glacial (~117-75 ka) derived from micro-facies analyses of**
3 **deep Dead Sea sediments**

4
5 **I. Neugebauer¹, M.J. Schwab¹, N.D. Waldmann², R. Tjallingii¹, U. Frank¹, E.**
6 **Hadzhiivanova², R. Naumann³, N. Taha², A. Agnon⁴, Y. Enzel⁴ and A.**
7 **Brauer^{1,5}**

8 [1] GFZ German Research Centre for Geosciences, Section 5.2 – Climate Dynamics and Landscape
9 Evolution, Telegrafenberg, 14473 Potsdam, Germany

10 [2] University of Haifa, Department of Marine Geosciences, Leon H. Charney School of Marine
11 Sciences, Mount Carmel 31905, Israel

12 [3] GFZ German Research Centre for Geosciences, Section 4.2 – Inorganic and Isotope
13 Geochemistry, Telegrafenberg, 14473 Potsdam, Germany

14 [4] The Hebrew University of Jerusalem, The Fredy & Nadine Herrmann Institute of Earth
15 Sciences, Givat Ram, Jerusalem 91904, Israel

16 [5] University of Potsdam, Institute of Earth and Environmental Science, Karl-Liebnecht-Str. 24-
17 25, 14476 Potsdam-Golm, Germany

18 Correspondence to: I. Neugebauer (inaneu@gfz-potsdam.de)

19
20 **Abstract**

21 The new sediment record from the deep Dead Sea basin (ICDP core 5017-1) provides a unique
22 archive for hydroclimatic variability in the Levant. Here, we present high-resolution sediment
23 facies analysis and elemental composition by [micro-X-ray fluorescence \(μXRF\)](#) scanning of core
24 5017-1 to trace lake levels and responses of the regional hydroclimatology during the time interval
25 from ca 117-75 ka, i.e. the transition between the last interglacial and the onset of the last glaciation.
26 We distinguished six major micro-facies types and interpreted these and their alterations in the core
27 in terms of relative lake level changes. The two end-member facies for highest and lowest lake

28 levels are (a) up to several meters thick, greenish sediments of alternating aragonite and detrital
29 marl laminae (aad) and (b) thick halite facies, respectively. Intermediate lake levels are
30 characterised by detrital marls with varying amounts of aragonite, gypsum or halite, reflecting
31 lower-amplitude, shorter-term variability. Two intervals of pronounced lake level drops occurred
32 at $\sim 110\text{-}108 \pm 5$ ka and $\sim 93\text{-}87 \pm 7$ ka. They likely coincide with stadial conditions in the central
33 Mediterranean (Melisey I and II pollen zones in Monticchio) and low global sea levels during [the](#)
34 [marine isotope stages \(MIS\) 5d and 5b](#). However, our data do not support the current hypothesis of
35 an almost complete desiccation of the Dead Sea during the earlier of these lake level low stands
36 based on a recovered gravel layer. Based on new petrographic analyses, we propose that, although
37 it was a low stand, this well-sorted gravel layer may be a vestige of a thick turbidite that has been
38 washed out during drilling rather than an in-situ beach deposit. Two intervals of higher lake stands
39 at $\sim 108\text{-}93 \pm 6$ ka and $\sim 87\text{-}75 \pm 7$ ka correspond to interstadial conditions in the central
40 Mediterranean, i.e. pollen zones St. Germain I and II in Monticchio, and GI 24+23 and 21 in
41 Greenland, as well as to sapropels S4 and S3 in the Mediterranean Sea. These apparent correlations
42 suggest a close link of the climate in the Levant to North Atlantic and Mediterranean climates
43 during the time of the build-up of Northern Hemisphere ice shields in the early last glacial period.

44 **1 Introduction**

45 The Dead Sea and its Pleistocene precursor Lakes Amora, Samra and Lisan (e.g. Bartov et al.,
46 2003; Torfstein et al., 2009; Waldmann et al., 2009) experienced major lake level fluctuations in
47 the past as a sensitive response to changing hydroclimatic conditions in the lake's watershed (e.g.
48 Enzel et al., 2008). The lakes expanded during glacial intervals due to up to twice modern
49 precipitation, whereas interglacials are generally characterised by a lake contraction due to reduced
50 precipitation and runoff (Enzel et al., 2008; Rohling, 2013). Hence, the last glacial Lake Lisan,
51 which occupied the Dead Sea basin between ~ 70 and 14 ka, reached up to ~ 270 m higher lake
52 stands than the Holocene Dead Sea and the last interglacial Lake Samra (e.g. Bartov et al., 2002;
53 2007; Waldmann et al., 2007; Torfstein et al., 2013). The highest amplitudes of lake level drops
54 occurred at the glacial to interglacial transitions triggered by lower rainfall (e.g. Yechieli et al.,
55 1993; Bartov et al., 2007; Waldmann et al., 2009; Stein et al., 2010). For example, the fresher Lake
56 Lisan water body turned into the hypersaline Holocene Dead Sea during the last termination leading

57 to the deposition of a thick halite sequence during the early Holocene (~11-10 ka; e.g. Stein et al.,
58 2010).

59 Less information is available about lake level changes during the transition from interglacial to
60 glacial climate conditions. Previous studies from exposed sediment sections of the Samra
61 Formation at the south-western margin of the Dead Sea suggested a relatively shallow Lake Samra
62 from ca 135 to 75 ka (Waldmann et al., 2007; 2009; 2010). The main lake level rise at the transition
63 from Lake Samra to Lake Lisan was assumed from a sedimentological change from sand deposits
64 to sediments of alternating fine laminae of aragonite and detritus at a major unconformity ~75-70
65 ka (e.g. Waldmann et al., 2009; Torfstein et al., 2013). However, the early glacial time interval
66 between the last interglacial low stand (Lake Samra) and the full glacial high stand (Lake Lisan),
67 i.e. coinciding with MIS 5d to 5a, is not well represented in the exposed sediments (Waldmann et
68 al., 2009).

69 Sediments from this time interval have been for the first time recovered by ICDP drilling project
70 DSDDP from the deepest part of the Dead Sea basin (Neugebauer et al., 2014). Based on a new
71 chronology and interpretation of a well-sorted gravel deposit, Torfstein et al. (2015) inferred an
72 almost complete drawdown of the Dead Sea leading to a sedimentary hiatus between 116 and 110
73 ka at around MIS 5d, which is considered the most extreme lake level drop during the last ~220 ka,
74 i.e. the time period covered by the DSDDP sediment record. Furthermore, Torfstein et al. (2015)
75 suggest moisture supply through the African monsoon to the southern Levant during more humid
76 intervals in the early last glacial, which are considered to coincide with MIS 5c and 5a, whereas
77 marine and terrestrial records from across the Mediterranean region responded to long-term
78 orbitally induced temperature fluctuations, ice sheet waxing and waning in the Northern
79 Hemisphere and climatic changes in the North Atlantic (e.g. Tzedakis, 2005; Martin-Puertas et al.,
80 2014).

81 In this study, we apply a combination of petrographic, micro-facies and high-resolution XRF
82 analyses to investigate in more detail the sedimentological changes in the new ICDP Dead Sea
83 record between the last interglacial and the onset of Lake Lisan (~117-75 ka). These sediments and
84 their alterations serve as indicators for hydroclimatic variations in the southern Levant. In addition,
85 we focus on the sedimentology of the gravel layer to add information on the drawdown hypothesis
86 of the Dead Sea (Stein et al., 2011; Torfstein et al., 2015).

87 **2 Regional Setting**

88 With a lake level of 429 m (in 2015) below mean sea level (m bmsl) and a water depth of ca 300
89 m the Dead Sea is located in one of the lowest continental depressions on earth. The basin is
90 bounded by the Judean Mountains on the west and the Jordan Plateau on the east, rising to heights
91 of ~1000 m and ~1200 m above mean sea level, respectively (Fig. 1). The modern watershed of the
92 lake, which is one of the largest in the Levant (~40,000 km²), experiences subhumid (>1000 mm
93 yr⁻¹ in the northernmost point) to semiarid Mediterranean climate in its north and arid to hyperarid
94 (~30 mm yr⁻¹ in the southernmost point) conditions in the southern part characterised by winter-
95 rain of the Saharo-Arabian environment. These climate conditions combined with the particular
96 steep topography of the basin margins create hyperarid conditions at the lake itself. The modern
97 Dead Sea is a hypersaline Ca-chloride brine (e.g. Katz et al., 1977; Lensky et al., 2005) and a
98 terminal lake, mainly fed by the Jordan River (Fig. 1). Precipitation primarily arrives in the
99 watershed in fall to late spring (Oct-May) through eastern Mediterranean mid-latitude cyclones
100 (Cyprus Lows; Ziv et al., 2006; Enzel et al., 2008) and tropical plumes in winter and spring (also
101 termed subtropical jet storms by Kahana et al., 2002; Rubin et al., 2007). Occasionally, the region
102 is influenced by the Active Red Sea Trough from the south during fall and winter (e.g. Enzel et al.,
103 2008) with sources of its moisture also in the Mediterranean. The geology of the catchment is
104 predominantly characterised by Cretaceous carbonate sedimentary rocks, with some Palaeozoic to
105 Mesozoic sandstones and Pleistocene volcanic units (Bentor, 1961; Sneh, 1998).

106 **3 Material and Methods**

107 **3.1 Dead Sea deep-basin core 5017-1**

108 The 5017-1 sediment core from the deep Dead Sea basin (31°30'29" N, E 35°28'16" E; ca 300 m
109 water depth in 2010; sediment surface ~725 m bmsl; Fig. 1) was obtained during the drilling
110 campaign of the ICDP Dead Sea Deep Drilling Project (DSDDP) in winter 2010-11 (Stein et al.,
111 2011). The record is ~455 m long and comprises two full glacial-interglacial cycles (Neugebauer
112 et al., 2014; Torfstein et al., 2015). Here, we focus on a ~65 m long section from ~180 to ~245 m
113 below lake floor (mblf). Sediment facies were described with an accuracy of 1 cm based on line-
114 scanning images of the split sediment cores. Magnetic susceptibility data in 1 mm resolution were
115 routinely obtained for the entire 5017-1 record (see Neugebauer et al., 2014 for details).

116 **3.2 Micro-facies analyses**

117 For micro-facies analyses we applied a combination of petrographic thin section microscopy and
118 high-resolution μ XRF element scanning. A total of 26 large-scale thin section samples (10 x 2 cm)
119 were prepared representing changes in facies types along the section. Preparation largely followed
120 the standard procedure for soft sediments (e.g. Brauer et al., 1999), but were performed under dry
121 conditions to avoid salt crystallization during the preparation process. Thin sections were analysed
122 with a petrographic microscope (Leica DMLP) and images were taken with a digital camera
123 (Olympus DP72). Fluorescence was analysed using a Nikon AZ100M microscope, operated with
124 violet and polarised light conditions, and Nikon photo software (NIS Elements AR 4.3).

125 The μ XRF measurements were acquired every 200 μ m for 10 s using the ITRAX μ XRF core
126 scanner at GFZ, Germany. The core scanner is equipped with a Cr tube operated at 30 kV and 30
127 mA to irradiate the split-core sediment surface. This non-destructive method acquires element
128 intensities of Si, S, Cl, K, Ca, Ti, Fe, Br and Sr (Neugebauer et al., 2014), which are presented as
129 count rates (counts per second – cps). The element intensity records reflect relative changes in the
130 composition of the Dead Sea sediments, but are also influenced by physical sediment properties
131 (e.g. density, water content, grain size) and the sample geometry. The easiest and most convenient
132 way to minimize the physical and geometrical sample effects is by the transformation of element
133 intensities into ratios or log-ratios (Weltje and Tjallingii, 2008).

134 **3.3 Grain size analyses and gravel petrography**

135 Laminated sediments were sampled for grain size distributions with 1 cm³ sample volume at 1-3
136 cm vertical resolution and a total of 363 samples. Sample preparation included decomposing
137 organic matter using 30 mL H₂O₂ (30%) and distilled water (1:1 concentration), and breaking
138 aggregates with Calgon detergent ((NaPO₃)₆, 1%) and ultrasonic bath. The particle size distribution
139 was measured using an LS 13 320 laser diffraction particle size analyser for (1) the total sample
140 and (2) the carbonate-free sample after dissolution through HCl (32%, dilution of 1:9 with distilled
141 water). Less than 1 g of sediment was required for measurement.

142 In total, 22 gravel layers detected in core 5017-1 were sampled for petrographic analyses. The
143 samples were wet-sieved for five grain size fractions (>4 mm, 2-4 mm, 1-2 mm, 0.5-1 mm and <0.5

144 mm), for which strewn slides have been prepared for microscopic inspections. Here, we focus on
145 two gravel units occurring within the studied core section (180-245 mblf).

146 **3.4 XRD and TOC/CaCO₃ measurements**

147 For X-ray powder diffraction ([XRD](#)) measurements 25 samples were collected from about the same
148 depths as thin sections to complement microscopic inspections. Powder X-ray patterns were
149 collected using a PANalytical Empyrean powder diffractometer with Cu K α radiation, automatic
150 divergent and antiscatter slits and a PIXcel^{3D} detector. The diffraction data were recorded from 5°
151 to 85° 2 Θ via a continuous scan with a step-size of 0.013 and a scan time of 60 s per step. The
152 generator settings were 40 kV and 40 mA.

153 Total organic carbon (TOC) and calcium carbonate (CaCO₃) contents have been determined from
154 19 of these samples using an elemental analyser (EA3000-CHNS Eurovector). First, 5-10 mg dried
155 and homogenized sample material was weighed in Sn-capsules for total carbon (TC) determination.
156 Subsequently, second sample aliquots of 3-4 mg of the samples were decalcified in Ag-capsules in
157 three steps through treatment with (1) 3% HCl, (2) 20% HCl and (3) drying at 75°C for TOC
158 determination. Data were calibrated with standards (BBOT, Sulfanilamide, for TOC additionally
159 Boden3) and empty Sn- and Ag-capsules. The relative standard deviation is <1%. CaCO₃ contents
160 were calculated from the difference TC-TOC.

161 **4 Results**

162 **4.1 Micro-facies, sedimentology and geochemistry**

163 The sediments of the analysed ~65 m long section of core 5017-1 mainly consist of laminated marl
164 of the aad facies (alternating aragonite and detritus; e.g. Machlus et al., 2000), gypsum and **massive**
165 halite deposits (Neugebauer et al., 2014). Commonly, detrital material is composed of clay to silt-
166 sized calcite, quartz, dolomite and minor feldspar and clay minerals. [The](#) ~~F~~thickness of detrital
167 layers ranges from <1 mm to several cm and their colour is greyish to black, if iron sulphides are
168 present (pyrite or greigite), or brownish and greenish, if terrestrial organic or algal remains are
169 dominant. Aragonite formed as 5-15 μ m small stellate aggregates of orthorhombic crystals building
170 ~0.1-4 mm thick white laminae. Monoclinic, euhedral ~10-60 μ m gypsum crystals build ~0.2-3 cm
171 thick beige layers. Larger, up to 1 mm gypsum crystals appear scattered within detrital layers.

172 Cubic, ~1 mm to several cm long halite crystals are either embedded in predominantly detrital marl
173 or build thick deposits. These thick halite deposits contain only minor detrital material and are often
174 layered.

175 Six micro-facies types were identified (Fig. 2):

- 176 i) green aad: alternating white aragonite and greenish detrital marl laminae (~1 mm thick
177 couplets; Fig. 2a), the greenish laminae exhibit some diatoms and very strong fluorescence
178 pointing to a significant amount of chlorophyll preserved in the sediment (Fig. 2f);
- 179 ii) aad-n: alternating white aragonite and greyish detrital marl laminae (~1 mm thick couplets,
180 occurrence as normal type; defined by Machlus et al., 2000);
- 181 iii) aad-II: alternating white aragonite and greyish detrital marl laminae with thicker aragonite
182 layers than normal type (~1-5 mm thick couplets, Fig. 2b);
- 183 iv) gd: well-laminated to massive, cm-thick gypsum deposits and detrital marl (Fig. 2de);
- 184 v) hd: cubic halite crystals (mm-cm) scattered in detrital marl;
- 185 vi) lh/hh: layered or homogeneous consolidated halite; the layered type often alternates with thin
186 detrital marl laminae (Fig. 2ed).

187 In addition, up to 1.7 m thick graded layers and up to 3 m thick slump deposits are predominantly
188 associated to the aad micro-facies types and less frequent and thinner in the halite-dominated
189 sections. In cm to tens of cm thick basal layers of 22 thick turbidites and slump deposits, matrix-
190 supported ~2-8 mm sized, angular to rounded gravels occur. In the studied section of core 5017-1,
191 four such mass-waste deposits with gravel-rich basal layers were identified at composite depths of
192 ~233.5 m, ~192.8 m, ~183.5 m and ~183 m (Fig. 4) of which the ~58 cm thick turbidite at ~233.5
193 m depth was analysed in detail (Fig. 3). The matrix-supported gravels are composed of carbonates
194 (limestone, dolomite, with a presence of aragonite) in the form of sparite, (bio)micrite or peloid,
195 and sulphates (gypsum, anhydrite) as well as halite and minor quartz. The fine and medium gravel
196 fractions constitute ~40% of the total dry weight (Fig. 3b).

197 In one exceptional case at ~239 m composite depth, a ~35 cm thick layer of well-sorted gravels
198 with <2% clay- to sand-matrix appears (Figs. 3 and 4). The petrographic composition of this gravel
199 deposit is identical to that of the other mud-supported gravels (Fig. 3). This gravel layer is from a
200 core section that suffered a major loss of core material during the drilling process (core 5017-1-A-
201 92-1). From the 130 cm long core drive only a cumulative thickness of 35 cm gravels and almost

202 no fine material were recovered in the liner. Therefore, the sedimentological contacts to over- and
203 underlying sediments are not preserved and are unknown (Fig. 3). Unfortunately, this prevents from
204 investigating sediment structures in the context of the complete depositional environment.
205 Interestingly, in the 10 cm wide core catcher of this core drive, matrix-supported gravel has been
206 caught. This core catcher sample largely resembles the basal layers of the abovementioned thick
207 turbidites and slumps.

208 Median grain size values of the laminated sediments, excluding the halite-facies types hd and lh/hh,
209 vary between ~7 and ~10 μm for samples with and without CaCO_3 (i.e. after dissolution of CaCO_3 ;
210 Supplement), respectively. These grain size distributions indicate mainly clay (~54% and ~43%
211 with and without CaCO_3 , respectively), very fine silt (~45% and ~55% with and without CaCO_3 ,
212 respectively) and very little sand (~0.1% and ~0.9% with and without CaCO_3 , respectively).
213 Gypsum-detritus samples (gd-facies) revealed the coarsest mean grain size of ~8 μm (~12.5 μm
214 without CaCO_3) and the highest sand fraction (~0.5% and ~2.2%, with and without CaCO_3 ,
215 respectively) due to gypsum which was not removed during sample treatment. The aad-n and aad-
216 II micro-facies show similar and low mean grain sizes of ~6 μm (~9 μm without CaCO_3), while
217 the green aad type exhibits a slightly higher mean value of ~7 μm (~11 μm without CaCO_3). Also
218 the silt and sand fractions of the green aad type are enhanced in comparison to the other two aad
219 types (Supplement).

220 The differentiation of the laminated micro-facies types gd, aad-II, aad-n and green aad is supported
221 by total organic carbon and calcium carbonate contents (Fig. 2g). The gd facies is characterised by
222 lowest TOC values of 0.25-0.5% and ~18% CaCO_3 , whereas the aad-II facies (0.35-0.57% TOC,
223 30-47% CaCO_3) and the aad-n facies (0.6-0.7% TOC, ~47% CaCO_3) exhibit higher values. The
224 green aad facies is characterised by highest TOC (0.65% and ~0.9%) and CaCO_3 contents (~40-
225 50% and 62%).

226 The elements Si, S, Cl, K, Ca, Ti, Fe, Br and Sr were obtained by μXRF scanning and used to
227 characterise the Dead Sea sediments (Fig. 2; see also Neugebauer et al., 2014; 2015). Aragonite
228 laminae are revealed by high Sr/Ca values, gypsum is represented by high S/Ca values and halite
229 is best characterised by the Cl/Br ratio (Fig. 2). The elements Si, K, Ti and Fe are constrained to
230 siliciclastics in the detrital sediment fraction. More ambiguous is the interpretation of Ca that occurs
231 in aragonite, gypsum and detrital calcite. The $\text{Ca}/(\text{Sr}+\text{S})$ ratio indicates the detrital carbonate

232 fraction because the authigenic Ca sources, i.e. aragonite and gypsum, are removed. The Ti/Ca ratio
233 represents the relative siliciclastic fraction (Fig. 2). The sum of Ca/(Sr+S) and Ti/Ca ratios best
234 represents the total amount of carbonate and siliciclastic detritus (Fig. 4). A correlation plot of these
235 two element ratios shows low, but significant, correlation ($R^2 = 0.4$) for the carbonate and
236 siliciclastic detrital fractions (Fig. 2h); the plot also indicates an additional Ca-bearing detrital
237 fraction.

238 **4.2 Lithostratigraphy**

239 The analysed section of core 5017-1 is sub-divided into four main lithostratigraphic units (Fig. 4).
240 Units I and III are predominantly composed of halite (controlled by hd and lh/hh facies), some
241 gypsum and detrital marl. Units II and IV present primarily aad (green aad, aad-n and aad-II) and
242 gd facies. These lithostratigraphic units are tied to the stratigraphic framework (Neugebauer et al.,
243 2014) and the U-Th chronology (Torfstein et al., 2015) of the 5017-1 core.

244 The lowermost unit I (245-237.5 m composite depth) is the upper part of a ca 40 m thick halite
245 sequence, the thickest halite deposit in the entire core, and is part of the last interglacial Samra
246 Formation (Neugebauer et al., 2014). This unit has very low magnetic susceptibility values and
247 Sr/Ca ratios with high Cl/Br ratios (Fig. 4). The abovementioned well-sorted gravel deposit, mainly
248 composed of limestone and dolomite clasts and halite, was identified ~2 m below the top of this
249 halite unit (Figs. 3 and 4). U-Th ages proposed a sedimentary hiatus between ca 116 and -110 ± 3
250 ka marked by this gravel layer (Torfstein et al., 2015).

251 The ~25 m thick unit II (237.5-212.5 m) presents mainly aad and gd facies. It is divided into two
252 sub-units: (1) sub-unit II-a (237.5-228 m) comprises aad-II, aad-n and gd facies and is characterised
253 by low Sr/Ca and Cl/Br ratios and distinct peaks in magnetic susceptibility. (2) Sub-unit II-b (228-
254 212.5 m) differs from sub-unit II-a as in addition to the above facies it presents three thick
255 sequences characterised by green aad facies and partly high Sr/Ca ratios. Unit II is characterised
256 by frequent, up to several m thick, graded detrital layers and slump deposits (Fig. 4). U-Th ages
257 place unit II between ca 108 ± 5 and 93 ± 7 ka (Torfstein et al., 2015), i.e. an interval of ~3-27
258 thousand years. Preliminary varve counting on the core photographs of this unit reveals a minimum
259 of 4050 ± 250 varves, which is at the lower end of the range and uncertainty of the U-Th ages. It is
260 likely that much of the sediments were eroded through the frequent mass-waste events. Unit II
261 builds the upper part of the Samra Formation of core 5017-1 as defined by Neugebauer et al. (2014).

262 Unit III (212.5-201.5 m) is dominated by halite deposits of the hd and lh/hh facies, which is well
263 reflected in high Cl/Br ratios. The lower ca 4 m of this unit could not be recovered due to the
264 hardness of the salt. Some cm- to dm-thick occurrences of aad-n, aad-II and gd facies are
265 intercalated in the halite deposits, as reflected by higher magnetic susceptibility, Ca/(Sr+S) + Ti/Ca
266 and Sr/Ca ratios. Unit III was deposited between ca 93 and 87 ± 7 ka (Torfstein et al., 2015) and
267 probably marks the transition between the Samra and Lisan Formations in the deep-basin core
268 5017-1 (Neugebauer et al., 2014). Compared to the chronology of the outcrops at the margin where
269 the Samra-Lisan transition has been traditionally considered at 75-70 ka (e.g. Waldmann et al.,
270 2009), probably because of transgressive truncation, the deep core may indicate that the transition
271 occurred ca 15 thousand years earlier (Torfstein et al., 2015).

272 The uppermost unit IV (201.5-180 m) compares to unit II and is characterised by the three aad
273 facies, as indicated by higher Ca/(Sr+S) + Ti/Ca and Sr/Ca ratios and the absence of halite (Fig. 4).
274 In contrast to unit II, where magnetic susceptibility values strongly fluctuate, constantly low
275 magnetic susceptibility characterises unit IV (Fig. 4). This unit can be divided into three sub-units:
276 (1) sub-unit IV-a is composed of aad-n, aad-II and gd facies, (2) sub-unit IV-b is a green aad section,
277 and (3) sub-unit IV-c is composed of aad-n and aad-II. Several cm- to m-thick slumped deposits
278 and graded detrital layers occur in unit IV. At a composite core depth of ~195 m the sediment is ca
279 85.5 ± 8 ka and six m above unit IV (i.e. at 174.5 m depth) an age of 70.5 ± 5 ka has been reported
280 (Torfstein et al., 2015). The interpolated age of the upper boundary of unit IV at 180 m depth is ca
281 75 ± 6 ka. Unit IV builds the lowermost part of the Lisan Formation of core 5017-1 (Neugebauer
282 et al., 2014).

283 **5 Discussion**

284 **5.1 Micro-facies as relative lake level indicators**

285 Lake levels of the water bodies occupying the Dead Sea basin are sensitive responders to changing
286 hydro-climatic conditions in the lake's catchment (Enzel et al., 2003; Bookman et al., 2006; Enzel
287 et al., 2008). Lake level reconstructions based on on-shore sequences indicate a total amplitude of
288 lake level fluctuation of at least ~270 m, with lowest levels of ~430 m bmsl occurring during parts
289 of the last interglacial, the last termination and potentially the Holocene, and anthropogenically-
290 induced in modern times (e.g. Bookman (Ken-Tor) et al., 2004; Bartov et al., 2007; Waldmann et

291 al., 2009; Stein et al., 2010). The highest lake level of Lake Lisan of ~160 m bmsl was reached
292 during the last glacial maximum (Bartov et al., 2003). These exposed sediments at the Dead Sea
293 margins also showed that in general different lake levels resulted in different sedimentary facies
294 (e.g. Machlus et al., 2000; Migowski et al., 2006). Hence, facies types can be considered as relative
295 lake level indicators, but without assigning an absolute level change (Figs. 4 and 5). Unlike the
296 near-shore environment, where lateral changes can alter the sedimentary facies which may lead to
297 erroneous relative lake level interpretations, in the deep basin such lateral changes are uncommon
298 and, therefore, facies changes are better related to changes in relative lake levels. These relative
299 lake levels are crucial ~~in inference of~~ to infer regional, basin-scale hydroclimatic changes that
300 control the direction of lake level trends (i.e. rising or falling), which are the net product of the
301 respective positive or negative lake budget over decades to millennia. To avoid complexities in
302 inferring minor relative lake level changes and to remain reasonable within the resolution of the U-
303 Th chronology, we concentrated only on reconstructing the millennial-scale facies alterations and
304 interpret them in terms of relative lake level variations.

305 The typical sediment facies during rising levels and the resulted episodic high stands of both the
306 deep last glacial Lake Lisan and the much shallower Holocene Dead Sea is the aad facies composed
307 of alternating aragonite and detritus (e.g. Machlus et al., 2000; Bookman (Ken-Tor) et al., 2004).
308 As the lake is devoid of bicarbonate, deposition of aad requires large amounts of bicarbonate supply
309 by freshwater reaching the lake through runoff during the winter rainy season to trigger
310 precipitation of primary aragonite (Stein et al., 1997; Barkan et al., 2001). Three different sub-types
311 of aad were distinguished in the investigated sediment section through micro-facies analyses. (i)
312 Green aad (Fig. 2) comprises greenish detrital laminae containing green algae remains and
313 represents highest lake levels and less salty limnological conditions. This facies depicts the
314 sediments deposited in core 5017-1 during the Last Glacial Maximum high stands (Neugebauer et
315 al., 2014), when Lake Lisan reached its maximum extent (e.g. Begin et al., 1974; Bartov et al.,
316 2002). (ii) The aad-n and (iii) the aad-II facies are similar, except that aad-II is characterised by
317 commonly thicker, but irregularly spacing aragonite laminae (Fig. 2). This may indicate insufficient
318 supply of bicarbonate to support regular annual aragonite formation. Therefore, the aad-II facies
319 ~~likely~~ likely was deposited during episodes of somewhat lower lake levels compared to the aad-n
320 facies. The aad-II facies also differs from the Id facies-type (laminated detritus), which exhibits
321 coarser detritus (50-60 μm) than aad (8-10 μm ; Haliva-Cohen et al., 2012) and which is a

322 characteristic facies for intermediate lake levels of the interglacial Samra and Ze'elim Formations
323 (e.g. Migowski et al., 2006; Waldmann et al., 2009; Neugebauer et al., 2014). The ld facies-type
324 was, however, not detected in the studied core section, [which is supported by the constantly very](#)
325 [fine grain sizes of the sediments \(Supplement\)](#).

326 The deposition of well-laminated or massive gypsum (gd facies, Fig. 2) is associated with mixing
327 of the water body due to lake level fall and a thinning of the upper freshwater layer (Torfstein et
328 al., 2008). Halite deposition is related to a negative water balance during times of decreased lake
329 levels (e.g. Lazar et al., 2014). Here, we distinguish between a mixed halite-detritus facies (hd) and
330 ~~massive or~~ layered [or homogeneous](#), consolidated halite (lh/hh facies, Fig. 2). Whereas the presence
331 of detritus suggests freshwater influx during extreme runoff events, deposition of thick halite
332 indicates episodes of lowest lake levels.

333 Lake level trends inferred from micro-facies analysis are supported by μ XRF element scanning
334 data (Figs. 4 and 5). Halite sequences associated with a negative water balance are well-expressed
335 in increased Cl/Br ratios. The detrital input depends on the erosion in the catchment, aeolian
336 deposition over the lake and the catchment, and freshwater supply to the lake. The relative detrital
337 input can be estimated using the Ca/(Sr+S) ratio (for carbonate fraction) and the Ti/Ca ratio (for
338 siliciclastic fraction). The Sr/Ca ratio resembles the aragonite amount that increases with enhanced
339 supply of freshwater. The combination of these ratios by summing up both detrital fractions and
340 aragonite and subtracting halite, results in a curve that can be interpreted as [a proxy](#) for water
341 balance (Fig. 5), with negative values for halite and gypsum deposits and positive values for detritus
342 and aragonite.

343 **5.2 Gravel deposits in the deep basin**

344 Gravel deposits are rather common in the deep basin and have been identified as matrix-supported
345 material mainly in basal layers of up to several meter thick turbidites and slumps reflecting mass-
346 waste deposits, which can be triggered by either extreme runoff or seismic events and slope
347 instabilities (Kagan and Marco, 2013; Neugebauer et al., 2014; Waldmann et al., 2014). Only in
348 one case at ~239 m composite sediment depth a 35 cm thick well-sorted gravel deposit lacking
349 fine-grained components has been documented (Figs. 3 and 4). This gravel has been interpreted as
350 beach deposit and in turn used to argue for a major drawdown or even almost desiccation of the
351 lake at the end of the last interglacial (Stein et al., 2011; Torfstein et al., 2015). Combined U-Th

352 ages and oxygen isotope stratigraphy suggest a ~116 to 110 ka hiatus at around the position of the
353 gravel deposit, which is assumed to support the drawdown hypothesis (Torfstein et al., 2015).
354 However, both, petrographic composition and grain characteristics of the well-sorted gravel are
355 identical with gravel in basal layers of thick slumps and turbidites as the one deposited only 6 m
356 above (at ~233 m composite sediment depth; Fig. 3). This suggests the possibility of a similar
357 source and even the same transport mechanism. Due to the massive core loss of 65% in the core
358 section where the well-sorted gravel has been found, no direct information about the in-situ contacts
359 of this gravel to over- and underlying sediment units is available (Fig. 3a) and its primary
360 sedimentological context remains unknown. However, the core catcher material supports the
361 interpretation even of the well-sorted gravel as the vestige of a major mass-waste deposit, since it
362 consists of matrix-supported gravel exactly resembling basal layers from at least 22 turbidites and
363 slumps occurring in the entire record. It is likely that the fine-grained sediment components of the
364 turbidite were washed out during the drilling process. Low core recoveries and loss of material
365 often occurred in sediment sections with alternating hard halite and soft mud (Neugebauer et al.,
366 2014) as in this section of the record above the major halite deposit. Therefore, we are convinced
367 that the well-sorted gravels are the result of a drilling artefact and should not be interpreted as an
368 in-situ beach layer, but as the washed-out relict of the basal sediments of a major mass-waste
369 deposit. The deposition of a thick turbidite could have also caused the supposed hiatus although its
370 length should be critically tested.

371 Accepting our re-interpretation of the well-sorted gravel as primarily a drilling relict of a turbidite
372 ~~and not a clear~~instead of an in-situ beach deposit implies that the Dead Sea not necessarily
373 desiccated at the end of the last interglacial, although it ~~could~~might have been at a low stage. This
374 consideration ~~probably~~ accords better with thermodynamic calculations and water balance
375 simulations concluding that the ~~geo~~chemistry of the brine and the geometry of the basin ~~do not~~
376 ~~allow~~should prevent a dry down of the lake from drying up (Yechieli et al., 1998; Krumgalz et al.,
377 2000). First, the specific chemical composition of the Dead Sea brine (mainly Mg, Na, Ca and Cl)
378 allows reaching a very high salinity with a low water activity and vapour pressure. Therefore, the
379 rate of evaporation decreases with increasing salinity. Second, the low surface area to volume ratio
380 of the lake basin limits the amount of evaporated water. In addition, the relative humidity of the air
381 above the brine has to be close to zero in order to further evaporate a highly concentrated brine

382 [which, however, was never observed \(Katz and Starinsky, 2015\) and is considered unlikely](#)
383 [especially at very low lake levels due to the wind-protected topography of the deep Dead Sea basin.](#)

384 **5.3 Relative lake level fluctuations between ~117 and 75 ka**

385 Relative lake levels have been reconstructed for the ~117-75 ka interval based on the six micro-
386 facies types introduced above (Figs. 4 and 5). Relatively lowest lake levels are reflected by the
387 halite-dominated units I (~117-108 ka) and III (~93-87 ka). Intermediate to relatively higher lake
388 levels inferred for aad facies dominated units II (~108-93 ka) and IV (~87-75 ka) because this facies
389 indicates increased fresh water inflow.

390 The age estimate of unit I indicates that the low stand of Lake Samra commenced during the later
391 part of the last interglacial and may have continued until $\sim 108 \pm 5$ ka BP (Fig. 5). However, there
392 is no information for the time interval from ~ 116 to 110 ± 4 ka, due to the erosional unconformity
393 revealed from the chronological data (Torfstein et al., 2015). The deposition of ca 2 m of halite
394 above the hiatus indicates that low levels of the lake continued until $\sim 108 \pm 5$ ka because for times
395 of halite deposition in the Dead Sea basin a lake level below 400 m bmsl can be assumed (Neev
396 and Emery, 1967; Bookman (Ken-Tor) et al., 2004; Waldmann et al., 2009; Stein et al., 2010).

397 During $\sim 108-93 \pm 6$ ka (unit II) a trend of general increase in lake level is indicated by the
398 succession from aad-II to aad-n and finally to the green aad facies (Fig.4). Intercalated gypsum
399 deposits from $\sim 108-100$ ka indicate frequent short-term drops in lake levels. In the last glacial Lisan
400 Formation such gypsum deposits were associated with reduced precipitation, intensified winds and
401 probably increased evaporation during Heinrich events (Bartov et al., 2003; Torfstein et al., 2008;
402 Rohling, 2013; Torfstein et al., 2013). A Lake Samra high-stand between $\sim 100-93$ ka is in
403 agreement with a level from exposures at the lake's margins, where a relatively high level of ~ 320
404 m bmsl was proposed (Fig. 5; Waldmann et al., 2009; 2010).

405 An abrupt lake level decline and a subsequent millennial-scale low stand, probably below 400 m
406 bmsl, is inferred from the ~ 7 m thick halite deposit during the $\sim 93-87 \pm 7$ ka interval (unit III, Figs.
407 4 and 5). Within this unit some aad-n, aad-II and gd facies alternate with the thick and mainly
408 layered halite deposits indicating superimposed, probably centennial-scale, lake level fluctuations.
409 This halite sequence represents the final stage of the Samra Formation and marks the last
410 appearance of halite for the next $\sim 70,000$ years (Neugebauer et al., 2014) until the early Holocene

411 salt formation (e.g. Yechieli et al., 1993; Stein et al., 2010). The late Lake Samra halite indicates a
412 more pronounced lake level drop than the limited lake level decline inferred from coarser clastic
413 deposits in the exposed lake margin sediments (Fig. 5; Waldmann et al., 2009).

414 During $\sim 87-79 \pm 7$ ka (units IV-a and IV-b) lake level increased again as evidenced from the
415 succession from aad-II and aad-n facies, intercalated by some gd facies, to green aad facies (Fig.
416 4). At ~ 79 ka (unit IV-c) the lake probably has shortly declined again as indicated by aad-II facies,
417 before continuing to rise again at $\sim 77 \pm 6$ ka (Fig. 5). Earlier studies of the exposed sediments of
418 the Samra and Lisan Formations suggested that a depositional unconformity between ~ 75 and 70
419 ka separated these two formations at the lake's margins (Bartov et al., 2003; Waldmann et al., 2009;
420 Torfstein et al., 2013). Above this assumed unconformity, aad facies characterise the lower and
421 upper members of the Lisan Formation (e.g. Bartov et al., 2002). Below the unconformity, the on-
422 shore Samra Formation is composed of reddish ld facies, sands and gravels (Waldmann et al.,
423 2009). In the deep core, however, there is no obvious sedimentological hint for a low stand of the
424 lake at around this time, but aad facies apparently continuously deposited since ~ 87 ka. This
425 suggests that Lake Lisan commenced ca 10-15 kyr earlier than was assumed from the exposures
426 where its deposits were in part truncated. This difference between shallow- and deep-basin
427 sediments might be explained by (1) the abundant occurrence of slumping deposits and graded
428 layers in the deep core (Fig. 4) or (2) by a lake level rise from a lower level to the level of the
429 observed unconformity at the margins during that time. Combining these two possibilities suggests
430 that these slumping deposits might indicate transgressive erosion at the outcrop locations during
431 times of lake level rise of the early Lake Lisan (Bartov et al., 2007). This is likely causing
432 unconformities in the near-shore marginal areas of the basin. The large number of slump deposits
433 within this sediment section might point to several short-term level oscillations during this
434 generally rising level trend, but there is no further evidence for this proposition.

435 **5.4 Hydroclimatic implications**

436 The Dead Sea is situated at a key transitional zone between predominantly Atlantic and tropical
437 influenced climates. The zone of interaction between both climate regimes is expected to have
438 changed during major climatic transitions like from glacial to interglacial modes and vice versa. In
439 contrast to the scarce and sometimes contradicting information from the Levant, several records
440 from the entire Mediterranean realm provide evidence for teleconnections of large-scale climate

441 variations with the North Atlantic climate regime during the early last glacial. The alternation of
442 cold stadial intervals from ~111 to 108 ka (GS 25) and ~90 to 85 ka (GS 23+22) (Rasmussen et al.,
443 2014), as reflected in Greenland ice cores (Fig. 5; Wolff et al., 2010) and North Atlantic ice rafting
444 events C24 and C22+C21 (Chapman and Shackleton, 1999), and warmer interstadials (GI 24+23
445 and GI 21; Rasmussen et al., 2014) is well expressed in the western (marine core MD952042 off
446 the Iberian margin; Sánchez Goñi et al., 1999), the central (Lago Grande di Monticchio; Fig. 5;
447 Brauer et al., 2007; Martin-Puertas et al., 2014) and the eastern Mediterranean (Tenaghi Philippon
448 (Tzedakis, 2005), in Lake Van (Litt et al., 2014) and marine sediments (Cheddadi and Rossignol-
449 Strick, 1995)). The same pattern of large-scale fluctuations are proposed from Lebanon (Lake
450 Yammoûneh; Develle et al., 2011; Gasse et al., 2015) and the Soreq and Peqin speleothem records
451 in Israel (Fig. 5; Bar-Matthews et al., 1999; 2000; 2003). Finally, also the Dead Sea record reveals
452 low water levels at $\sim 110\text{-}108 \pm 5$ ka and $\sim 93\text{-}87 \pm 7$ ka, reflecting dry periods corresponding to
453 Northern Hemisphere stadials, and higher lake levels at $\sim 108\text{-}93 \pm 6$ ka and $\sim 87\text{-}75 \pm 6$ ka
454 coinciding with Greenland interstadials (Fig. 5).

455 The ~~fluctuations between stadials and~~long interstadials interrupted by short stadials in the North
456 Atlantic realm, ~~which are reflected in the waxing and waning of glaciers~~ during the build-up phase
457 of the large continental ice sheets (e.g. Mangerud et al., 1996; 1998; Clark et al., 1999; Svendsen
458 et al., 2004) are related to changes in Northern Hemisphere orbital insolation (Fig. 5; Laskar et al.,
459 2004). At the same time, orbital insolation-driven changes of the ITCZ controlled the monsoon
460 system and led to a strengthening of the African summer monsoon and widespread vegetation cover
461 in the Sahel and in the southern Sahara regions (Fig. 5; deMenocal et al., 2000; Tjallingii et al.,
462 2008; Herold and Lohmann, 2009). Enhanced precipitation in eastern Africa induced the formation
463 of organic-rich sapropel layers S4 and S3 (Fig. 5) in the eastern Mediterranean basin due to
464 enhanced Nile River runoff (e.g. Rossignol-Strick, 1985; Rohling et al., 2015). These changes in
465 freshwater flow further influenced the isotopic composition of the eastern Mediterranean Sea water,
466 i.e. the source region for precipitation in the region of the Soreq and Peqin speleothems (Fig. 5;
467 Bar-Matthews et al., 2000; 2003). This is an indirect mechanism explaining a monsoonal influence
468 in the speleothem records of the Levant.

469 Two issues must be discussed when precipitation increase and decrease are considered for
470 explaining rising and falling trends in lake levels and their maxima: (a) winter vs. summer
471 precipitation, and (b) tropical vs. Atlantic-Mediterranean sources. ~~All combinations~~Different

472 [scenarios](#) have been proposed ~~for various time intervals, i.e. but~~ the source of moisture for the
473 precipitation leading to higher Dead Sea lake levels during the early glacial and related atmospheric
474 teleconnections is still debated. ~~In addition, the opposite should be asked as well: which is the~~
475 ~~significant source or season that its moisture delivery to the Dead Sea basin was shut off to control~~
476 ~~minor and drastic lake level falls?~~ Northward shifts of the tropical rain belt as far north as the
477 Levant ~~can have been~~ excluded (Tzedakis, 2007 and references therein); ~~and~~ ~~A~~also Enzel et al.
478 (2015) ~~have~~ argued that summer rains associated with either the African or Indian monsoons are
479 unlikely even in the southernmost point of the Dead Sea watershed. Based on hyperarid soils, Amit
480 et al (2006; 2011) demonstrated that the southern Negev, including the southern watershed of the
481 Dead Sea, was hyperarid since the early Pleistocene. This ~~was later~~ [is further](#) supported by a
482 diminishing speleothem growth southward and a proposal for a predominating Atlantic-
483 Mediterranean source of winter precipitation in the Negev during relatively short episodes of the
484 last interglacial (Vaks et al., 2010). This ~~probably~~ [apparently](#) contradicts the ~~proposal of~~ [hypothesis](#)
485 [that](#) a northward shift of summer rains from monsoonal sources to the southern Levant ~~that were~~
486 ~~suggested to have~~ contributed to the slightly increased Dead Sea lake level during the early last
487 glacial (Torfstein et al., 2015). [Less attention has been paid to seasonal shifts in precipitation as a](#)
488 [factor for lake level fluctuations. One reason is that most model studies focus on the summer season](#)
489 [\(e.g. Liu et al., 2004; Herold and Lohmann, 2009\), while information about the winter season](#)
490 [atmospheric circulation during intervals of maximum insolation are still scarce. One exception is](#)
491 [the study by Kutzbach et al. \(2014\), which suggests that an increase in winter storm tracks could](#)
492 [have caused the wetter intervals in the Levant during maximum Northern Hemisphere seasonality.](#)

493 Present-day observations identified a third possible mechanism of moisture supply to the southern
494 Levant. Winter to spring tropical plumes originating from the tropical eastern Atlantic and western
495 Africa transport moisture across the Sahara into the southern Levant deserts usually when the sub-
496 tropical jet is at a southern latitudinal position (e.g. Kahana et al., 2002; Rubin et al., 2007; Tubi
497 and Dayan, 2014). Increased frequency of such atmospheric circulation pattern that cause
498 widespread ample rainstorms are probably the only type that can increase runoff yield in southern
499 Negev drainage basins (e.g. Enzel et al., 2012) to a volume that will be noticed as a level change,
500 although minor, in the Dead Sea. Low-latitude tropical plumes have been also proposed as moisture
501 source in the past when Northern Hemisphere insolation reached maxima during times of the last
502 interglacial Lake Samra (Waldmann et al., 2009; 2010).

503 Disentangling the interactions of low-latitude/tropical and mid-latitude (Atlantic and
504 Mediterranean) moisture sources and related mechanisms that triggered the reconstructed long-
505 term and large-scale lake level fluctuations of the Dead Sea during the first 40 millennia of the last
506 glacial is ~~not straightforward~~ challenging and remains partly speculative. One reason for this
507 difficulty might be that orbital-driven changes in insolation and seasonality are the common
508 external trigger for both, high and low latitude climatic fluctuations during that time. Nevertheless,
509 the striking coincidence with palaeoclimatic records across the Mediterranean suggests a strong
510 role of the Atlantic-Mediterranean atmospheric circulation for the moisture supply to the Levant
511 during the last glacial inception.

512 The observed coincidence of a cold North Atlantic and dry southern Levant during the last glacial
513 inception apparently contradicts with the long-term observations of glacial high stands and
514 interglacial low stands at the Dead Sea. This apparent difference in the Dead Sea lake level response
515 to North Atlantic climate changes at different time scales might be explained by threshold effects
516 in the growth of the Fennoscandian ice sheet. Once the ice shield reached a certain height, it became
517 a morphological barrier causing a major system shift in the atmospheric circulation pattern (Webb
518 III et al., 1993) which, in turn, forces the Mediterranean storm tracks to shift southward and to be
519 funnelled and intensified towards the central Levant. This would explain the doubling of annual
520 rainfall in this region (Enzel et al., 2003; 2008) and the high Lake Lisan levels during the last glacial
521 by a major increase in precipitation in the Dead Sea basin (Rohling, 2013). During the glacial
522 inception different atmospheric boundary conditions prevailed likely because the ice shield
523 elevation was still below the threshold, which forces the large-scale circulation pattern to change.
524 To test this hypothesis, more high-resolution proxy records from the southern Levant and advanced
525 modelling studies are needed.

526 ~~A possible teleconnecting mechanism even to the high latitudes, where synchronous changes are~~
527 ~~evidenced from the Greenland ice cores, might be in the build-up of the Fennoscandian ice sheet,~~
528 ~~which might have acted as morphological obstacle forcing changes in the flow paths of the~~
529 ~~Northern Hemisphere jet stream. Furthermore, the large positive long-term changes in glacial and~~
530 ~~interglacial Dead Sea levels demand a very large volume of inflow (Enzel et al., 2003; 2008),~~
531 ~~leaving this source with its eastern Mediterranean cyclones as the best candidate. Shutting down or~~
532 ~~reducing this source was suggested as the prime cause for sharp declines in levels during both the~~
533 ~~Holocene and the last glacial (e.g. Bartov et al., 2003; Enzel et al., 2003; Torfstein et al., 2013). So~~

534 ~~far, in contrast with the summer season, little modelling efforts were conducted on the winter~~
535 ~~season atmospheric circulation during intervals of maximum insolation. An exception is a model~~
536 ~~simulation by Kutzbach et al. (2014), which supports an increased winter storm track that could~~
537 ~~have caused the wetter intervals in the Levant during maximum Northern Hemisphere seasonality.~~

538 6 Conclusions

- 539 - Investigation of a ~65 m long sediment section of the 5017-1 core from the deep Dead Sea
540 basin confirmed the sensitivity of sediment deposition to lake level variations. Therefore,
541 micro-facies is a suitable proxy for relative lake level variations and water balance allowing
542 to trace changing hydroclimatic conditions in the southern Levant during the early last
543 glacial from ~117 to 75 ka.
- 544 - Matrix-supported gravel deposits are more common in the deepest part of the Dead Sea
545 basin than previously documented. They are probably transported by mass-waste events
546 during major lake level fluctuations. We propose that the appearance of one well-sorted
547 gravel deposit, which was previously suggested as an in-situ beach deposit, is likely an
548 artefact of the drilling process and that this gravel was originally deposited by mass-wasting
549 as well. Therefore, we conclude that there is, yet, no proof for an almost complete drying
550 of the Dead Sea at the end of the last interglacial.
- 551 - We suggest that the first phase of an early Lake Lisan commenced ca 15 kyr earlier than
552 was suggested from the main sedimentological shift in exposed sediments at the lake's
553 margins at ~75-70 ka. In the deep basin, Lisan-type sediments, i.e. aad, were deposited
554 already since ~108-93 ka, but again interrupted by a final period of halite deposition
555 marking the end of Lake Samra at ~87 ka.
- 556 - Large-scale lake level fluctuations of the Dead Sea during the early last glacial (MIS 5d-
557 5a) are in concert with Mediterranean records and climate conditions in the North Atlantic.
558 ~~suggesting~~ This suggests that the insolation-driven Atlantic-Mediterranean ~~storm-track~~
559 ~~position~~ cyclone activity and seasonality changes ~~over and off the eastern Mediterranean is~~
560 are the main cause ~~of these rising and falling lake levels~~ for the observed lower lake levels
561 during colder intervals. ~~These shifts are related to large scale shifts of the Northern~~
562 ~~Hemisphere circulation triggered by the growing and shrinking continental ice sheets.~~ On
563 longer time scales, this pattern changed and highest lake levels during the Lake Lisan phase

564 [occurred during the cold Pleniglacial \(MIS 4-2\). This might be related to a southward shift](#)
565 [and intensification of Mediterranean cyclones towards the Levant due to a shift in](#)
566 [atmospheric circulation boundary conditions caused by the growth of Northern Hemisphere](#)
567 [ice sheets.](#)

568

569 **Acknowledgements**

570 [We like to thank the editor and two anonymous reviewers for their constructive comments, which](#)
571 [helped to improve the quality of the manuscript.](#) Funding by the International Continental Scientific
572 Drilling Program (ICDP), the German Science Foundation (DFG grants FR 1672/2-1 and BR
573 2208/10-1), the GFZ German Research Centre for Geosciences and the Israel Science Foundation
574 (ISF) Dead Sea Core-Center of Excellence Research (Grant # 1436/14 to YE) is gratefully
575 acknowledged. AA was supported by DESERVE Helmholtz Virtual Institute. We thank G. Arnold,
576 D. Berger and B. Brademann for preparing excellent thin sections and for technical support, P.
577 Dulski and F. Ott for help with μ XRF, B. Plessen and P. Meier for TOC and CaCO_3 measurements,
578 J. Mingram for support with the fluorescence microscope, G. Schlolaut (all GFZ German Research
579 Centre for Geosciences) and K. Schorling (HU Berlin) for grain size sampling, S. Baltruschat (TU
580 Darmstadt) for assistance with XRD samples and all people that have been involved in the drilling,
581 core opening and sampling campaigns [of the Dead Sea Deep Drilling Project](#). This study is a
582 contribution to the Helmholtz Association (HGF) climate initiative REKLIM Topic 8 "Rapid
583 climate change derived from proxy data".

584

1 **References**

- 2 Almogi-Labin, A., Bar-Matthews, M., Shriki, D., Kolosovsky, E., Paterne, M., Schilman, B., Ayalon,
3 A., Aizenshtat, Z., and Matthews, A.: Climatic variability during the last ~90 ka of the southern
4 and northern Levantine Basin as evident from marine records and speleothems, *Quaternary*
5 *Science Reviews*, 28, 2882-2896, <http://dx.doi.org/10.1016/j.quascirev.2009.07.017>, 2009.
- 6 Amit, R., Enzel, Y., and Sharon, D.: Permanent Quaternary hyperaridity in the Negev, Israel,
7 resulting from regional tectonics blocking Mediterranean frontal systems, *Geology*, 34, 509-
8 512, 10.1130/g22354.1, 2006.
- 9 Amit, R., Simhai, O., Ayalon, A., Enzel, Y., Matmon, A., Crouvi, O., Porat, N., and McDonald, E.:
10 Transition from arid to hyper-arid environment in the southern Levant deserts as recorded by
11 early Pleistocene cummulitic Aridisols, *Quaternary Science Reviews*, 30, 312-323,
12 <http://dx.doi.org/10.1016/j.quascirev.2010.11.007>, 2011.
- 13 Bar-Matthews, M., Ayalon, A., Kaufman, A., and Wasserburg, G. J.: The Eastern Mediterranean
14 paleoclimate as a reflection of regional events: Soreq cave, Israel, *Earth and Planetary Science*
15 *Letters*, 166, 85-95, Doi: 10.1016/s0012-821x(98)00275-1, 1999.
- 16 Bar-Matthews, M., Ayalon, A., and Kaufman, A.: Timing and hydrological conditions of Sapropel
17 events in the Eastern Mediterranean, as evident from speleothems, Soreq cave, Israel,
18 *Chemical Geology*, 169, 145-156, [http://dx.doi.org/10.1016/S0009-2541\(99\)00232-6](http://dx.doi.org/10.1016/S0009-2541(99)00232-6), 2000.
- 19 Bar-Matthews, M., Ayalon, A., Gilmour, M., Matthews, A., and Hawkesworth, C. J.: Sea–land
20 oxygen isotopic relationships from planktonic foraminifera and speleothems in the Eastern
21 Mediterranean region and their implication for paleorainfall during interglacial intervals,
22 *Geochimica et Cosmochimica Acta*, 67, 3181-3199, [http://dx.doi.org/10.1016/S0016-](http://dx.doi.org/10.1016/S0016-7037(02)01031-1)
23 [7037\(02\)01031-1](http://dx.doi.org/10.1016/S0016-7037(02)01031-1), 2003.
- 24 Barkan, E., Luz, B., and Lazar, B.: Dynamics of the carbon dioxide system in the Dead Sea,
25 *Geochimica et Cosmochimica Acta*, 65, 355-368, [http://dx.doi.org/10.1016/S0016-](http://dx.doi.org/10.1016/S0016-7037(00)00540-8)
26 [7037\(00\)00540-8](http://dx.doi.org/10.1016/S0016-7037(00)00540-8), 2001.
- 27 Bartov, Y., Stein, M., Enzel, Y., Agnon, A., and Reches, Z.: Lake Levels and Sequence Stratigraphy
28 of Lake Lisan, the Late Pleistocene Precursor of the Dead Sea, *Quaternary Research*, 57, 9-21,
29 DOI: 10.1006/qres.2001.2284, 2002.
- 30 Bartov, Y., Goldstein, S. L., Stein, M., and Enzel, Y.: Catastrophic arid episodes in the Eastern
31 Mediterranean linked with the North Atlantic Heinrich events, *Geology*, 31, 439-442,
32 10.1130/0091-7613(2003)031<0439:caeite>2.0.co;2, 2003.
- 33 Bartov, Y., Enzel, Y., Porat, N., and Stein, M.: Evolution of the Late Pleistocene–Holocene Dead
34 Sea Basin from Sequence Stratigraphy of Fan Deltas and Lake-Level Reconstruction, *Journal of*
35 *Sedimentary Research*, 77, 680-692, 10.2110/jsr.2007.070, 2007.
- 36 Begin, Z. B., Ehrlich, A., and Nathan, Y.: Lake Lisan -The Pleistocene precursor of the Dead Sea,
37 *Geological Survey of Israel Bulletin* 63, 1974.
- 38 Bentor, Y. K.: Some geochemical aspects of the Dead Sea and the question of its age, *Geochimica*
39 *et Cosmochimica Acta*, 25, 239-260, [http://dx.doi.org/10.1016/0016-7037\(61\)90061-8](http://dx.doi.org/10.1016/0016-7037(61)90061-8), 1961.
- 40 Bookman (Ken-Tor), R., Enzel, Y., Agnon, A., and Stein, M.: Late Holocene lake levels of the Dead
41 Sea, *Geological Society of America Bulletin*, 116, 555-571, 10.1130/b25286.1, 2004.

42 Bookman, R., Bartov, Y., Enzel, Y., and Stein, M.: Quaternary lake levels in the Dead Sea basin:
43 Two centuries of research, Geological Society of America Special Papers, 401, 155-170,
44 10.1130/2006.2401(10), 2006.

45 Brauer, A., Endres, C., and Negendank, J. F. W.: Lateglacial calendar year chronology based on
46 annually laminated sediments from Lake Meerfelder Maar, Germany, Quaternary
47 International, 61, 17-25, [http://dx.doi.org/10.1016/S1040-6182\(99\)00014-2](http://dx.doi.org/10.1016/S1040-6182(99)00014-2), 1999.

48 Brauer, A., Allen, J. R. M., Mingram, J., Dulski, P., Wulf, S., and Huntley, B.: Evidence for last
49 interglacial chronology and environmental change from Southern Europe, Proceedings of the
50 National Academy of Sciences, 104, 450-455, 10.1073/pnas.0603321104, 2007.

51 Chapman, M. R., and Shackleton, N. J.: Global ice-volume fluctuations, North Atlantic ice-rafting
52 events, and deep-ocean circulation changes between 130 and 70 ka, Geology, 27, 795-798,
53 10.1130/0091-7613(1999)027<0795:givfna>2.3.co;2, 1999.

54 Cheddadi, R., and Rossignol-Strick, M.: Eastern Mediterranean Quaternary paleoclimates from
55 pollen and isotope records of marine cores in the Nile Cone Area, Paleoceanography, 10, 291-
56 300, 10.1029/94pa02672, 1995.

57 Clark, P. U., Alley, R. B., and Pollard, D.: Northern Hemisphere Ice-Sheet Influences on Global
58 Climate Change, Science, 286, 1104-1111, 10.1126/science.286.5442.1104, 1999.

59 deMenocal, P., Ortiz, J., Guilderson, T., Adkins, J., Sarnthein, M., Baker, L., and Yarusinsky, M.:
60 Abrupt onset and termination of the African Humid Period: rapid climate responses to gradual
61 insolation forcing, Quaternary Science Reviews, 19, 347-361,
62 [http://dx.doi.org/10.1016/S0277-3791\(99\)00081-5](http://dx.doi.org/10.1016/S0277-3791(99)00081-5), 2000.

63 Develle, A. L., Gasse, F., Vidal, L., Williamson, D., Demory, F., Van Campo, E., Ghaleb, B., and
64 Thouveny, N.: A 250 ka sedimentary record from a small karstic lake in the Northern Levant
65 (Yammoûneh, Lebanon): Paleoclimatic implications, Palaeogeography, Palaeoclimatology,
66 Palaeoecology, 305, 10-27, <http://dx.doi.org/10.1016/j.palaeo.2011.02.008>, 2011.

67 Enzel, Y., Bookman, R., Sharon, D., Gvirtzman, H., Dayan, U., Ziv, B., and Stein, M.: Late Holocene
68 climates of the Near East deduced from Dead Sea level variations and modern regional winter
69 rainfall, Quaternary Research, 60, 263-273, DOI: 10.1016/j.yqres.2003.07.011, 2003.

70 Enzel, Y., Amit, R., Dayan, U., Crouvi, O., Kahana, R., Ziv, B., and Sharon, D.: The climatic and
71 physiographic controls of the eastern Mediterranean over the late Pleistocene climates in the
72 southern Levant and its neighboring deserts, Global and Planetary Change, 60, 165-192,
73 10.1016/j.gloplacha.2007.02.003, 2008.

74 Enzel, Y., Amit, R., Grodek, T., Ayalon, A., Lekach, J., Porat, N., Bierman, P., Blum, J. D., and Erel,
75 Y.: Late Quaternary weathering, erosion, and deposition in Nahal Yael, Israel: An “impact of
76 climatic change on an arid watershed”?, Geological Society of America Bulletin, 124, 705-722,
77 10.1130/b30538.1, 2012.

78 Enzel, Y., Kushnir, Y., and Quade, J.: The middle Holocene climatic records from Arabia:
79 Reassessing lacustrine environments, shift of ITCZ in Arabian Sea, and impacts of the southwest
80 Indian and African monsoons, Global and Planetary Change, 129, 69-91,
81 <http://dx.doi.org/10.1016/j.gloplacha.2015.03.004>, 2015.

82 Gasse, F., Vidal, L., Van Campo, E., Demory, F., Develle, A.-L., Tachikawa, K., Elias, A., Bard, E.,
83 Garcia, M., Sonzogni, C., and Thouveny, N.: Hydroclimatic changes in northern Levant over the
84 past 400,000 years, Quaternary Science Reviews, 111, 1-8,
85 <http://dx.doi.org/10.1016/j.quascirev.2014.12.019>, 2015.

86 Haliva-Cohen, A., Stein, M., Goldstein, S. L., Sandler, A., and Starinsky, A.: Sources and transport
87 routes of fine detritus material to the Late Quaternary Dead Sea basin, *Quaternary Science*
88 *Reviews*, 50, 55-70, [10.1016/j.quascirev.2012.06.014](https://doi.org/10.1016/j.quascirev.2012.06.014), 2012.

89 Herold, M., and Lohmann, G.: Eemian tropical and subtropical African moisture transport: an
90 isotope modelling study, *Clim Dyn*, 33, 1075-1088, [10.1007/s00382-008-0515-2](https://doi.org/10.1007/s00382-008-0515-2), 2009.

91 Kagan, E. J., and Marco, S.: Seismically triggered mass movement events from the Dead Sea
92 depocentre, International Workshop "Tectonics of the Levant fault and Northern Red Sea", IPG
93 Paris, 2013,

94 Kahana, R., Ziv, B., Enzel, Y., and Dayan, U.: Synoptic climatology of major floods in the Negev
95 Desert, Israel, *International Journal of Climatology*, 22, 867-882, [10.1002/joc.766](https://doi.org/10.1002/joc.766), 2002.

96 Katz, A., Kolodny, Y., and Nissenbaum, A.: The geochemical evolution of the Pleistocene Lake
97 Lisan-Dead Sea system, *Geochimica et Cosmochimica Acta*, 41, 1609-1626,
98 [http://dx.doi.org/10.1016/0016-7037\(77\)90172-7](http://dx.doi.org/10.1016/0016-7037(77)90172-7), 1977.

99 Katz, A., and Starinsky, A.: No drawdown and no hyperaridity in the ancient Dead Sea: (Comments
100 to Torfstein's et al. (2015) paper, *EPSL* 412, 235–244), *Earth and Planetary Science Letters*, 427,
101 303-305, <http://dx.doi.org/10.1016/j.epsl.2015.07.006>, 2015.

102 Krumgalz, B. S., Hecht, A., Starinsky, A., and Katz, A.: Thermodynamic constraints on Dead Sea
103 evaporation: can the Dead Sea dry up?, *Chemical Geology*, 165, 1-11,
104 [http://dx.doi.org/10.1016/S0009-2541\(99\)00156-4](http://dx.doi.org/10.1016/S0009-2541(99)00156-4), 2000.

105 Kutzbach, J. E., Chen, G., Cheng, H., Edwards, R. L., and Liu, Z.: Potential role of winter rainfall in
106 explaining increased moisture in the Mediterranean and Middle East during periods of
107 maximum orbitally-forced insolation seasonality, *Clim Dyn*, 42, 1079-1095, [10.1007/s00382-](https://doi.org/10.1007/s00382-013-1692-1)
108 [013-1692-1](https://doi.org/10.1007/s00382-013-1692-1), 2014.

109 Laskar, J., Robutel, P., Joutel, F., Gastineau, M., Correia, A. C. M., and Levrard, B.: A long-term
110 numerical solution for the insolation quantities of the Earth, *Astronomy & Astrophysics*, 428,
111 261-285, 2004.

112 Lazar, B., Sivan, O., Yechieli, Y., Levy, E. J., Antler, G., Gavrieli, I., and Stein, M.: Long-term
113 freshening of the Dead Sea brine revealed by porewater Cl⁻ and δ¹⁸O in ICDP Dead Sea deep-
114 drill, *Earth and Planetary Science Letters*, 400, 94-101,
115 <http://dx.doi.org/10.1016/j.epsl.2014.03.019>, 2014.

116 Lensky, N. G., Dvorkin, Y., Lyakhovskiy, V., Gertman, I., and Gavrieli, I.: Water, salt, and energy
117 balances of the Dead Sea, *Water Resources Research*, 41, W12418, [10.1029/2005wr004084](https://doi.org/10.1029/2005wr004084),
118 2005.

119 Litt, T., Pickarski, N., Heumann, G., Stockhecke, M., and Tzedakis, P. C.: A 600,000 year long
120 continental pollen record from Lake Van, eastern Anatolia (Turkey), *Quaternary Science*
121 *Reviews*, 104, 30-41, <http://dx.doi.org/10.1016/j.quascirev.2014.03.017>, 2014.

122 Liu, Z., Harrison, S. P., Kutzbach, J., and Otto-Bliesner, B.: Global monsoons in the mid-Holocene
123 and oceanic feedback, *Clim Dyn*, 22, 157-182, [10.1007/s00382-003-0372-y](https://doi.org/10.1007/s00382-003-0372-y), 2004.

124 Machlus, M., Enzel, Y., Goldstein, S. L., Marco, S., and Stein, M.: Reconstructing low levels of Lake
125 Lisan by correlating fan-delta and lacustrine deposits, *Quaternary International*, 73-74, 137-
126 144, Doi: [10.1016/S1040-6182\(00\)00070-7](https://doi.org/10.1016/S1040-6182(00)00070-7), 2000.

127 Mangerud, J., Jansen, E., and Landvik, J. Y.: Late Cenozoic history of the Scandinavian and Barents
128 Sea ice sheets, *Global and Planetary Change*, 12, 11-26, [http://dx.doi.org/10.1016/0921-](http://dx.doi.org/10.1016/0921-8181(95)00009-7)
129 [8181\(95\)00009-7](http://dx.doi.org/10.1016/0921-8181(95)00009-7), 1996.

130 Mangerud, J., Dokken, T., Hebbeln, D., Heggen, B., Ingólfsson, Ó., Landvik, J. Y., Mejdahl, V.,
131 Svendsen, J. I., and Vorren, T. O.: Fluctuations of the Svalbard–Barents Sea ice sheet during the
132 last 150 000 years, *Quaternary Science Reviews*, 17, 11-42, [http://dx.doi.org/10.1016/S0277-](http://dx.doi.org/10.1016/S0277-3791(97)00069-3)
133 [3791\(97\)00069-3](http://dx.doi.org/10.1016/S0277-3791(97)00069-3), 1998.

134 Martin-Puertas, C., Brauer, A., Wulf, S., Ott, F., Lauterbach, S., and Dulski, P.: Annual proxy data
135 from Lago Grande di Monticchio (southern Italy) between 76 and 112 ka: new chronological
136 constraints and insights on abrupt climatic oscillations, *Climate of the Past*, 10, 2099-2114,
137 10.5194/cp-10-2099-2014, 2014.

138 Migowski, C., Stein, M., Prasad, S., Negendank, J. F. W., and Agnon, A.: Holocene climate variability
139 and cultural evolution in the Near East from the Dead Sea sedimentary record, *Quaternary*
140 *Research*, 66, 421-431, DOI: 10.1016/j.yqres.2006.06.010, 2006.

141 Neugebauer, I., Brauer, A., Schwab, M. J., Waldmann, N. D., Enzel, Y., Kitagawa, H., Torfstein, A.,
142 Frank, U., Dulski, P., Agnon, A., Ariztegui, D., Ben-Avraham, Z., Goldstein, S. L., Stein, M., and
143 DSDDP Scientific Party: Lithology of the long sediment record recovered by the ICDP Dead Sea
144 Deep Drilling Project (DSDDP), *Quaternary Science Reviews*, 102, 149-165,
145 <http://dx.doi.org/10.1016/j.quascirev.2014.08.013>, 2014.

146 Neugebauer, I., Brauer, A., Schwab, M. J., Dulski, P., Frank, U., Hadzhiivanova, E., Kitagawa, H.,
147 Litt, T., Schiebel, V., Taha, N., Waldmann, N. D., and DSDDP Scientific Party: Evidences for
148 centennial dry periods at ~3300 and ~2800 cal. yr BP from micro-facies analyses of the Dead
149 Sea sediments, *The Holocene*, 25, 1358-1371, 10.1177/0959683615584208, 2015.

150 Rasmussen, S. O., Bigler, M., Blockley, S. P., Blunier, T., Buchardt, S. L., Clausen, H. B., Cvijanovic,
151 I., Dahl-Jensen, D., Johnsen, S. J., Fischer, H., Gkinis, V., Guillevic, M., Hoek, W. Z., Lowe, J. J.,
152 Pedro, J. B., Popp, T., Seierstad, I. K., Steffensen, J. P., Svensson, A. M., Vallenga, P., Vinther,
153 B. M., Walker, M. J. C., Wheatley, J. J., and Winstrup, M.: A stratigraphic framework for abrupt
154 climatic changes during the Last Glacial period based on three synchronized Greenland ice-
155 core records: refining and extending the INTIMATE event stratigraphy, *Quaternary Science*
156 *Reviews*, 106, 14-28, <http://dx.doi.org/10.1016/j.quascirev.2014.09.007>, 2014.

157 Rohling, E. J.: Quantitative assessment of glacial fluctuations in the level of Lake Lisan, Dead Sea
158 rift, *Quaternary Science Reviews*, 70, 63-72,
159 <http://dx.doi.org/10.1016/j.quascirev.2013.03.013>, 2013.

160 Rohling, E. J., Marino, G., and Grant, K. M.: Mediterranean climate and oceanography, and the
161 periodic development of anoxic events (sapropels), *Earth-Science Reviews*, 143, 62-97,
162 <http://dx.doi.org/10.1016/j.earscirev.2015.01.008>, 2015.

163 Rossignol-Strick, M.: Mediterranean Quaternary sapropels, an immediate response of the African
164 monsoon to variation of insolation, *Palaeogeography, Palaeoclimatology, Palaeoecology*, 49,
165 237-263, [http://dx.doi.org/10.1016/0031-0182\(85\)90056-2](http://dx.doi.org/10.1016/0031-0182(85)90056-2), 1985.

166 Rubin, S., Ziv, B., and Paldor, N.: Tropical Plumes over Eastern North Africa as a Source of Rain in
167 the Middle East, *Monthly Weather Review*, 135, 4135-4148, 10.1175/2007mwr1919.1, 2007.

168 Sade, A., Hall, J. K., Sade, H., Amit, G., Tibor, G., Schulze, B., Gur-Arieh, L., ten Brink, U., Ben-
169 Avraham, Z., Keller, C., Gertman, I., Beaudoin, J., Al-Zoubi, A., Akawwi, E., Rimawi, O.,
170 Abueladas, A., Mayer, L., Calder, B., and Maratos, A.: Multibeam Bathymetric Map of the Dead
171 Sea, Geological Survey of Israel Report GSI/01, 2014.

172 Sánchez Goñi, M. F., Eynaud, F., Turon, J. L., and Shackleton, N. J.: High resolution palynological
173 record off the Iberian margin: direct land-sea correlation for the Last Interglacial complex,

174 Earth and Planetary Science Letters, 171, 123-137, [http://dx.doi.org/10.1016/S0012-](http://dx.doi.org/10.1016/S0012-821X(99)00141-7)
175 [821X\(99\)00141-7](http://dx.doi.org/10.1016/S0012-821X(99)00141-7), 1999.

176 Sneh, A., Bartov, Y., Weissbrod, T., Rosensaft, M.: Geological Map of Israel, 1:200,000, Israel
177 Geological Survey (4 sheets), 1998.

178 Stein, M., Starinsky, A., Katz, A., Goldstein, S. L., Machlus, M., and Schramm, A.: Strontium
179 isotopic, chemical, and sedimentological evidence for the evolution of Lake Lisan and the Dead
180 Sea, *Geochimica et Cosmochimica Acta*, 61, 3975-3992, 10.1016/s0016-7037(97)00191-9,
181 1997.

182 Stein, M., Torfstein, A., Gavrieli, I., and Yechieli, Y.: Abrupt aridities and salt deposition in the post-
183 glacial Dead Sea and their North Atlantic connection, *Quaternary Science Reviews*, 29, 567-
184 575, DOI: 10.1016/j.quascirev.2009.10.015, 2010.

185 Stein, M., Ben-Avraham, Z., and Goldstein, S. L.: Dead Sea deep cores: A window into past climate
186 and seismicity, *Eos, Transactions American Geophysical Union*, 92, 453-454,
187 10.1029/2011eo490001, 2011.

188 Svendsen, J. I., Alexanderson, H., Astakhov, V. I., Demidov, I., Dowdeswell, J. A., Funder, S.,
189 Gataullin, V., Henriksen, M., Hjort, C., Houmark-Nielsen, M., Hubberten, H. W., Ingólfsson, Ó.,
190 Jakobsson, M., Kjær, K. H., Larsen, E., Lokrantz, H., Lunkka, J. P., Lyså, A., Mangerud, J.,
191 Matiouchkov, A., Murray, A., Möller, P., Niessen, F., Nikolskaya, O., Polyak, L., Saarnisto, M.,
192 Siegert, C., Siegert, M. J., Spielhagen, R. F., and Stein, R.: Late Quaternary ice sheet history of
193 northern Eurasia, *Quaternary Science Reviews*, 23, 1229-1271,
194 <http://dx.doi.org/10.1016/j.quascirev.2003.12.008>, 2004.

195 Tjallingii, R., Claussen, M., Stuut, J.-B. W., Fohlmeister, J., Jahn, A., Bickert, T., Lamy, F., and Rohl,
196 U.: Coherent high- and low-latitude control of the northwest African hydrological balance,
197 *Nature Geoscience*, 1, 670-675,
198 http://www.nature.com/ngeo/journal/v1/n10/supinfo/ngeo289_S1.html, 2008.

199 Torfstein, A., Gavrieli, I., Katz, A., Kolodny, Y., and Stein, M.: Gypsum as a monitor of the paleo-
200 limnological-hydrological conditions in Lake Lisan and the Dead Sea, *Geochimica et*
201 *Cosmochimica Acta*, 72, 2491-2509, DOI: 10.1016/j.gca.2008.02.015, 2008.

202 Torfstein, A., Haase-Schramm, A., Waldmann, N., Kolodny, Y., and Stein, M.: U-series and oxygen
203 isotope chronology of the mid-Pleistocene Lake Amora (Dead Sea basin), *Geochimica et*
204 *Cosmochimica Acta*, 73, 2603-2630, 10.1016/j.gca.2009.02.010, 2009.

205 Torfstein, A., Goldstein, S. L., Stein, M., and Enzel, Y.: Impacts of abrupt climate changes in the
206 Levant from Last Glacial Dead Sea levels, *Quaternary Science Reviews*, 69, 1-7,
207 <http://dx.doi.org/10.1016/j.quascirev.2013.02.015>, 2013.

208 Torfstein, A., Goldstein, S. L., Kushnir, Y., Enzel, Y., Haug, G., and Stein, M.: Dead Sea drawdown
209 and monsoonal impacts in the Levant during the last interglacial, *Earth and Planetary Science*
210 *Letters*, 412, 235-244, <http://dx.doi.org/10.1016/j.epsl.2014.12.013>, 2015.

211 Tubi, A., and Dayan, U.: Tropical Plumes over the Middle East: Climatology and synoptic
212 conditions, *Atmospheric Research*, 145-146, 168-181,
213 <http://dx.doi.org/10.1016/j.atmosres.2014.03.028>, 2014.

214 Tzedakis, P. C.: Towards an understanding of the response of southern European vegetation to
215 orbital and suborbital climate variability, *Quaternary Science Reviews*, 24, 1585-1599,
216 <http://dx.doi.org/10.1016/j.quascirev.2004.11.012>, 2005.

217 Tzedakis, P. C.: Seven ambiguities in the Mediterranean palaeoenvironmental narrative,
218 Quaternary Science Reviews, 26, 2042-2066,
219 <http://dx.doi.org/10.1016/j.quascirev.2007.03.014>, 2007.

220 Vaks, A., Bar-Matthews, M., Matthews, A., Ayalon, A., and Frumkin, A.: Middle-Late Quaternary
221 paleoclimate of northern margins of the Saharan-Arabian Desert: reconstruction from
222 speleothems of Negev Desert, Israel, Quaternary Science Reviews, 29, 2647-2662,
223 <http://dx.doi.org/10.1016/j.quascirev.2010.06.014>, 2010.

224 Waldmann, N., Starinsky, A., and Stein, M.: Primary carbonates and Ca-chloride brines as monitors
225 of a paleo-hydrological regime in the Dead Sea basin, Quaternary Science Reviews, 26, 2219-
226 2228, DOI: 10.1016/j.quascirev.2007.04.019, 2007.

227 Waldmann, N., Stein, M., Ariztegui, D., and Starinsky, A.: Stratigraphy, depositional environments
228 and level reconstruction of the last interglacial Lake Samra in the Dead Sea basin, Quaternary
229 Research, 72, 1-15, 10.1016/j.yqres.2009.03.005, 2009.

230 Waldmann, N., Torfstein, A., and Stein, M.: Northward intrusions of low- and mid-latitude storms
231 across the Saharo-Arabian belt during past interglacials, Geology, 38, 567-570,
232 10.1130/g30654.1, 2010.

233 Waldmann, N., Hadzhiivanova, E., Neugebauer, I., Brauer, A., Schwab, M. J., Frank, U., and Dulski,
234 P.: Anatomy of mass transport deposits in the Dead Sea; sedimentary processes in an active
235 tectonic hypersaline basin, EGU General Assembly, EGU-2014-11281, Vienna, Austria, 2014,

236 Webb III, T., Ruddiman, W. F., Street-Perrott, F. A., Markgraf, V., Kutzbach, J. E., Bartlein, P. J.,
237 Wright Jr., H. E., and Prell, W. L.: Climatic changes during the past 18,000 years: regional
238 syntheses, mechanisms, and causes, in: Global Climates since the Last Glacial Maximum, edited
239 by: Wright Jr., H. E., Kutzbach, J. E., and Webb III, T., 514-535, 1993.

240 Weltje, G. J., and Tjallingii, R.: Calibration of XRF core scanners for quantitative geochemical
241 logging of sediment cores: Theory and application, Earth and Planetary Science Letters, 274,
242 423-438, <http://dx.doi.org/10.1016/j.epsl.2008.07.054>, 2008.

243 Wolff, E. W., Chappellaz, J., Blunier, T., Rasmussen, S. O., and Svensson, A.: Millennial-scale
244 variability during the last glacial: The ice core record, Quaternary Science Reviews, 29, 2828-
245 2838, <http://dx.doi.org/10.1016/j.quascirev.2009.10.013>, 2010.

246 Wright, J. D.: Global Climate Change in Marine Stable Isotope Records, in: Quaternary
247 Geochronology: Methods and Applications, edited by: Noller, J. S., Sowers, J. M., and Lettis, W.
248 R., American Geophysical Union, 427-433, 2000.

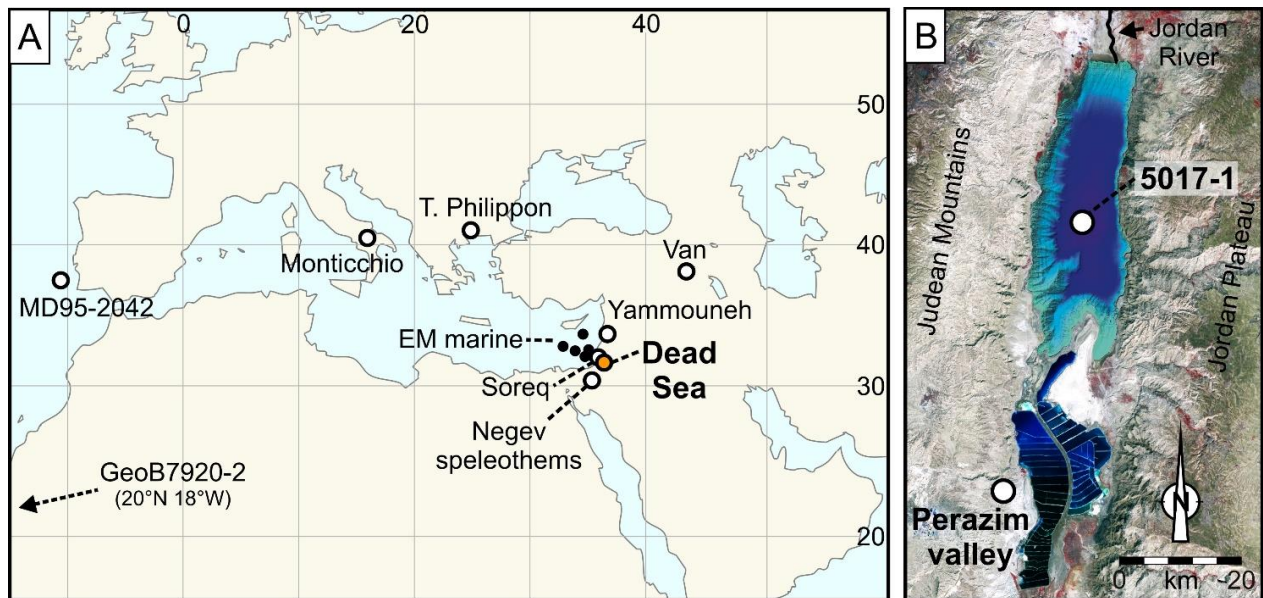
249 Yechieli, Y., Magaritz, M., Levy, Y., Weber, U., Kafri, U., Woelfli, W., and Bonani, G.: Late
250 Quaternary Geological History of the Dead Sea Area, Israel, Quaternary Research, 39, 59-67,
251 10.1006/qres.1993.1007, 1993.

252 Yechieli, Y., Gavrieli, I., Berkowitz, B., and Ronen, D.: Will the Dead Sea die?, Geology, 26, 755-
253 758, 10.1130/0091-7613(1998)026<0755:wtdsd>2.3.co;2, 1998.

254 Ziv, B., Dayan, U., Kushnir, Y., Roth, C., and Enzel, Y.: Regional and global atmospheric patterns
255 governing rainfall in the southern Levant, International Journal of Climatology, 26, 55-73,
256 10.1002/joc.1238, 2006.

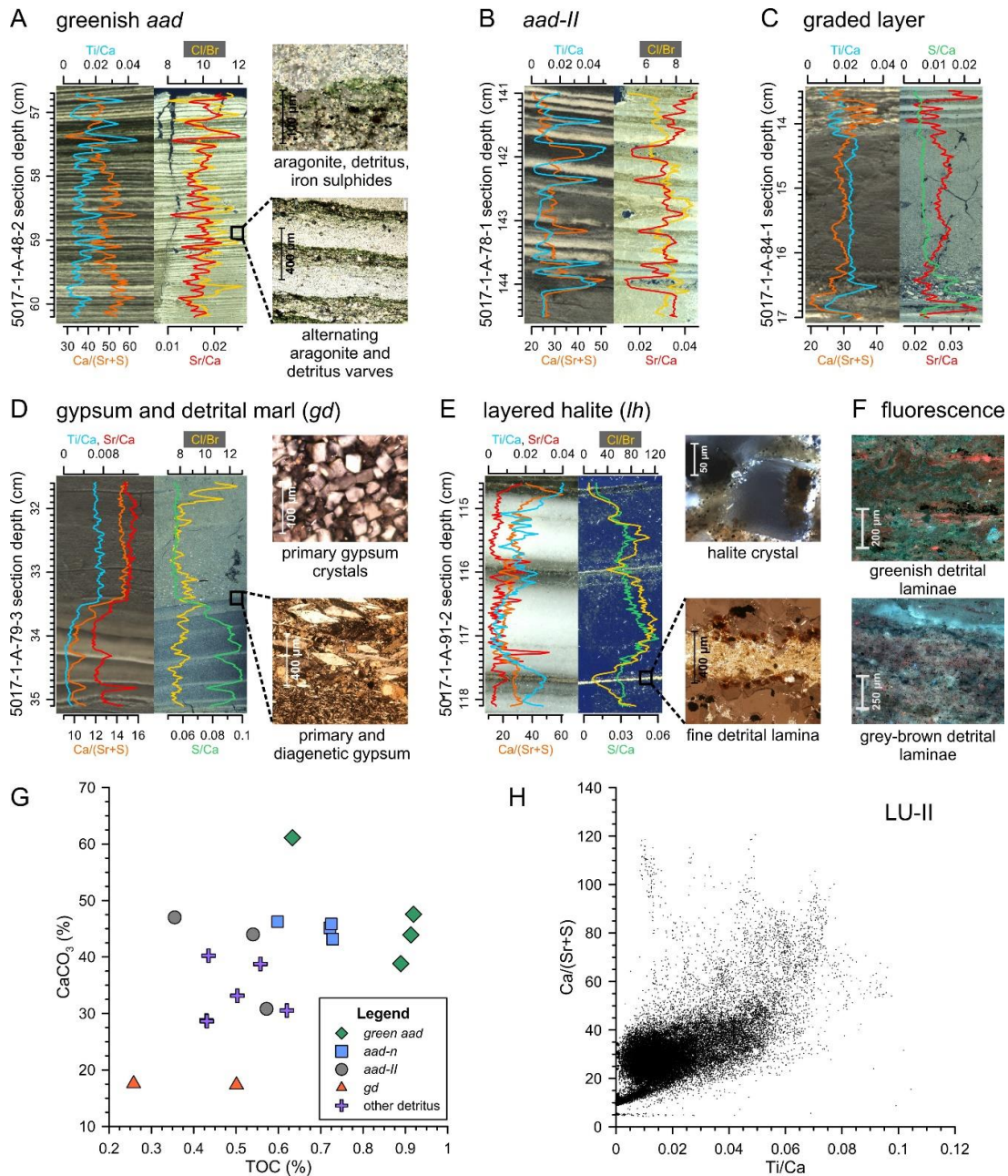
257

1 **Figures and figure captions**



2
3 Figure 1. (A) Location of Mediterranean records discussed in the text; EM marine – eastern
4 Mediterranean marine cores (Cheddadi and Rossignol-Strick, 1995; Almogi-Labin et al., 2009);
5 Negev speleothems – various caves in the northern, central and southern Negev (Vaks et al., 2010);
6 for references of the other records the reader is referred to the text. (B) Map of the Dead Sea (NASA
7 image by R. Simmon using Landsat data (2011) from USGS, www.visibleearth.nasa.gov/),
8 bathymetry of [the](#) northern Dead Sea basin from Sade et al. (2014), 5017-1 coring location, Perazim
9 valley Samra outcrop PZ-7 (Waldmann et al., 2009).

10

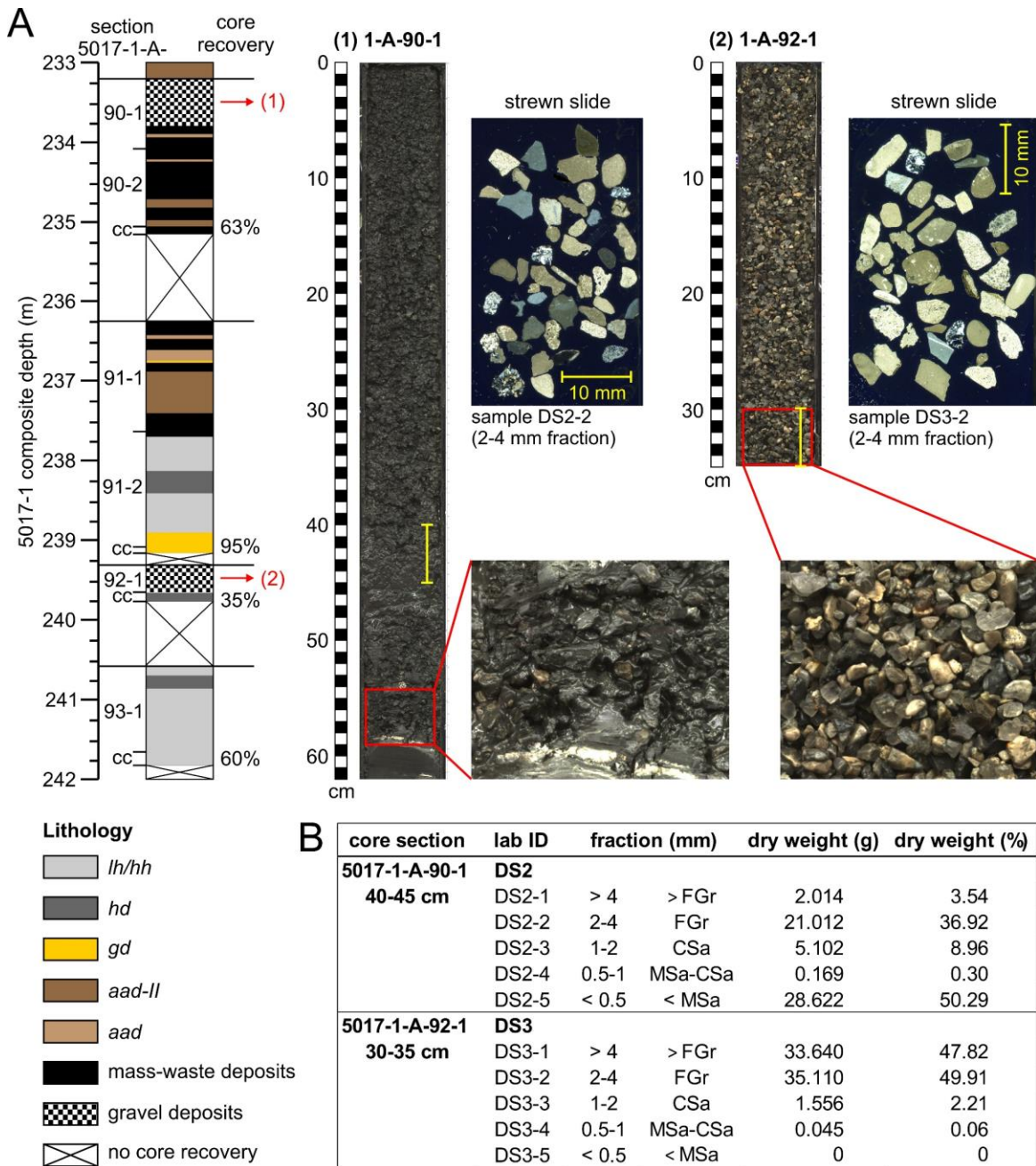


11

12 Figure 2. Micro-facies (core photos, polarised thin section scans and microscopic images with
 13 varying magnification and polarisation conditions) and μ XRF characteristics (element ratios): (A)
 14 green aad facies with peaks in Sr/Ca typical for aragonite layers and peaks in Ti/Ca and Ca/(Sr+S)
 15 indicating detrital layers; (B) aad-II facies containing greyish detritus and thicker aragonite layers
 16 than the green aad facies; (C) example of a mass-waste deposit: graded layer with high Ti/Ca ratio
 17 and increased S/Ca at the base due to diagenetic gypsum; (D) gd facies characterised by high S/Ca
 18 ratio; (E) lh facies with high Cl/Br and positively correlated S/Ca, but peaks of all other elements
 19 only in the thin detrital laminae; (F) fluorescence (violet light) microscope images of greenish

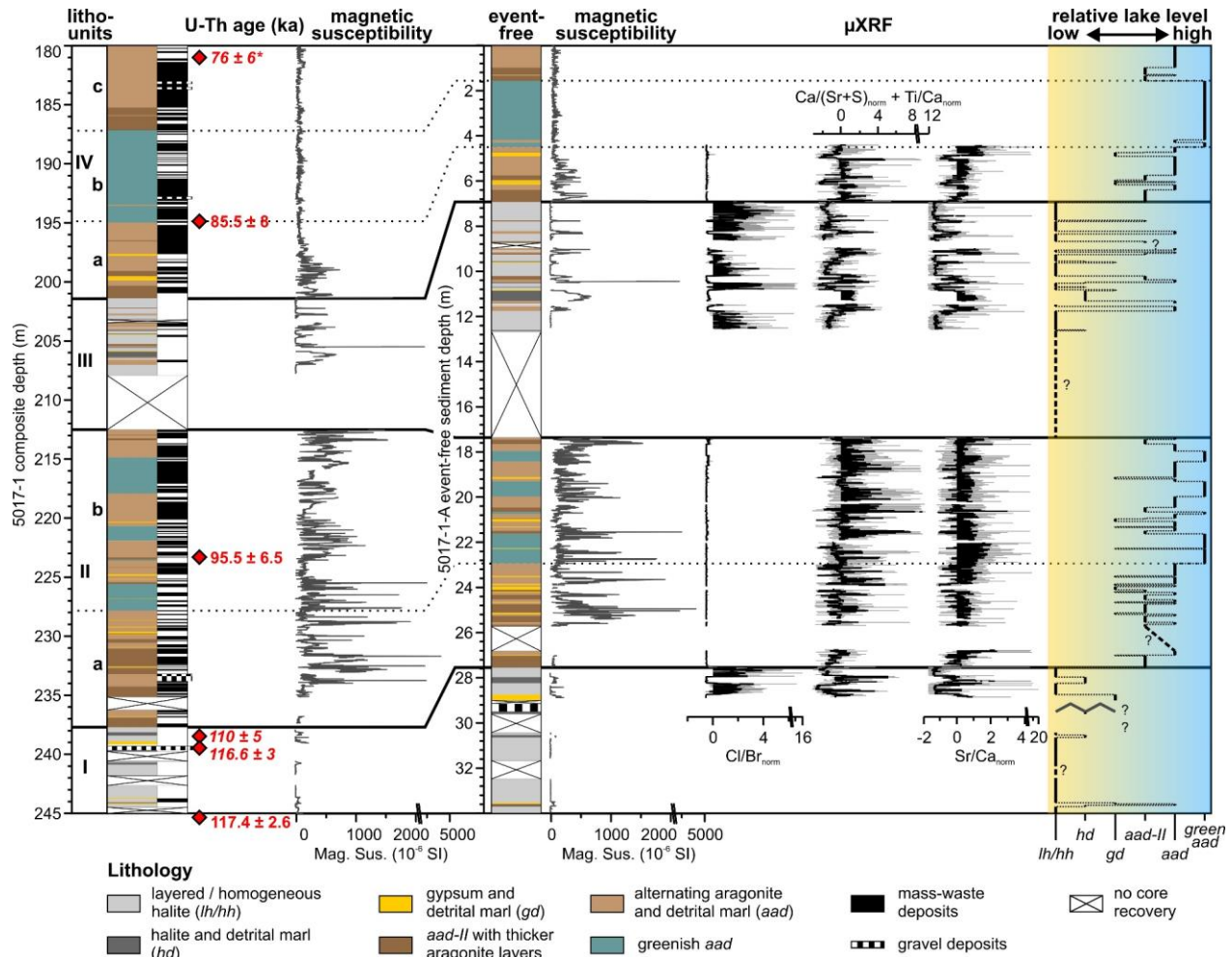
20 detrital laminae (upper photo, core section 5017-A-1-87-1, at ~72 cm) with very strong
21 fluorescence (red colour) and greyish-brownish detrital laminae (lower photo, core section 5017-
22 1-A-78-1, at ~140 cm) that are characterised by a weaker fluorescence; (G) correlation plot of TOC
23 against CaCO_3 contents of 19 samples distinguished for different micro-facies types; (H)
24 correlation plot of the two detrital fractions as derived from μXRF element scanning, exemplary
25 for lithological unit (LU) II: Ti/Ca as proxy for the siliciclastic detrital fraction and $\text{Ca}/(\text{Sr}+\text{S})$ as
26 proxy for the detrital carbonate fraction, $R^2 = 0.4$.

27



28

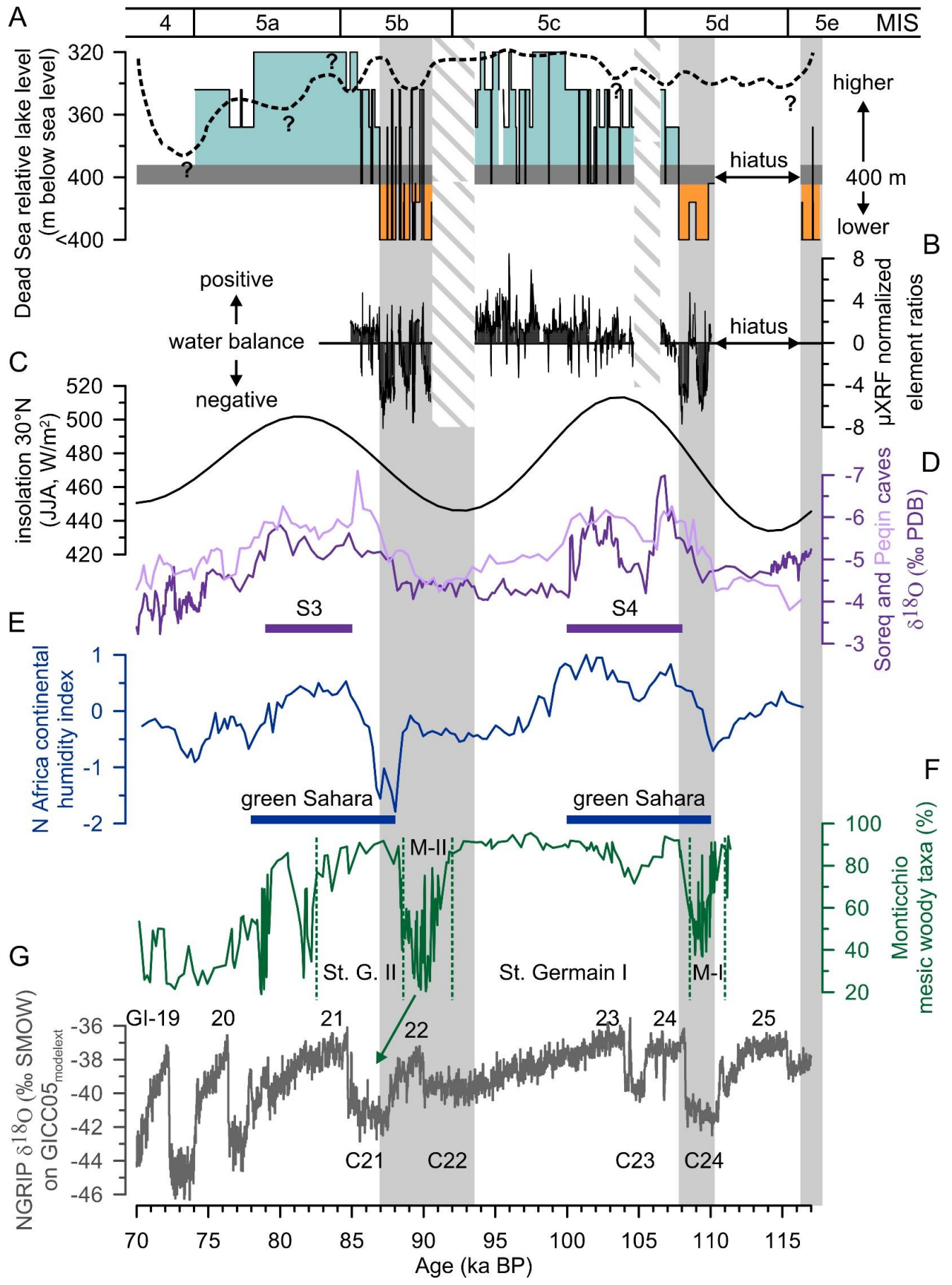
29 Figure 3. (A) Lithological profile from 233-242 m composite depth (cc – core catcher), two gravel
 30 deposits in core sections (1) 5017-1-A-90-1 (233.17 m composite depth) and (2) 5017-1-A-92-1
 31 (239.27 m composite depth) and strewn thin slide scans (polarised light) of the 2-4 mm grain
 32 fractions; yellow bars indicate sampling positions in the two core sections. (B) table of grain size
 33 fractions after sieving for one example of a mud-supported gravel occurrence and the pure gravel
 34 layer, both as shown in (A).



36

37 Figure 4. Lithology of the ~65 m long 5017-1 core section: lithostratigraphic units, U-Th ages (from
 38 Torfstein et al., 2015), with extrapolated ages in italic, * - interpolated age (see text for explanation),
 39 magnetic susceptibility (1 mm resolution, 10^{-6} SI); event-free lithology, μ XRF data (grey: 200 μ m
 40 steps, black: 101-steps running means of counts) and the relative lake level changes inferred from
 41 the changing micro-facies. All mass-waste deposits thicker than 1 cm were excluded from the
 42 event-free lithological profile and data, event-free sediment depth starts with zero at 180 m below
 43 lake floor. μ XRF data of normalized ratios: Cl/Br representing halite, $(Ca/(Sr+S) + Ti/Ca)$ indicating
 44 the total carbonate and siliciclastic detritus, Sr/Ca indicating aragonite.

45



47 Figure 5. Comparison of the Dead Sea to other records: (A) the relative Dead Sea lake level curve
48 inferred from micro-facies analysis of the deep-basin core 5017-1 (this study; right y-axis) and
49 from site PZ-7 from the Perazim valley (dashed line; left y-axis, indicating maximum or minimum
50 relative lake levels) (Waldmann et al., 2009); (B) sum of normalized ratios of Ca/(Sr+S) and Ti/Ca
51 as proxies for carbonate and siliciclastic detritus, respectively, and of Sr/Ca, proxy for aragonite,
52 subtracted by the Cl/Br ratio, which is a proxy for halite, $[Ca/(Sr+S) + Ti/Ca + Sr/Ca - Cl/Br]$
53 indicating the water balance of the lake and agreeing well with the relative lake level curve; (C)
54 mean summer (JJA) insolation at 30°N (after Laskar et al., 2004); (D) $\delta^{18}O$ of Soreq and Peqin
55 speleothems, Israel (Bar-Matthews et al., 2003) and eastern Mediterranean sapropel events S3 and
56 S4 (according to Bar-Matthews et al., 2000); (E) humidity index of continental North Africa (core
57 GeoB7920-2) and “green Sahara” phases (Tjallingii et al., 2008); (F) Monticchio (southern Italy)
58 pollen record of mesic woody taxa and Mediterranean pollen zones Melisey (M) I and II, and St.
59 Germain I and II (Brauer et al., 2007; Martin-Puertas et al., 2014), note a possible chronological
60 shift of 3500 yr to the older for 92-76 ka according to Martin-Puertas et al. (2014); (G) Greenland
61 ice core $\delta^{18}O$ record on GICC05_{modelext} timescale (Wolff et al., 2010), indicated are also Greenland
62 interstadials (GI) after Rasmussen et al. (2014) and North Atlantic ice rafting events C21 to C24
63 (Chapman and Shackleton, 1999). Marine isotope stages are given according to Wright (2000).
64 Grey vertical bars indicate periods of negative water balance in the Dead Sea; obliquely banded
65 bars: no core recovery.

1 **Hydroclimatic variability in the Levant during the early last**
2 **glacial (~117-75 ka) derived from micro-facies analyses of**
3 **deep Dead Sea sediments**

4
5 **I. Neugebauer¹, M.J. Schwab¹, N.D. Waldmann², R. Tjallingii¹, U. Frank¹, E.**
6 **Hadzhiivanova², R. Naumann³, N. Taha², A. Agnon⁴, Y. Enzel⁴ and A.**
7 **Brauer^{1,5}**

8 [1] GFZ German Research Centre for Geosciences, Section 5.2 – Climate Dynamics and Landscape
9 Evolution, Telegrafenberg, 14473 Potsdam, Germany

10 [2] University of Haifa, Department of Marine Geosciences, Leon H. Charney School of Marine
11 Sciences, Mount Carmel 31905, Israel

12 [3] GFZ German Research Centre for Geosciences, Section 4.2 – Inorganic and Isotope
13 Geochemistry, Telegrafenberg, 14473 Potsdam, Germany

14 [4] The Hebrew University of Jerusalem, The Fredy & Nadine Herrmann Institute of Earth
15 Sciences, Givat Ram, Jerusalem 91904, Israel

16 [5] University of Potsdam, Institute of Earth and Environmental Science, Karl-Liebnecht-Str. 24-
17 25, 14476 Potsdam-Golm, Germany

18 Correspondence to: I. Neugebauer (inaneu@gfz-potsdam.de)

19
20 **Abstract**

21 The new sediment record from the deep Dead Sea basin (ICDP core 5017-1) provides a unique
22 archive for hydroclimatic variability in the Levant. Here, we present high-resolution sediment
23 facies analysis and elemental composition by [micro-X-ray fluorescence \(μXRF\)](#) scanning of core
24 5017-1 to trace lake levels and responses of the regional hydroclimatology during the time interval
25 from ca 117-75 ka, i.e. the transition between the last interglacial and the onset of the last glaciation.
26 We distinguished six major micro-facies types and interpreted these and their alterations in the core
27 in terms of relative lake level changes. The two end-member facies for highest and lowest lake

28 levels are (a) up to several meters thick, greenish sediments of alternating aragonite and detrital
29 marl laminae (aad) and (b) thick halite facies, respectively. Intermediate lake levels are
30 characterised by detrital marls with varying amounts of aragonite, gypsum or halite, reflecting
31 lower-amplitude, shorter-term variability. Two intervals of pronounced lake level drops occurred
32 at $\sim 110\text{-}108 \pm 5$ ka and $\sim 93\text{-}87 \pm 7$ ka. They likely coincide with stadial conditions in the central
33 Mediterranean (Melisey I and II pollen zones in Monticchio) and low global sea levels during [the](#)
34 [marine isotope stages \(MIS\) 5d and 5b](#). However, our data do not support the current hypothesis of
35 an almost complete desiccation of the Dead Sea during the earlier of these lake level low stands
36 based on a recovered gravel layer. Based on new petrographic analyses, we propose that, although
37 it was a low stand, this well-sorted gravel layer may be a vestige of a thick turbidite that has been
38 washed out during drilling rather than an in-situ beach deposit. Two intervals of higher lake stands
39 at $\sim 108\text{-}93 \pm 6$ ka and $\sim 87\text{-}75 \pm 7$ ka correspond to interstadial conditions in the central
40 Mediterranean, i.e. pollen zones St. Germain I and II in Monticchio, and GI 24+23 and 21 in
41 Greenland, as well as to sapropels S4 and S3 in the Mediterranean Sea. These apparent correlations
42 suggest a close link of the climate in the Levant to North Atlantic and Mediterranean climates
43 during the time of the build-up of Northern Hemisphere ice shields in the early last glacial period.

44 **1 Introduction**

45 The Dead Sea and its Pleistocene precursor Lakes Amora, Samra and Lisan (e.g. Bartov et al.,
46 2003; Torfstein et al., 2009; Waldmann et al., 2009) experienced major lake level fluctuations in
47 the past as a sensitive response to changing hydroclimatic conditions in the lake's watershed (e.g.
48 Enzel et al., 2008). The lakes expanded during glacial intervals due to up to twice modern
49 precipitation, whereas interglacials are generally characterised by a lake contraction due to reduced
50 precipitation and runoff (Enzel et al., 2008; Rohling, 2013). Hence, the last glacial Lake Lisan,
51 which occupied the Dead Sea basin between ~ 70 and 14 ka, reached up to ~ 270 m higher lake
52 stands than the Holocene Dead Sea and the last interglacial Lake Samra (e.g. Bartov et al., 2002;
53 2007; Waldmann et al., 2007; Torfstein et al., 2013). The highest amplitudes of lake level drops
54 occurred at the glacial to interglacial transitions triggered by lower rainfall (e.g. Yechieli et al.,
55 1993; Bartov et al., 2007; Waldmann et al., 2009; Stein et al., 2010). For example, the fresher Lake
56 Lisan water body turned into the hypersaline Holocene Dead Sea during the last termination leading

57 to the deposition of a thick halite sequence during the early Holocene (~11-10 ka; e.g. Stein et al.,
58 2010).

59 Less information is available about lake level changes during the transition from interglacial to
60 glacial climate conditions. Previous studies from exposed sediment sections of the Samra
61 Formation at the south-western margin of the Dead Sea suggested a relatively shallow Lake Samra
62 from ca 135 to 75 ka (Waldmann et al., 2007; 2009; 2010). The main lake level rise at the transition
63 from Lake Samra to Lake Lisan was assumed from a sedimentological change from sand deposits
64 to sediments of alternating fine laminae of aragonite and detritus at a major unconformity ~75-70
65 ka (e.g. Waldmann et al., 2009; Torfstein et al., 2013). However, the early glacial time interval
66 between the last interglacial low stand (Lake Samra) and the full glacial high stand (Lake Lisan),
67 i.e. coinciding with MIS 5d to 5a, is not well represented in the exposed sediments (Waldmann et
68 al., 2009).

69 Sediments from this time interval have been for the first time recovered by ICDP drilling project
70 DSDDP from the deepest part of the Dead Sea basin (Neugebauer et al., 2014). Based on a new
71 chronology and interpretation of a well-sorted gravel deposit, Torfstein et al. (2015) inferred an
72 almost complete drawdown of the Dead Sea leading to a sedimentary hiatus between 116 and 110
73 ka at around MIS 5d, which is considered the most extreme lake level drop during the last ~220 ka,
74 i.e. the time period covered by the DSDDP sediment record. Furthermore, Torfstein et al. (2015)
75 suggest moisture supply through the African monsoon to the southern Levant during more humid
76 intervals in the early last glacial, which are considered to coincide with MIS 5c and 5a, whereas
77 marine and terrestrial records from across the Mediterranean region responded to long-term
78 orbitally induced temperature fluctuations, ice sheet waxing and waning in the Northern
79 Hemisphere and climatic changes in the North Atlantic (e.g. Tzedakis, 2005; Martin-Puertas et al.,
80 2014).

81 In this study, we apply a combination of petrographic, micro-facies and high-resolution XRF
82 analyses to investigate in more detail the sedimentological changes in the new ICDP Dead Sea
83 record between the last interglacial and the onset of Lake Lisan (~117-75 ka). These sediments and
84 their alterations serve as indicators for hydroclimatic variations in the southern Levant. In addition,
85 we focus on the sedimentology of the gravel layer to add information on the drawdown hypothesis
86 of the Dead Sea (Stein et al., 2011; Torfstein et al., 2015).

87 **2 Regional Setting**

88 With a lake level of 429 m (in 2015) below mean sea level (m bmsl) and a water depth of ca 300
89 m the Dead Sea is located in one of the lowest continental depressions on earth. The basin is
90 bounded by the Judean Mountains on the west and the Jordan Plateau on the east, rising to heights
91 of ~1000 m and ~1200 m above mean sea level, respectively (Fig. 1). The modern watershed of the
92 lake, which is one of the largest in the Levant (~40,000 km²), experiences subhumid (>1000 mm
93 yr⁻¹ in the northernmost point) to semiarid Mediterranean climate in its north and arid to hyperarid
94 (~30 mm yr⁻¹ in the southernmost point) conditions in the southern part characterised by winter-
95 rain of the Saharo-Arabian environment. These climate conditions combined with the particular
96 steep topography of the basin margins create hyperarid conditions at the lake itself. The modern
97 Dead Sea is a hypersaline Ca-chloride brine (e.g. Katz et al., 1977; Lensky et al., 2005) and a
98 terminal lake, mainly fed by the Jordan River (Fig. 1). Precipitation primarily arrives in the
99 watershed in fall to late spring (Oct-May) through eastern Mediterranean mid-latitude cyclones
100 (Cyprus Lows; Ziv et al., 2006; Enzel et al., 2008) and tropical plumes in winter and spring (also
101 termed subtropical jet storms by Kahana et al., 2002; Rubin et al., 2007). Occasionally, the region
102 is influenced by the Active Red Sea Trough from the south during fall and winter (e.g. Enzel et al.,
103 2008) with sources of its moisture also in the Mediterranean. The geology of the catchment is
104 predominantly characterised by Cretaceous carbonate sedimentary rocks, with some Palaeozoic to
105 Mesozoic sandstones and Pleistocene volcanic units (Bentor, 1961; Sneh, 1998).

106 **3 Material and Methods**

107 **3.1 Dead Sea deep-basin core 5017-1**

108 The 5017-1 sediment core from the deep Dead Sea basin (31°30'29" N, E 35°28'16" E; ca 300 m
109 water depth in 2010; sediment surface ~725 m bmsl; Fig. 1) was obtained during the drilling
110 campaign of the ICDP Dead Sea Deep Drilling Project (DSDDP) in winter 2010-11 (Stein et al.,
111 2011). The record is ~455 m long and comprises two full glacial-interglacial cycles (Neugebauer
112 et al., 2014; Torfstein et al., 2015). Here, we focus on a ~65 m long section from ~180 to ~245 m
113 below lake floor (mblf). Sediment facies were described with an accuracy of 1 cm based on line-
114 scanning images of the split sediment cores. Magnetic susceptibility data in 1 mm resolution were
115 routinely obtained for the entire 5017-1 record (see Neugebauer et al., 2014 for details).

116 **3.2 Micro-facies analyses**

117 For micro-facies analyses we applied a combination of petrographic thin section microscopy and
118 high-resolution μ XRF element scanning. A total of 26 large-scale thin section samples (10 x 2 cm)
119 were prepared representing changes in facies types along the section. Preparation largely followed
120 the standard procedure for soft sediments (e.g. Brauer et al., 1999), but were performed under dry
121 conditions to avoid salt crystallization during the preparation process. Thin sections were analysed
122 with a petrographic microscope (Leica DMLP) and images were taken with a digital camera
123 (Olympus DP72). Fluorescence was analysed using a Nikon AZ100M microscope, operated with
124 violet and polarised light conditions, and Nikon photo software (NIS Elements AR 4.3).

125 The μ XRF measurements were acquired every 200 μ m for 10 s using the ITRAX μ XRF core
126 scanner at GFZ, Germany. The core scanner is equipped with a Cr tube operated at 30 kV and 30
127 mA to irradiate the split-core sediment surface. This non-destructive method acquires element
128 intensities of Si, S, Cl, K, Ca, Ti, Fe, Br and Sr (Neugebauer et al., 2014), which are presented as
129 count rates (counts per second – cps). The element intensity records reflect relative changes in the
130 composition of the Dead Sea sediments, but are also influenced by physical sediment properties
131 (e.g. density, water content, grain size) and the sample geometry. The easiest and most convenient
132 way to minimize the physical and geometrical sample effects is by the transformation of element
133 intensities into ratios or log-ratios (Weltje and Tjallingii, 2008).

134 **3.3 Grain size analyses and gravel petrography**

135 Laminated sediments were sampled for grain size distributions with 1 cm³ sample volume at 1-3
136 cm vertical resolution and a total of 363 samples. Sample preparation included decomposing
137 organic matter using 30 mL H₂O₂ (30%) and distilled water (1:1 concentration), and breaking
138 aggregates with Calgon detergent ((NaPO₃)₆, 1%) and ultrasonic bath. The particle size distribution
139 was measured using an LS 13 320 laser diffraction particle size analyser for (1) the total sample
140 and (2) the carbonate-free sample after dissolution through HCl (32%, dilution of 1:9 with distilled
141 water). Less than 1 g of sediment was required for measurement.

142 In total, 22 gravel layers detected in core 5017-1 were sampled for petrographic analyses. The
143 samples were wet-sieved for five grain size fractions (>4 mm, 2-4 mm, 1-2 mm, 0.5-1 mm and <0.5

144 mm), for which strewn slides have been prepared for microscopic inspections. Here, we focus on
145 two gravel units occurring within the studied core section (180-245 mblf).

146 **3.4 XRD and TOC/CaCO₃ measurements**

147 For X-ray powder diffraction ([XRD](#)) measurements 25 samples were collected from about the same
148 depths as thin sections to complement microscopic inspections. Powder X-ray patterns were
149 collected using a PANalytical Empyrean powder diffractometer with Cu K α radiation, automatic
150 divergent and antiscatter slits and a PIXcel^{3D} detector. The diffraction data were recorded from 5°
151 to 85° 2 Θ via a continuous scan with a step-size of 0.013 and a scan time of 60 s per step. The
152 generator settings were 40 kV and 40 mA.

153 Total organic carbon (TOC) and calcium carbonate (CaCO₃) contents have been determined from
154 19 of these samples using an elemental analyser (EA3000-CHNS Eurovector). First, 5-10 mg dried
155 and homogenized sample material was weighed in Sn-capsules for total carbon (TC) determination.
156 Subsequently, second sample aliquots of 3-4 mg of the samples were decalcified in Ag-capsules in
157 three steps through treatment with (1) 3% HCl, (2) 20% HCl and (3) drying at 75°C for TOC
158 determination. Data were calibrated with standards (BBOT, Sulfanilamide, for TOC additionally
159 Boden3) and empty Sn- and Ag-capsules. The relative standard deviation is <1%. CaCO₃ contents
160 were calculated from the difference TC-TOC.

161 **4 Results**

162 **4.1 Micro-facies, sedimentology and geochemistry**

163 The sediments of the analysed ~65 m long section of core 5017-1 mainly consist of laminated marl
164 of the aad facies (alternating aragonite and detritus; e.g. Machlus et al., 2000), gypsum and **massive**
165 halite deposits (Neugebauer et al., 2014). Commonly, detrital material is composed of clay to silt-
166 sized calcite, quartz, dolomite and minor feldspar and clay minerals. [The](#) **T**hickness of detrital
167 layers ranges from <1 mm to several cm and their colour is greyish to black, if iron sulphides are
168 present (pyrite or greigite), or brownish and greenish, if terrestrial organic or algal remains are
169 dominant. Aragonite formed as 5-15 μ m small stellate aggregates of orthorhombic crystals building
170 ~0.1-4 mm thick white laminae. Monoclinic, euhedral ~10-60 μ m gypsum crystals build ~0.2-3 cm
171 thick beige layers. Larger, up to 1 mm gypsum crystals appear scattered within detrital layers.

172 Cubic, ~1 mm to several cm long halite crystals are either embedded in predominantly detrital marl
173 or build thick deposits. These thick halite deposits contain only minor detrital material and are often
174 layered.

175 Six micro-facies types were identified (Fig. 2):

- 176 i) green aad: alternating white aragonite and greenish detrital marl laminae (~1 mm thick
177 couplets; Fig. 2a), the greenish laminae exhibit some diatoms and very strong fluorescence
178 pointing to a significant amount of chlorophyll preserved in the sediment (Fig. 2f);
- 179 ii) aad-n: alternating white aragonite and greyish detrital marl laminae (~1 mm thick couplets,
180 occurrence as normal type; defined by Machlus et al., 2000);
- 181 iii) aad-II: alternating white aragonite and greyish detrital marl laminae with thicker aragonite
182 layers than normal type (~1-5 mm thick couplets, Fig. 2b);
- 183 iv) gd: well-laminated to massive, cm-thick gypsum deposits and detrital marl (Fig. 2de);
- 184 v) hd: cubic halite crystals (mm-cm) scattered in detrital marl;
- 185 vi) lh/hh: layered or homogeneous consolidated halite; the layered type often alternates with thin
186 detrital marl laminae (Fig. 2ed).

187 In addition, up to 1.7 m thick graded layers and up to 3 m thick slump deposits are predominantly
188 associated to the aad micro-facies types and less frequent and thinner in the halite-dominated
189 sections. In cm to tens of cm thick basal layers of 22 thick turbidites and slump deposits, matrix-
190 supported ~2-8 mm sized, angular to rounded gravels occur. In the studied section of core 5017-1,
191 four such mass-waste deposits with gravel-rich basal layers were identified at composite depths of
192 ~233.5 m, ~192.8 m, ~183.5 m and ~183 m (Fig. 4) of which the ~58 cm thick turbidite at ~233.5
193 m depth was analysed in detail (Fig. 3). The matrix-supported gravels are composed of carbonates
194 (limestone, dolomite, with a presence of aragonite) in the form of sparite, (bio)micrite or peloid,
195 and sulphates (gypsum, anhydrite) as well as halite and minor quartz. The fine and medium gravel
196 fractions constitute ~40% of the total dry weight (Fig. 3b).

197 In one exceptional case at ~239 m composite depth, a ~35 cm thick layer of well-sorted gravels
198 with <2% clay- to sand-matrix appears (Figs. 3 and 4). The petrographic composition of this gravel
199 deposit is identical to that of the other mud-supported gravels (Fig. 3). This gravel layer is from a
200 core section that suffered a major loss of core material during the drilling process (core 5017-1-A-
201 92-1). From the 130 cm long core drive only a cumulative thickness of 35 cm gravels and almost

202 no fine material were recovered in the liner. Therefore, the sedimentological contacts to over- and
203 underlying sediments are not preserved and are unknown (Fig. 3). Unfortunately, this prevents from
204 investigating sediment structures in the context of the complete depositional environment.
205 Interestingly, in the 10 cm wide core catcher of this core drive, matrix-supported gravel has been
206 caught. This core catcher sample largely resembles the basal layers of the abovementioned thick
207 turbidites and slumps.

208 Median grain size values of the laminated sediments, excluding the halite-facies types hd and lh/hh,
209 vary between ~7 and ~10 μm for samples with and without CaCO_3 (i.e. after dissolution of CaCO_3 ;
210 Supplement), respectively. These grain size distributions indicate mainly clay (~54% and ~43%
211 with and without CaCO_3 , respectively), very fine silt (~45% and ~55% with and without CaCO_3 ,
212 respectively) and very little sand (~0.1% and ~0.9% with and without CaCO_3 , respectively).
213 Gypsum-detritus samples (gd-facies) revealed the coarsest mean grain size of ~8 μm (~12.5 μm
214 without CaCO_3) and the highest sand fraction (~0.5% and ~2.2%, with and without CaCO_3 ,
215 respectively) due to gypsum which was not removed during sample treatment. The aad-n and aad-
216 II micro-facies show similar and low mean grain sizes of ~6 μm (~9 μm without CaCO_3), while
217 the green aad type exhibits a slightly higher mean value of ~7 μm (~11 μm without CaCO_3). Also
218 the silt and sand fractions of the green aad type are enhanced in comparison to the other two aad
219 types (Supplement).

220 The differentiation of the laminated micro-facies types gd, aad-II, aad-n and green aad is supported
221 by total organic carbon and calcium carbonate contents (Fig. 2g). The gd facies is characterised by
222 lowest TOC values of 0.25-0.5% and ~18% CaCO_3 , whereas the aad-II facies (0.35-0.57% TOC,
223 30-47% CaCO_3) and the aad-n facies (0.6-0.7% TOC, ~47% CaCO_3) exhibit higher values. The
224 green aad facies is characterised by highest TOC (0.65% and ~0.9%) and CaCO_3 contents (~40-
225 50% and 62%).

226 The elements Si, S, Cl, K, Ca, Ti, Fe, Br and Sr were obtained by μXRF scanning and used to
227 characterise the Dead Sea sediments (Fig. 2; see also Neugebauer et al., 2014; 2015). Aragonite
228 laminae are revealed by high Sr/Ca values, gypsum is represented by high S/Ca values and halite
229 is best characterised by the Cl/Br ratio (Fig. 2). The elements Si, K, Ti and Fe are constrained to
230 siliciclastics in the detrital sediment fraction. More ambiguous is the interpretation of Ca that occurs
231 in aragonite, gypsum and detrital calcite. The $\text{Ca}/(\text{Sr}+\text{S})$ ratio indicates the detrital carbonate

232 fraction because the authigenic Ca sources, i.e. aragonite and gypsum, are removed. The Ti/Ca ratio
233 represents the relative siliciclastic fraction (Fig. 2). The sum of Ca/(Sr+S) and Ti/Ca ratios best
234 represents the total amount of carbonate and siliciclastic detritus (Fig. 4). A correlation plot of these
235 two element ratios shows low, but significant, correlation ($R^2 = 0.4$) for the carbonate and
236 siliciclastic detrital fractions (Fig. 2h); the plot also indicates an additional Ca-bearing detrital
237 fraction.

238 **4.2 Lithostratigraphy**

239 The analysed section of core 5017-1 is sub-divided into four main lithostratigraphic units (Fig. 4).
240 Units I and III are predominantly composed of halite (controlled by hd and lh/hh facies), some
241 gypsum and detrital marl. Units II and IV present primarily aad (green aad, aad-n and aad-II) and
242 gd facies. These lithostratigraphic units are tied to the stratigraphic framework (Neugebauer et al.,
243 2014) and the U-Th chronology (Torfstein et al., 2015) of the 5017-1 core.

244 The lowermost unit I (245-237.5 m composite depth) is the upper part of a ca 40 m thick halite
245 sequence, the thickest halite deposit in the entire core, and is part of the last interglacial Samra
246 Formation (Neugebauer et al., 2014). This unit has very low magnetic susceptibility values and
247 Sr/Ca ratios with high Cl/Br ratios (Fig. 4). The abovementioned well-sorted gravel deposit, mainly
248 composed of limestone and dolomite clasts and halite, was identified ~2 m below the top of this
249 halite unit (Figs. 3 and 4). U-Th ages proposed a sedimentary hiatus between ca 116 and -110 ± 3
250 ka marked by this gravel layer (Torfstein et al., 2015).

251 The ~25 m thick unit II (237.5-212.5 m) presents mainly aad and gd facies. It is divided into two
252 sub-units: (1) sub-unit II-a (237.5-228 m) comprises aad-II, aad-n and gd facies and is characterised
253 by low Sr/Ca and Cl/Br ratios and distinct peaks in magnetic susceptibility. (2) Sub-unit II-b (228-
254 212.5 m) differs from sub-unit II-a as in addition to the above facies it presents three thick
255 sequences characterised by green aad facies and partly high Sr/Ca ratios. Unit II is characterised
256 by frequent, up to several m thick, graded detrital layers and slump deposits (Fig. 4). U-Th ages
257 place unit II between ca 108 ± 5 and 93 ± 7 ka (Torfstein et al., 2015), i.e. an interval of ~3-27
258 thousand years. Preliminary varve counting on the core photographs of this unit reveals a minimum
259 of 4050 ± 250 varves, which is at the lower end of the range and uncertainty of the U-Th ages. It is
260 likely that much of the sediments were eroded through the frequent mass-waste events. Unit II
261 builds the upper part of the Samra Formation of core 5017-1 as defined by Neugebauer et al. (2014).

262 Unit III (212.5-201.5 m) is dominated by halite deposits of the hd and lh/hh facies, which is well
263 reflected in high Cl/Br ratios. The lower ca 4 m of this unit could not be recovered due to the
264 hardness of the salt. Some cm- to dm-thick occurrences of aad-n, aad-II and gd facies are
265 intercalated in the halite deposits, as reflected by higher magnetic susceptibility, Ca/(Sr+S) + Ti/Ca
266 and Sr/Ca ratios. Unit III was deposited between ca 93 and 87 ± 7 ka (Torfstein et al., 2015) and
267 probably marks the transition between the Samra and Lisan Formations in the deep-basin core
268 5017-1 (Neugebauer et al., 2014). Compared to the chronology of the outcrops at the margin where
269 the Samra-Lisan transition has been traditionally considered at 75-70 ka (e.g. Waldmann et al.,
270 2009), probably because of transgressive truncation, the deep core may indicate that the transition
271 occurred ca 15 thousand years earlier (Torfstein et al., 2015).

272 The uppermost unit IV (201.5-180 m) compares to unit II and is characterised by the three aad
273 facies, as indicated by higher Ca/(Sr+S) + Ti/Ca and Sr/Ca ratios and the absence of halite (Fig. 4).
274 In contrast to unit II, where magnetic susceptibility values strongly fluctuate, constantly low
275 magnetic susceptibility characterises unit IV (Fig. 4). This unit can be divided into three sub-units:
276 (1) sub-unit IV-a is composed of aad-n, aad-II and gd facies, (2) sub-unit IV-b is a green aad section,
277 and (3) sub-unit IV-c is composed of aad-n and aad-II. Several cm- to m-thick slumped deposits
278 and graded detrital layers occur in unit IV. At a composite core depth of ~195 m the sediment is ca
279 85.5 ± 8 ka and six m above unit IV (i.e. at 174.5 m depth) an age of 70.5 ± 5 ka has been reported
280 (Torfstein et al., 2015). The interpolated age of the upper boundary of unit IV at 180 m depth is ca
281 75 ± 6 ka. Unit IV builds the lowermost part of the Lisan Formation of core 5017-1 (Neugebauer
282 et al., 2014).

283 **5 Discussion**

284 **5.1 Micro-facies as relative lake level indicators**

285 Lake levels of the water bodies occupying the Dead Sea basin are sensitive responders to changing
286 hydro-climatic conditions in the lake's catchment (Enzel et al., 2003; Bookman et al., 2006; Enzel
287 et al., 2008). Lake level reconstructions based on on-shore sequences indicate a total amplitude of
288 lake level fluctuation of at least ~270 m, with lowest levels of ~430 m bmsl occurring during parts
289 of the last interglacial, the last termination and potentially the Holocene, and anthropogenically-
290 induced in modern times (e.g. Bookman (Ken-Tor) et al., 2004; Bartov et al., 2007; Waldmann et

291 al., 2009; Stein et al., 2010). The highest lake level of Lake Lisan of ~160 m bmsl was reached
292 during the last glacial maximum (Bartov et al., 2003). These exposed sediments at the Dead Sea
293 margins also showed that in general different lake levels resulted in different sedimentary facies
294 (e.g. Machlus et al., 2000; Migowski et al., 2006). Hence, facies types can be considered as relative
295 lake level indicators, but without assigning an absolute level change (Figs. 4 and 5). Unlike the
296 near-shore environment, where lateral changes can alter the sedimentary facies which may lead to
297 erroneous relative lake level interpretations, in the deep basin such lateral changes are uncommon
298 and, therefore, facies changes are better related to changes in relative lake levels. These relative
299 lake levels are crucial ~~in inference of~~ to infer regional, basin-scale hydroclimatic changes that
300 control the direction of lake level trends (i.e. rising or falling), which are the net product of the
301 respective positive or negative lake budget over decades to millennia. To avoid complexities in
302 inferring minor relative lake level changes and to remain reasonable within the resolution of the U-
303 Th chronology, we concentrated only on reconstructing the millennial-scale facies alterations and
304 interpret them in terms of relative lake level variations.

305 The typical sediment facies during rising levels and the resulted episodic high stands of both the
306 deep last glacial Lake Lisan and the much shallower Holocene Dead Sea is the aad facies composed
307 of alternating aragonite and detritus (e.g. Machlus et al., 2000; Bookman (Ken-Tor) et al., 2004).
308 As the lake is devoid of bicarbonate, deposition of aad requires large amounts of bicarbonate supply
309 by freshwater reaching the lake through runoff during the winter rainy season to trigger
310 precipitation of primary aragonite (Stein et al., 1997; Barkan et al., 2001). Three different sub-types
311 of aad were distinguished in the investigated sediment section through micro-facies analyses. (i)
312 Green aad (Fig. 2) comprises greenish detrital laminae containing green algae remains and
313 represents highest lake levels and less salty limnological conditions. This facies depicts the
314 sediments deposited in core 5017-1 during the Last Glacial Maximum high stands (Neugebauer et
315 al., 2014), when Lake Lisan reached its maximum extent (e.g. Begin et al., 1974; Bartov et al.,
316 2002). (ii) The aad-n and (iii) the aad-II facies are similar, except that aad-II is characterised by
317 commonly thicker, but irregularly spacing aragonite laminae (Fig. 2). This may indicate insufficient
318 supply of bicarbonate to support regular annual aragonite formation. Therefore, the aad-II facies
319 ~~likely~~ likely was deposited during episodes of somewhat lower lake levels compared to the aad-n
320 facies. The aad-II facies also differs from the Id facies-type (laminated detritus), which exhibits
321 coarser detritus (50-60 μm) than aad (8-10 μm ; Haliva-Cohen et al., 2012) and which is a

322 characteristic facies for intermediate lake levels of the interglacial Samra and Ze'elim Formations
323 (e.g. Migowski et al., 2006; Waldmann et al., 2009; Neugebauer et al., 2014). The ld facies-type
324 was, however, not detected in the studied core section, which is supported by the constantly very
325 fine grain sizes of the sediments (Supplement).

326 The deposition of well-laminated or massive gypsum (gd facies, Fig. 2) is associated with mixing
327 of the water body due to lake level fall and a thinning of the upper freshwater layer (Torfstein et
328 al., 2008). Halite deposition is related to a negative water balance during times of decreased lake
329 levels (e.g. Lazar et al., 2014). Here, we distinguish between a mixed halite-detritus facies (hd) and
330 ~~massive or~~ layered or homogeneous, consolidated halite (lh/hh facies, Fig. 2). Whereas the presence
331 of detritus suggests freshwater influx during extreme runoff events, deposition of thick halite
332 indicates episodes of lowest lake levels.

333 Lake level trends inferred from micro-facies analysis are supported by μ XRF element scanning
334 data (Figs. 4 and 5). Halite sequences associated with a negative water balance are well-expressed
335 in increased Cl/Br ratios. The detrital input depends on the erosion in the catchment, aeolian
336 deposition over the lake and the catchment, and freshwater supply to the lake. The relative detrital
337 input can be estimated using the Ca/(Sr+S) ratio (for carbonate fraction) and the Ti/Ca ratio (for
338 siliciclastic fraction). The Sr/Ca ratio resembles the aragonite amount that increases with enhanced
339 supply of freshwater. The combination of these ratios by summing up both detrital fractions and
340 aragonite and subtracting halite, results in a curve that can be interpreted as a proxy for water
341 balance (Fig. 5), with negative values for halite and gypsum deposits and positive values for detritus
342 and aragonite.

343 **5.2 Gravel deposits in the deep basin**

344 Gravel deposits are rather common in the deep basin and have been identified as matrix-supported
345 material mainly in basal layers of up to several meter thick turbidites and slumps reflecting mass-
346 waste deposits, which can be triggered by either extreme runoff or seismic events and slope
347 instabilities (Kagan and Marco, 2013; Neugebauer et al., 2014; Waldmann et al., 2014). Only in
348 one case at ~239 m composite sediment depth a 35 cm thick well-sorted gravel deposit lacking
349 fine-grained components has been documented (Figs. 3 and 4). This gravel has been interpreted as
350 beach deposit and in turn used to argue for a major drawdown or even almost desiccation of the
351 lake at the end of the last interglacial (Stein et al., 2011; Torfstein et al., 2015). Combined U-Th

352 ages and oxygen isotope stratigraphy suggest a ~116 to 110 ka hiatus at around the position of the
353 gravel deposit, which is assumed to support the drawdown hypothesis (Torfstein et al., 2015).
354 However, both, petrographic composition and grain characteristics of the well-sorted gravel are
355 identical with gravel in basal layers of thick slumps and turbidites as the one deposited only 6 m
356 above (at ~233 m composite sediment depth; Fig. 3). This suggests the possibility of a similar
357 source and even the same transport mechanism. Due to the massive core loss of 65% in the core
358 section where the well-sorted gravel has been found, no direct information about the in-situ contacts
359 of this gravel to over- and underlying sediment units is available (Fig. 3a) and its primary
360 sedimentological context remains unknown. However, the core catcher material supports the
361 interpretation even of the well-sorted gravel as the vestige of a major mass-waste deposit, since it
362 consists of matrix-supported gravel exactly resembling basal layers from at least 22 turbidites and
363 slumps occurring in the entire record. It is likely that the fine-grained sediment components of the
364 turbidite were washed out during the drilling process. Low core recoveries and loss of material
365 often occurred in sediment sections with alternating hard halite and soft mud (Neugebauer et al.,
366 2014) as in this section of the record above the major halite deposit. Therefore, we are convinced
367 that the well-sorted gravels are the result of a drilling artefact and should not be interpreted as an
368 in-situ beach layer, but as the washed-out relict of the basal sediments of a major mass-waste
369 deposit. The deposition of a thick turbidite could have also caused the supposed hiatus although its
370 length should be critically tested.

371 Accepting our re-interpretation of the well-sorted gravel as primarily a drilling relict of a turbidite
372 ~~and not a clear~~instead of an in-situ beach deposit implies that the Dead Sea not necessarily
373 desiccated at the end of the last interglacial, although it ~~could~~might have been at a low stage. This
374 consideration ~~probably~~ accords better with thermodynamic calculations and water balance
375 simulations concluding that the ~~geo~~chemistry of the brine and the geometry of the basin ~~do not~~
376 ~~allow~~should prevent a dry down of the lake from drying up (Yechieli et al., 1998; Krumgalz et al.,
377 2000). First, the specific chemical composition of the Dead Sea brine (mainly Mg, Na, Ca and Cl)
378 allows reaching a very high salinity with a low water activity and vapour pressure. Therefore, the
379 rate of evaporation decreases with increasing salinity. Second, the low surface area to volume ratio
380 of the lake basin limits the amount of evaporated water. In addition, the relative humidity of the air
381 above the brine has to be close to zero in order to further evaporate a highly concentrated brine

382 [which, however, was never observed \(Katz and Starinsky, 2015\) and is considered unlikely](#)
383 [especially at very low lake levels due to the wind-protected topography of the deep Dead Sea basin.](#)

384 **5.3 Relative lake level fluctuations between ~117 and 75 ka**

385 Relative lake levels have been reconstructed for the ~117-75 ka interval based on the six micro-
386 facies types introduced above (Figs. 4 and 5). Relatively lowest lake levels are reflected by the
387 halite-dominated units I (~117-108 ka) and III (~93-87 ka). Intermediate to relatively higher lake
388 levels inferred for aad facies dominated units II (~108-93 ka) and IV (~87-75 ka) because this facies
389 indicates increased fresh water inflow.

390 The age estimate of unit I indicates that the low stand of Lake Samra commenced during the later
391 part of the last interglacial and may have continued until $\sim 108 \pm 5$ ka BP (Fig. 5). However, there
392 is no information for the time interval from ~ 116 to 110 ± 4 ka, due to the erosional unconformity
393 revealed from the chronological data (Torfstein et al., 2015). The deposition of ca 2 m of halite
394 above the hiatus indicates that low levels of the lake continued until $\sim 108 \pm 5$ ka because for times
395 of halite deposition in the Dead Sea basin a lake level below 400 m bmsl can be assumed (Neev
396 and Emery, 1967; Bookman (Ken-Tor) et al., 2004; Waldmann et al., 2009; Stein et al., 2010).

397 During $\sim 108-93 \pm 6$ ka (unit II) a trend of general increase in lake level is indicated by the
398 succession from aad-II to aad-n and finally to the green aad facies (Fig.4). Intercalated gypsum
399 deposits from $\sim 108-100$ ka indicate frequent short-term drops in lake levels. In the last glacial Lisan
400 Formation such gypsum deposits were associated with reduced precipitation, intensified winds and
401 probably increased evaporation during Heinrich events (Bartov et al., 2003; Torfstein et al., 2008;
402 Rohling, 2013; Torfstein et al., 2013). A Lake Samra high-stand between $\sim 100-93$ ka is in
403 agreement with a level from exposures at the lake's margins, where a relatively high level of ~ 320
404 m bmsl was proposed (Fig. 5; Waldmann et al., 2009; 2010).

405 An abrupt lake level decline and a subsequent millennial-scale low stand, probably below 400 m
406 bmsl, is inferred from the ~ 7 m thick halite deposit during the $\sim 93-87 \pm 7$ ka interval (unit III, Figs.
407 4 and 5). Within this unit some aad-n, aad-II and gd facies alternate with the thick and mainly
408 layered halite deposits indicating superimposed, probably centennial-scale, lake level fluctuations.
409 This halite sequence represents the final stage of the Samra Formation and marks the last
410 appearance of halite for the next $\sim 70,000$ years (Neugebauer et al., 2014) until the early Holocene

411 salt formation (e.g. Yechieli et al., 1993; Stein et al., 2010). The late Lake Samra halite indicates a
412 more pronounced lake level drop than the limited lake level decline inferred from coarser clastic
413 deposits in the exposed lake margin sediments (Fig. 5; Waldmann et al., 2009).

414 During $\sim 87-79 \pm 7$ ka (units IV-a and IV-b) lake level increased again as evidenced from the
415 succession from aad-II and aad-n facies, intercalated by some gd facies, to green aad facies (Fig.
416 4). At ~ 79 ka (unit IV-c) the lake probably has shortly declined again as indicated by aad-II facies,
417 before continuing to rise again at $\sim 77 \pm 6$ ka (Fig. 5). Earlier studies of the exposed sediments of
418 the Samra and Lisan Formations suggested that a depositional unconformity between ~ 75 and 70
419 ka separated these two formations at the lake's margins (Bartov et al., 2003; Waldmann et al., 2009;
420 Torfstein et al., 2013). Above this assumed unconformity, aad facies characterise the lower and
421 upper members of the Lisan Formation (e.g. Bartov et al., 2002). Below the unconformity, the on-
422 shore Samra Formation is composed of reddish ld facies, sands and gravels (Waldmann et al.,
423 2009). In the deep core, however, there is no obvious sedimentological hint for a low stand of the
424 lake at around this time, but aad facies apparently continuously deposited since ~ 87 ka. This
425 suggests that Lake Lisan commenced ca 10-15 kyr earlier than was assumed from the exposures
426 where its deposits were in part truncated. This difference between shallow- and deep-basin
427 sediments might be explained by (1) the abundant occurrence of slumping deposits and graded
428 layers in the deep core (Fig. 4) or (2) by a lake level rise from a lower level to the level of the
429 observed unconformity at the margins during that time. Combining these two possibilities suggests
430 that these slumping deposits might indicate transgressive erosion at the outcrop locations during
431 times of lake level rise of the early Lake Lisan (Bartov et al., 2007). This is likely causing
432 unconformities in the near-shore marginal areas of the basin. The large number of slump deposits
433 within this sediment section might point to several short-term level oscillations during this
434 generally rising level trend, but there is no further evidence for this proposition.

435 **5.4 Hydroclimatic implications**

436 The Dead Sea is situated at a key transitional zone between predominantly Atlantic and tropical
437 influenced climates. The zone of interaction between both climate regimes is expected to have
438 changed during major climatic transitions like from glacial to interglacial modes and vice versa. In
439 contrast to the scarce and sometimes contradicting information from the Levant, several records
440 from the entire Mediterranean realm provide evidence for teleconnections of large-scale climate

441 variations with the North Atlantic climate regime during the early last glacial. The alternation of
442 cold stadial intervals from ~111 to 108 ka (GS 25) and ~90 to 85 ka (GS 23+22) (Rasmussen et al.,
443 2014), as reflected in Greenland ice cores (Fig. 5; Wolff et al., 2010) and North Atlantic ice rafting
444 events C24 and C22+C21 (Chapman and Shackleton, 1999), and warmer interstadials (GI 24+23
445 and GI 21; Rasmussen et al., 2014) is well expressed in the western (marine core MD952042 off
446 the Iberian margin; Sánchez Goñi et al., 1999), the central (Lago Grande di Monticchio; Fig. 5;
447 Brauer et al., 2007; Martin-Puertas et al., 2014) and the eastern Mediterranean (Tenaghi Philippon
448 (Tzedakis, 2005), in Lake Van (Litt et al., 2014) and marine sediments (Cheddadi and Rossignol-
449 Strick, 1995)). The same pattern of large-scale fluctuations are proposed from Lebanon (Lake
450 Yammoûneh; Develle et al., 2011; Gasse et al., 2015) and the Soreq and Peqin speleothem records
451 in Israel (Fig. 5; Bar-Matthews et al., 1999; 2000; 2003). Finally, also the Dead Sea record reveals
452 low water levels at $\sim 110\text{-}108 \pm 5$ ka and $\sim 93\text{-}87 \pm 7$ ka, reflecting dry periods corresponding to
453 Northern Hemisphere stadials, and higher lake levels at $\sim 108\text{-}93 \pm 6$ ka and $\sim 87\text{-}75 \pm 6$ ka
454 coinciding with Greenland interstadials (Fig. 5).

455 The ~~fluctuations between stadials and~~long interstadials interrupted by short stadials in the North
456 Atlantic realm, ~~which are reflected in the waxing and waning of glaciers~~ during the build-up phase
457 of the large continental ice sheets (e.g. Mangerud et al., 1996; 1998; Clark et al., 1999; Svendsen
458 et al., 2004) are related to changes in Northern Hemisphere orbital insolation (Fig. 5; Laskar et al.,
459 2004). At the same time, orbital insolation-driven changes of the ITCZ controlled the monsoon
460 system and led to a strengthening of the African summer monsoon and widespread vegetation cover
461 in the Sahel and in the southern Sahara regions (Fig. 5; deMenocal et al., 2000; Tjallingii et al.,
462 2008; Herold and Lohmann, 2009). Enhanced precipitation in eastern Africa induced the formation
463 of organic-rich sapropel layers S4 and S3 (Fig. 5) in the eastern Mediterranean basin due to
464 enhanced Nile River runoff (e.g. Rossignol-Strick, 1985; Rohling et al., 2015). These changes in
465 freshwater flow further influenced the isotopic composition of the eastern Mediterranean Sea water,
466 i.e. the source region for precipitation in the region of the Soreq and Peqin speleothems (Fig. 5;
467 Bar-Matthews et al., 2000; 2003). This is an indirect mechanism explaining a monsoonal influence
468 in the speleothem records of the Levant.

469 Two issues must be discussed when precipitation increase and decrease are considered for
470 explaining rising and falling trends in lake levels and their maxima: (a) winter vs. summer
471 precipitation, and (b) tropical vs. Atlantic-Mediterranean sources. ~~All combinations~~Different

472 [scenarios](#) have been proposed ~~for various time intervals, i.e. but~~ the source of moisture for the
473 precipitation leading to higher Dead Sea lake levels during the early glacial and related atmospheric
474 teleconnections is still debated. ~~In addition, the opposite should be asked as well: which is the~~
475 ~~significant source or season that its moisture delivery to the Dead Sea basin was shut off to control~~
476 ~~minor and drastic lake level falls?~~ Northward shifts of the tropical rain belt as far north as the
477 Levant ~~can have been~~ excluded (Tzedakis, 2007 and references therein); ~~and~~ ~~A~~also Enzel et al.
478 (2015) ~~have~~ argued that summer rains associated with either the African or Indian monsoons are
479 unlikely even in the southernmost point of the Dead Sea watershed. Based on hyperarid soils, Amit
480 et al (2006; 2011) demonstrated that the southern Negev, including the southern watershed of the
481 Dead Sea, was hyperarid since the early Pleistocene. This ~~was later~~ [is further](#) supported by a
482 diminishing speleothem growth southward and a proposal for a predominating Atlantic-
483 Mediterranean source of winter precipitation in the Negev during relatively short episodes of the
484 last interglacial (Vaks et al., 2010). This ~~probably~~ [apparently](#) contradicts the ~~proposal of~~ [hypothesis](#)
485 [that](#) a northward shift of summer rains from monsoonal sources to the southern Levant ~~that were~~
486 ~~suggested to have~~ contributed to the slightly increased Dead Sea lake level during the early last
487 glacial (Torfstein et al., 2015). [Less attention has been paid to seasonal shifts in precipitation as a](#)
488 [factor for lake level fluctuations. One reason is that most model studies focus on the summer season](#)
489 [\(e.g. Liu et al., 2004; Herold and Lohmann, 2009\), while information about the winter season](#)
490 [atmospheric circulation during intervals of maximum insolation are still scarce. One exception is](#)
491 [the study by Kutzbach et al. \(2014\), which suggests that an increase in winter storm tracks could](#)
492 [have caused the wetter intervals in the Levant during maximum Northern Hemisphere seasonality.](#)

493 Present-day observations identified a third possible mechanism of moisture supply to the southern
494 Levant. Winter to spring tropical plumes originating from the tropical eastern Atlantic and western
495 Africa transport moisture across the Sahara into the southern Levant deserts usually when the sub-
496 tropical jet is at a southern latitudinal position (e.g. Kahana et al., 2002; Rubin et al., 2007; Tubi
497 and Dayan, 2014). Increased frequency of such atmospheric circulation pattern that cause
498 widespread ample rainstorms are probably the only type that can increase runoff yield in southern
499 Negev drainage basins (e.g. Enzel et al., 2012) to a volume that will be noticed as a level change,
500 although minor, in the Dead Sea. Low-latitude tropical plumes have been also proposed as moisture
501 source in the past when Northern Hemisphere insolation reached maxima during times of the last
502 interglacial Lake Samra (Waldmann et al., 2009; 2010).

503 Disentangling the interactions of low-latitude/tropical and mid-latitude (Atlantic and
504 Mediterranean) moisture sources and related mechanisms that triggered the reconstructed long-
505 term and large-scale lake level fluctuations of the Dead Sea during the first 40 millennia of the last
506 glacial is ~~not straightforward~~ challenging and remains partly speculative. One reason for this
507 difficulty might be that orbital-driven changes in insolation and seasonality are the common
508 external trigger for both, high and low latitude climatic fluctuations during that time. Nevertheless,
509 the striking coincidence with palaeoclimatic records across the Mediterranean suggests a strong
510 role of the Atlantic-Mediterranean atmospheric circulation for the moisture supply to the Levant
511 during the last glacial inception.

512 The observed coincidence of a cold North Atlantic and dry southern Levant during the last glacial
513 inception apparently contradicts with the long-term observations of glacial high stands and
514 interglacial low stands at the Dead Sea. This apparent difference in the Dead Sea lake level response
515 to North Atlantic climate changes at different time scales might be explained by threshold effects
516 in the growth of the Fennoscandian ice sheet. Once the ice shield reached a certain height, it became
517 a morphological barrier causing a major system shift in the atmospheric circulation pattern (Webb
518 III et al., 1993) which, in turn, forces the Mediterranean storm tracks to shift southward and to be
519 funnelled and intensified towards the central Levant. This would explain the doubling of annual
520 rainfall in this region (Enzel et al., 2003; 2008) and the high Lake Lisan levels during the last glacial
521 by a major increase in precipitation in the Dead Sea basin (Rohling, 2013). During the glacial
522 inception different atmospheric boundary conditions prevailed likely because the ice shield
523 elevation was still below the threshold, which forces the large-scale circulation pattern to change.
524 To test this hypothesis, more high-resolution proxy records from the southern Levant and advanced
525 modelling studies are needed.

526 ~~A possible teleconnecting mechanism even to the high latitudes, where synchronous changes are~~
527 ~~evidenced from the Greenland ice cores, might be in the build-up of the Fennoscandian ice sheet,~~
528 ~~which might have acted as morphological obstacle forcing changes in the flow paths of the~~
529 ~~Northern Hemisphere jet stream. Furthermore, the large positive long-term changes in glacial and~~
530 ~~interglacial Dead Sea levels demand a very large volume of inflow (Enzel et al., 2003; 2008),~~
531 ~~leaving this source with its eastern Mediterranean cyclones as the best candidate. Shutting down or~~
532 ~~reducing this source was suggested as the prime cause for sharp declines in levels during both the~~
533 ~~Holocene and the last glacial (e.g. Bartov et al., 2003; Enzel et al., 2003; Torfstein et al., 2013). So~~

534 ~~far, in contrast with the summer season, little modelling efforts were conducted on the winter~~
535 ~~season atmospheric circulation during intervals of maximum insolation. An exception is a model~~
536 ~~simulation by Kutzbach et al. (2014), which supports an increased winter storm track that could~~
537 ~~have caused the wetter intervals in the Levant during maximum Northern Hemisphere seasonality.~~

538 6 Conclusions

- 539 - Investigation of a ~65 m long sediment section of the 5017-1 core from the deep Dead Sea
540 basin confirmed the sensitivity of sediment deposition to lake level variations. Therefore,
541 micro-facies is a suitable proxy for relative lake level variations and water balance allowing
542 to trace changing hydroclimatic conditions in the southern Levant during the early last
543 glacial from ~117 to 75 ka.
- 544 - Matrix-supported gravel deposits are more common in the deepest part of the Dead Sea
545 basin than previously documented. They are probably transported by mass-waste events
546 during major lake level fluctuations. We propose that the appearance of one well-sorted
547 gravel deposit, which was previously suggested as an in-situ beach deposit, is likely an
548 artefact of the drilling process and that this gravel was originally deposited by mass-wasting
549 as well. Therefore, we conclude that there is, yet, no proof for an almost complete drying
550 of the Dead Sea at the end of the last interglacial.
- 551 - We suggest that the first phase of an early Lake Lisan commenced ca 15 kyr earlier than
552 was suggested from the main sedimentological shift in exposed sediments at the lake's
553 margins at ~75-70 ka. In the deep basin, Lisan-type sediments, i.e. aad, were deposited
554 already since ~108-93 ka, but again interrupted by a final period of halite deposition
555 marking the end of Lake Samra at ~87 ka.
- 556 - Large-scale lake level fluctuations of the Dead Sea during the early last glacial (MIS 5d-
557 5a) are in concert with Mediterranean records and climate conditions in the North Atlantic.
558 ~~suggesting~~ This suggests that the insolation-driven Atlantic-Mediterranean ~~storm-track~~
559 ~~position~~ cyclone activity and seasonality changes ~~over and off the eastern Mediterranean is~~
560 are the main cause ~~of these rising and falling lake levels~~ for the observed lower lake levels
561 during colder intervals. ~~These shifts are related to large scale shifts of the Northern~~
562 ~~Hemisphere circulation triggered by the growing and shrinking continental ice sheets.~~ On
563 longer time scales, this pattern changed and highest lake levels during the Lake Lisan phase

564 [occurred during the cold Pleniglacial \(MIS 4-2\). This might be related to a southward shift](#)
565 [and intensification of Mediterranean cyclones towards the Levant due to a shift in](#)
566 [atmospheric circulation boundary conditions caused by the growth of Northern Hemisphere](#)
567 [ice sheets.](#)

568

569 **Acknowledgements**

570 [We like to thank the editor and two anonymous reviewers for their constructive comments, which](#)
571 [helped to improve the quality of the manuscript.](#) Funding by the International Continental Scientific
572 Drilling Program (ICDP), the German Science Foundation (DFG grants FR 1672/2-1 and BR
573 2208/10-1), the GFZ German Research Centre for Geosciences and the Israel Science Foundation
574 (ISF) Dead Sea Core-Center of Excellence Research (Grant # 1436/14 to YE) is gratefully
575 acknowledged. AA was supported by DESERVE Helmholtz Virtual Institute. We thank G. Arnold,
576 D. Berger and B. Brademann for preparing excellent thin sections and for technical support, P.
577 Dulski and F. Ott for help with μ XRF, B. Plessen and P. Meier for TOC and CaCO_3 measurements,
578 J. Mingram for support with the fluorescence microscope, G. Schlolaut (all GFZ German Research
579 Centre for Geosciences) and K. Schorling (HU Berlin) for grain size sampling, S. Baltruschat (TU
580 Darmstadt) for assistance with XRD samples and all people that have been involved in the drilling,
581 core opening and sampling campaigns [of the Dead Sea Deep Drilling Project](#). This study is a
582 contribution to the Helmholtz Association (HGF) climate initiative REKLIM Topic 8 "Rapid
583 climate change derived from proxy data".

584

1 **References**

- 2 Almogi-Labin, A., Bar-Matthews, M., Shriki, D., Kolosovsky, E., Paterne, M., Schilman, B., Ayalon,
3 A., Aizenshtat, Z., and Matthews, A.: Climatic variability during the last ~90 ka of the southern
4 and northern Levantine Basin as evident from marine records and speleothems, *Quaternary*
5 *Science Reviews*, 28, 2882-2896, <http://dx.doi.org/10.1016/j.quascirev.2009.07.017>, 2009.
- 6 Amit, R., Enzel, Y., and Sharon, D.: Permanent Quaternary hyperaridity in the Negev, Israel,
7 resulting from regional tectonics blocking Mediterranean frontal systems, *Geology*, 34, 509-
8 512, 10.1130/g22354.1, 2006.
- 9 Amit, R., Simhai, O., Ayalon, A., Enzel, Y., Matmon, A., Crouvi, O., Porat, N., and McDonald, E.:
10 Transition from arid to hyper-arid environment in the southern Levant deserts as recorded by
11 early Pleistocene cummulic Aridisols, *Quaternary Science Reviews*, 30, 312-323,
12 <http://dx.doi.org/10.1016/j.quascirev.2010.11.007>, 2011.
- 13 Bar-Matthews, M., Ayalon, A., Kaufman, A., and Wasserburg, G. J.: The Eastern Mediterranean
14 paleoclimate as a reflection of regional events: Soreq cave, Israel, *Earth and Planetary Science*
15 *Letters*, 166, 85-95, Doi: 10.1016/s0012-821x(98)00275-1, 1999.
- 16 Bar-Matthews, M., Ayalon, A., and Kaufman, A.: Timing and hydrological conditions of Sapropel
17 events in the Eastern Mediterranean, as evident from speleothems, Soreq cave, Israel,
18 *Chemical Geology*, 169, 145-156, [http://dx.doi.org/10.1016/S0009-2541\(99\)00232-6](http://dx.doi.org/10.1016/S0009-2541(99)00232-6), 2000.
- 19 Bar-Matthews, M., Ayalon, A., Gilmour, M., Matthews, A., and Hawkesworth, C. J.: Sea–land
20 oxygen isotopic relationships from planktonic foraminifera and speleothems in the Eastern
21 Mediterranean region and their implication for paleorainfall during interglacial intervals,
22 *Geochimica et Cosmochimica Acta*, 67, 3181-3199, [http://dx.doi.org/10.1016/S0016-](http://dx.doi.org/10.1016/S0016-7037(02)01031-1)
23 [7037\(02\)01031-1](http://dx.doi.org/10.1016/S0016-7037(02)01031-1), 2003.
- 24 Barkan, E., Luz, B., and Lazar, B.: Dynamics of the carbon dioxide system in the Dead Sea,
25 *Geochimica et Cosmochimica Acta*, 65, 355-368, [http://dx.doi.org/10.1016/S0016-](http://dx.doi.org/10.1016/S0016-7037(00)00540-8)
26 [7037\(00\)00540-8](http://dx.doi.org/10.1016/S0016-7037(00)00540-8), 2001.
- 27 Bartov, Y., Stein, M., Enzel, Y., Agnon, A., and Reches, Z.: Lake Levels and Sequence Stratigraphy
28 of Lake Lisan, the Late Pleistocene Precursor of the Dead Sea, *Quaternary Research*, 57, 9-21,
29 DOI: 10.1006/qres.2001.2284, 2002.
- 30 Bartov, Y., Goldstein, S. L., Stein, M., and Enzel, Y.: Catastrophic arid episodes in the Eastern
31 Mediterranean linked with the North Atlantic Heinrich events, *Geology*, 31, 439-442,
32 10.1130/0091-7613(2003)031<0439:caeite>2.0.co;2, 2003.
- 33 Bartov, Y., Enzel, Y., Porat, N., and Stein, M.: Evolution of the Late Pleistocene–Holocene Dead
34 Sea Basin from Sequence Statigraphy of Fan Deltas and Lake-Level Reconstruction, *Journal of*
35 *Sedimentary Research*, 77, 680-692, 10.2110/jsr.2007.070, 2007.
- 36 Begin, Z. B., Ehrlich, A., and Nathan, Y.: Lake Lisan -The Pleistocene precursor of the Dead Sea,
37 *Geological Survey of Israel Bulletin* 63, 1974.
- 38 Bentor, Y. K.: Some geochemical aspects of the Dead Sea and the question of its age, *Geochimica*
39 *et Cosmochimica Acta*, 25, 239-260, [http://dx.doi.org/10.1016/0016-7037\(61\)90061-8](http://dx.doi.org/10.1016/0016-7037(61)90061-8), 1961.
- 40 Bookman (Ken-Tor), R., Enzel, Y., Agnon, A., and Stein, M.: Late Holocene lake levels of the Dead
41 Sea, *Geological Society of America Bulletin*, 116, 555-571, 10.1130/b25286.1, 2004.

42 Bookman, R., Bartov, Y., Enzel, Y., and Stein, M.: Quaternary lake levels in the Dead Sea basin:
43 Two centuries of research, Geological Society of America Special Papers, 401, 155-170,
44 10.1130/2006.2401(10), 2006.

45 Brauer, A., Endres, C., and Negendank, J. F. W.: Lateglacial calendar year chronology based on
46 annually laminated sediments from Lake Meerfelder Maar, Germany, Quaternary
47 International, 61, 17-25, [http://dx.doi.org/10.1016/S1040-6182\(99\)00014-2](http://dx.doi.org/10.1016/S1040-6182(99)00014-2), 1999.

48 Brauer, A., Allen, J. R. M., Mingram, J., Dulski, P., Wulf, S., and Huntley, B.: Evidence for last
49 interglacial chronology and environmental change from Southern Europe, Proceedings of the
50 National Academy of Sciences, 104, 450-455, 10.1073/pnas.0603321104, 2007.

51 Chapman, M. R., and Shackleton, N. J.: Global ice-volume fluctuations, North Atlantic ice-rafting
52 events, and deep-ocean circulation changes between 130 and 70 ka, Geology, 27, 795-798,
53 10.1130/0091-7613(1999)027<0795:givfna>2.3.co;2, 1999.

54 Cheddadi, R., and Rossignol-Strick, M.: Eastern Mediterranean Quaternary paleoclimates from
55 pollen and isotope records of marine cores in the Nile Cone Area, Paleoceanography, 10, 291-
56 300, 10.1029/94pa02672, 1995.

57 Clark, P. U., Alley, R. B., and Pollard, D.: Northern Hemisphere Ice-Sheet Influences on Global
58 Climate Change, Science, 286, 1104-1111, 10.1126/science.286.5442.1104, 1999.

59 deMenocal, P., Ortiz, J., Guilderson, T., Adkins, J., Sarnthein, M., Baker, L., and Yarusinsky, M.:
60 Abrupt onset and termination of the African Humid Period: rapid climate responses to gradual
61 insolation forcing, Quaternary Science Reviews, 19, 347-361,
62 [http://dx.doi.org/10.1016/S0277-3791\(99\)00081-5](http://dx.doi.org/10.1016/S0277-3791(99)00081-5), 2000.

63 Develle, A. L., Gasse, F., Vidal, L., Williamson, D., Demory, F., Van Campo, E., Ghaleb, B., and
64 Thouveny, N.: A 250 ka sedimentary record from a small karstic lake in the Northern Levant
65 (Yammoûneh, Lebanon): Paleoclimatic implications, Palaeogeography, Palaeoclimatology,
66 Palaeoecology, 305, 10-27, <http://dx.doi.org/10.1016/j.palaeo.2011.02.008>, 2011.

67 Enzel, Y., Bookman, R., Sharon, D., Gvirtzman, H., Dayan, U., Ziv, B., and Stein, M.: Late Holocene
68 climates of the Near East deduced from Dead Sea level variations and modern regional winter
69 rainfall, Quaternary Research, 60, 263-273, DOI: 10.1016/j.yqres.2003.07.011, 2003.

70 Enzel, Y., Amit, R., Dayan, U., Crouvi, O., Kahana, R., Ziv, B., and Sharon, D.: The climatic and
71 physiographic controls of the eastern Mediterranean over the late Pleistocene climates in the
72 southern Levant and its neighboring deserts, Global and Planetary Change, 60, 165-192,
73 10.1016/j.gloplacha.2007.02.003, 2008.

74 Enzel, Y., Amit, R., Grodek, T., Ayalon, A., Lekach, J., Porat, N., Bierman, P., Blum, J. D., and Erel,
75 Y.: Late Quaternary weathering, erosion, and deposition in Nahal Yael, Israel: An “impact of
76 climatic change on an arid watershed”?, Geological Society of America Bulletin, 124, 705-722,
77 10.1130/b30538.1, 2012.

78 Enzel, Y., Kushnir, Y., and Quade, J.: The middle Holocene climatic records from Arabia:
79 Reassessing lacustrine environments, shift of ITCZ in Arabian Sea, and impacts of the southwest
80 Indian and African monsoons, Global and Planetary Change, 129, 69-91,
81 <http://dx.doi.org/10.1016/j.gloplacha.2015.03.004>, 2015.

82 Gasse, F., Vidal, L., Van Campo, E., Demory, F., Develle, A.-L., Tachikawa, K., Elias, A., Bard, E.,
83 Garcia, M., Sonzogni, C., and Thouveny, N.: Hydroclimatic changes in northern Levant over the
84 past 400,000 years, Quaternary Science Reviews, 111, 1-8,
85 <http://dx.doi.org/10.1016/j.quascirev.2014.12.019>, 2015.

86 Haliva-Cohen, A., Stein, M., Goldstein, S. L., Sandler, A., and Starinsky, A.: Sources and transport
87 routes of fine detritus material to the Late Quaternary Dead Sea basin, *Quaternary Science*
88 *Reviews*, 50, 55-70, [10.1016/j.quascirev.2012.06.014](https://doi.org/10.1016/j.quascirev.2012.06.014), 2012.

89 Herold, M., and Lohmann, G.: Eemian tropical and subtropical African moisture transport: an
90 isotope modelling study, *Clim Dyn*, 33, 1075-1088, [10.1007/s00382-008-0515-2](https://doi.org/10.1007/s00382-008-0515-2), 2009.

91 Kagan, E. J., and Marco, S.: Seismically triggered mass movement events from the Dead Sea
92 depocentre, International Workshop "Tectonics of the Levant fault and Northern Red Sea", IPG
93 Paris, 2013,

94 Kahana, R., Ziv, B., Enzel, Y., and Dayan, U.: Synoptic climatology of major floods in the Negev
95 Desert, Israel, *International Journal of Climatology*, 22, 867-882, [10.1002/joc.766](https://doi.org/10.1002/joc.766), 2002.

96 Katz, A., Kolodny, Y., and Nissenbaum, A.: The geochemical evolution of the Pleistocene Lake
97 Lisan-Dead Sea system, *Geochimica et Cosmochimica Acta*, 41, 1609-1626,
98 [http://dx.doi.org/10.1016/0016-7037\(77\)90172-7](http://dx.doi.org/10.1016/0016-7037(77)90172-7), 1977.

99 Katz, A., and Starinsky, A.: No drawdown and no hyperaridity in the ancient Dead Sea: (Comments
100 to Torfstein's et al. (2015) paper, *EPSL* 412, 235–244), *Earth and Planetary Science Letters*, 427,
101 303-305, <http://dx.doi.org/10.1016/j.epsl.2015.07.006>, 2015.

102 Krumgalz, B. S., Hecht, A., Starinsky, A., and Katz, A.: Thermodynamic constraints on Dead Sea
103 evaporation: can the Dead Sea dry up?, *Chemical Geology*, 165, 1-11,
104 [http://dx.doi.org/10.1016/S0009-2541\(99\)00156-4](http://dx.doi.org/10.1016/S0009-2541(99)00156-4), 2000.

105 Kutzbach, J. E., Chen, G., Cheng, H., Edwards, R. L., and Liu, Z.: Potential role of winter rainfall in
106 explaining increased moisture in the Mediterranean and Middle East during periods of
107 maximum orbitally-forced insolation seasonality, *Clim Dyn*, 42, 1079-1095, [10.1007/s00382-](https://doi.org/10.1007/s00382-013-1692-1)
108 [013-1692-1](https://doi.org/10.1007/s00382-013-1692-1), 2014.

109 Laskar, J., Robutel, P., Joutel, F., Gastineau, M., Correia, A. C. M., and Levrard, B.: A long-term
110 numerical solution for the insolation quantities of the Earth, *Astronomy & Astrophysics*, 428,
111 261-285, 2004.

112 Lazar, B., Sivan, O., Yechieli, Y., Levy, E. J., Antler, G., Gavrieli, I., and Stein, M.: Long-term
113 freshening of the Dead Sea brine revealed by porewater Cl⁻ and δ¹⁸O in ICDP Dead Sea deep-
114 drill, *Earth and Planetary Science Letters*, 400, 94-101,
115 <http://dx.doi.org/10.1016/j.epsl.2014.03.019>, 2014.

116 Lensky, N. G., Dvorkin, Y., Lyakhovsky, V., Gertman, I., and Gavrieli, I.: Water, salt, and energy
117 balances of the Dead Sea, *Water Resources Research*, 41, W12418, [10.1029/2005wr004084](https://doi.org/10.1029/2005wr004084),
118 2005.

119 Litt, T., Pickarski, N., Heumann, G., Stockhecke, M., and Tzedakis, P. C.: A 600,000 year long
120 continental pollen record from Lake Van, eastern Anatolia (Turkey), *Quaternary Science*
121 *Reviews*, 104, 30-41, <http://dx.doi.org/10.1016/j.quascirev.2014.03.017>, 2014.

122 Liu, Z., Harrison, S. P., Kutzbach, J., and Otto-Bliesner, B.: Global monsoons in the mid-Holocene
123 and oceanic feedback, *Clim Dyn*, 22, 157-182, [10.1007/s00382-003-0372-y](https://doi.org/10.1007/s00382-003-0372-y), 2004.

124 Machlus, M., Enzel, Y., Goldstein, S. L., Marco, S., and Stein, M.: Reconstructing low levels of Lake
125 Lisan by correlating fan-delta and lacustrine deposits, *Quaternary International*, 73-74, 137-
126 144, Doi: [10.1016/S1040-6182\(00\)00070-7](https://doi.org/10.1016/S1040-6182(00)00070-7), 2000.

127 Mangerud, J., Jansen, E., and Landvik, J. Y.: Late Cenozoic history of the Scandinavian and Barents
128 Sea ice sheets, *Global and Planetary Change*, 12, 11-26, [http://dx.doi.org/10.1016/0921-](http://dx.doi.org/10.1016/0921-8181(95)00009-7)
129 [8181\(95\)00009-7](http://dx.doi.org/10.1016/0921-8181(95)00009-7), 1996.

130 Mangerud, J., Dokken, T., Hebbeln, D., Heggen, B., Ingólfsson, Ó., Landvik, J. Y., Mejdahl, V.,
131 Svendsen, J. I., and Vorren, T. O.: Fluctuations of the Svalbard–Barents Sea ice sheet during the
132 last 150 000 years, *Quaternary Science Reviews*, 17, 11-42, [http://dx.doi.org/10.1016/S0277-](http://dx.doi.org/10.1016/S0277-3791(97)00069-3)
133 [3791\(97\)00069-3](http://dx.doi.org/10.1016/S0277-3791(97)00069-3), 1998.

134 Martin-Puertas, C., Brauer, A., Wulf, S., Ott, F., Lauterbach, S., and Dulski, P.: Annual proxy data
135 from Lago Grande di Monticchio (southern Italy) between 76 and 112 ka: new chronological
136 constraints and insights on abrupt climatic oscillations, *Climate of the Past*, 10, 2099-2114,
137 10.5194/cp-10-2099-2014, 2014.

138 Migowski, C., Stein, M., Prasad, S., Negendank, J. F. W., and Agnon, A.: Holocene climate variability
139 and cultural evolution in the Near East from the Dead Sea sedimentary record, *Quaternary*
140 *Research*, 66, 421-431, DOI: 10.1016/j.yqres.2006.06.010, 2006.

141 Neugebauer, I., Brauer, A., Schwab, M. J., Waldmann, N. D., Enzel, Y., Kitagawa, H., Torfstein, A.,
142 Frank, U., Dulski, P., Agnon, A., Ariztegui, D., Ben-Avraham, Z., Goldstein, S. L., Stein, M., and
143 DSDDP Scientific Party: Lithology of the long sediment record recovered by the ICDP Dead Sea
144 Deep Drilling Project (DSDDP), *Quaternary Science Reviews*, 102, 149-165,
145 <http://dx.doi.org/10.1016/j.quascirev.2014.08.013>, 2014.

146 Neugebauer, I., Brauer, A., Schwab, M. J., Dulski, P., Frank, U., Hadzhiivanova, E., Kitagawa, H.,
147 Litt, T., Schiebel, V., Taha, N., Waldmann, N. D., and DSDDP Scientific Party: Evidences for
148 centennial dry periods at ~3300 and ~2800 cal. yr BP from micro-facies analyses of the Dead
149 Sea sediments, *The Holocene*, 25, 1358-1371, 10.1177/0959683615584208, 2015.

150 Rasmussen, S. O., Bigler, M., Blockley, S. P., Blunier, T., Buchardt, S. L., Clausen, H. B., Cvijanovic,
151 I., Dahl-Jensen, D., Johnsen, S. J., Fischer, H., Gkinis, V., Guillevic, M., Hoek, W. Z., Lowe, J. J.,
152 Pedro, J. B., Popp, T., Seierstad, I. K., Steffensen, J. P., Svensson, A. M., Vallenga, P., Vinther,
153 B. M., Walker, M. J. C., Wheatley, J. J., and Winstrup, M.: A stratigraphic framework for abrupt
154 climatic changes during the Last Glacial period based on three synchronized Greenland ice-
155 core records: refining and extending the INTIMATE event stratigraphy, *Quaternary Science*
156 *Reviews*, 106, 14-28, <http://dx.doi.org/10.1016/j.quascirev.2014.09.007>, 2014.

157 Rohling, E. J.: Quantitative assessment of glacial fluctuations in the level of Lake Lisan, Dead Sea
158 rift, *Quaternary Science Reviews*, 70, 63-72,
159 <http://dx.doi.org/10.1016/j.quascirev.2013.03.013>, 2013.

160 Rohling, E. J., Marino, G., and Grant, K. M.: Mediterranean climate and oceanography, and the
161 periodic development of anoxic events (sapropels), *Earth-Science Reviews*, 143, 62-97,
162 <http://dx.doi.org/10.1016/j.earscirev.2015.01.008>, 2015.

163 Rossignol-Strick, M.: Mediterranean Quaternary sapropels, an immediate response of the African
164 monsoon to variation of insolation, *Palaeogeography, Palaeoclimatology, Palaeoecology*, 49,
165 237-263, [http://dx.doi.org/10.1016/0031-0182\(85\)90056-2](http://dx.doi.org/10.1016/0031-0182(85)90056-2), 1985.

166 Rubin, S., Ziv, B., and Paldor, N.: Tropical Plumes over Eastern North Africa as a Source of Rain in
167 the Middle East, *Monthly Weather Review*, 135, 4135-4148, 10.1175/2007mwr1919.1, 2007.

168 Sade, A., Hall, J. K., Sade, H., Amit, G., Tibor, G., Schulze, B., Gur-Arieh, L., ten Brink, U., Ben-
169 Avraham, Z., Keller, C., Gertman, I., Beaudoin, J., Al-Zoubi, A., Akawwi, E., Rimawi, O.,
170 Abueladas, A., Mayer, L., Calder, B., and Maratos, A.: Multibeam Bathymetric Map of the Dead
171 Sea, Geological Survey of Israel Report GSI/01, 2014.

172 Sánchez Goñi, M. F., Eynaud, F., Turon, J. L., and Shackleton, N. J.: High resolution palynological
173 record off the Iberian margin: direct land-sea correlation for the Last Interglacial complex,

174 Earth and Planetary Science Letters, 171, 123-137, [http://dx.doi.org/10.1016/S0012-](http://dx.doi.org/10.1016/S0012-821X(99)00141-7)
175 [821X\(99\)00141-7](http://dx.doi.org/10.1016/S0012-821X(99)00141-7), 1999.

176 Sneh, A., Bartov, Y., Weissbrod, T., Rosensaft, M.: Geological Map of Israel, 1:200,000, Israel
177 Geological Survey (4 sheets), 1998.

178 Stein, M., Starinsky, A., Katz, A., Goldstein, S. L., Machlus, M., and Schramm, A.: Strontium
179 isotopic, chemical, and sedimentological evidence for the evolution of Lake Lisan and the Dead
180 Sea, *Geochimica et Cosmochimica Acta*, 61, 3975-3992, 10.1016/s0016-7037(97)00191-9,
181 1997.

182 Stein, M., Torfstein, A., Gavrieli, I., and Yechieli, Y.: Abrupt aridities and salt deposition in the post-
183 glacial Dead Sea and their North Atlantic connection, *Quaternary Science Reviews*, 29, 567-
184 575, DOI: 10.1016/j.quascirev.2009.10.015, 2010.

185 Stein, M., Ben-Avraham, Z., and Goldstein, S. L.: Dead Sea deep cores: A window into past climate
186 and seismicity, *Eos, Transactions American Geophysical Union*, 92, 453-454,
187 10.1029/2011eo490001, 2011.

188 Svendsen, J. I., Alexanderson, H., Astakhov, V. I., Demidov, I., Dowdeswell, J. A., Funder, S.,
189 Gataullin, V., Henriksen, M., Hjort, C., Houmark-Nielsen, M., Hubberten, H. W., Ingólfsson, Ó.,
190 Jakobsson, M., Kjær, K. H., Larsen, E., Lokrantz, H., Lunkka, J. P., Lyså, A., Mangerud, J.,
191 Matiouchkov, A., Murray, A., Möller, P., Niessen, F., Nikolskaya, O., Polyak, L., Saarnisto, M.,
192 Siegert, C., Siegert, M. J., Spielhagen, R. F., and Stein, R.: Late Quaternary ice sheet history of
193 northern Eurasia, *Quaternary Science Reviews*, 23, 1229-1271,
194 <http://dx.doi.org/10.1016/j.quascirev.2003.12.008>, 2004.

195 Tjallingii, R., Claussen, M., Stuut, J.-B. W., Fohlmeister, J., Jahn, A., Bickert, T., Lamy, F., and Rohl,
196 U.: Coherent high- and low-latitude control of the northwest African hydrological balance,
197 *Nature Geoscience*, 1, 670-675,
198 http://www.nature.com/ngeo/journal/v1/n10/supinfo/ngeo289_S1.html, 2008.

199 Torfstein, A., Gavrieli, I., Katz, A., Kolodny, Y., and Stein, M.: Gypsum as a monitor of the paleo-
200 limnological-hydrological conditions in Lake Lisan and the Dead Sea, *Geochimica et*
201 *Cosmochimica Acta*, 72, 2491-2509, DOI: 10.1016/j.gca.2008.02.015, 2008.

202 Torfstein, A., Haase-Schramm, A., Waldmann, N., Kolodny, Y., and Stein, M.: U-series and oxygen
203 isotope chronology of the mid-Pleistocene Lake Amora (Dead Sea basin), *Geochimica et*
204 *Cosmochimica Acta*, 73, 2603-2630, 10.1016/j.gca.2009.02.010, 2009.

205 Torfstein, A., Goldstein, S. L., Stein, M., and Enzel, Y.: Impacts of abrupt climate changes in the
206 Levant from Last Glacial Dead Sea levels, *Quaternary Science Reviews*, 69, 1-7,
207 <http://dx.doi.org/10.1016/j.quascirev.2013.02.015>, 2013.

208 Torfstein, A., Goldstein, S. L., Kushnir, Y., Enzel, Y., Haug, G., and Stein, M.: Dead Sea drawdown
209 and monsoonal impacts in the Levant during the last interglacial, *Earth and Planetary Science*
210 *Letters*, 412, 235-244, <http://dx.doi.org/10.1016/j.epsl.2014.12.013>, 2015.

211 Tubi, A., and Dayan, U.: Tropical Plumes over the Middle East: Climatology and synoptic
212 conditions, *Atmospheric Research*, 145-146, 168-181,
213 <http://dx.doi.org/10.1016/j.atmosres.2014.03.028>, 2014.

214 Tzedakis, P. C.: Towards an understanding of the response of southern European vegetation to
215 orbital and suborbital climate variability, *Quaternary Science Reviews*, 24, 1585-1599,
216 <http://dx.doi.org/10.1016/j.quascirev.2004.11.012>, 2005.

217 Tzedakis, P. C.: Seven ambiguities in the Mediterranean palaeoenvironmental narrative,
218 Quaternary Science Reviews, 26, 2042-2066,
219 <http://dx.doi.org/10.1016/j.quascirev.2007.03.014>, 2007.

220 Vaks, A., Bar-Matthews, M., Matthews, A., Ayalon, A., and Frumkin, A.: Middle-Late Quaternary
221 paleoclimate of northern margins of the Saharan-Arabian Desert: reconstruction from
222 speleothems of Negev Desert, Israel, Quaternary Science Reviews, 29, 2647-2662,
223 <http://dx.doi.org/10.1016/j.quascirev.2010.06.014>, 2010.

224 Waldmann, N., Starinsky, A., and Stein, M.: Primary carbonates and Ca-chloride brines as monitors
225 of a paleo-hydrological regime in the Dead Sea basin, Quaternary Science Reviews, 26, 2219-
226 2228, DOI: 10.1016/j.quascirev.2007.04.019, 2007.

227 Waldmann, N., Stein, M., Ariztegui, D., and Starinsky, A.: Stratigraphy, depositional environments
228 and level reconstruction of the last interglacial Lake Samra in the Dead Sea basin, Quaternary
229 Research, 72, 1-15, 10.1016/j.yqres.2009.03.005, 2009.

230 Waldmann, N., Torfstein, A., and Stein, M.: Northward intrusions of low- and mid-latitude storms
231 across the Saharo-Arabian belt during past interglacials, Geology, 38, 567-570,
232 10.1130/g30654.1, 2010.

233 Waldmann, N., Hadzhiivanova, E., Neugebauer, I., Brauer, A., Schwab, M. J., Frank, U., and Dulski,
234 P.: Anatomy of mass transport deposits in the Dead Sea; sedimentary processes in an active
235 tectonic hypersaline basin, EGU General Assembly, EGU-2014-11281, Vienna, Austria, 2014,

236 Webb III, T., Ruddiman, W. F., Street-Perrott, F. A., Markgraf, V., Kutzbach, J. E., Bartlein, P. J.,
237 Wright Jr., H. E., and Prell, W. L.: Climatic changes during the past 18,000 years: regional
238 syntheses, mechanisms, and causes, in: Global Climates since the Last Glacial Maximum, edited
239 by: Wright Jr., H. E., Kutzbach, J. E., and Webb III, T., 514-535, 1993.

240 Weltje, G. J., and Tjallingii, R.: Calibration of XRF core scanners for quantitative geochemical
241 logging of sediment cores: Theory and application, Earth and Planetary Science Letters, 274,
242 423-438, <http://dx.doi.org/10.1016/j.epsl.2008.07.054>, 2008.

243 Wolff, E. W., Chappellaz, J., Blunier, T., Rasmussen, S. O., and Svensson, A.: Millennial-scale
244 variability during the last glacial: The ice core record, Quaternary Science Reviews, 29, 2828-
245 2838, <http://dx.doi.org/10.1016/j.quascirev.2009.10.013>, 2010.

246 Wright, J. D.: Global Climate Change in Marine Stable Isotope Records, in: Quaternary
247 Geochronology: Methods and Applications, edited by: Noller, J. S., Sowers, J. M., and Lettis, W.
248 R., American Geophysical Union, 427-433, 2000.

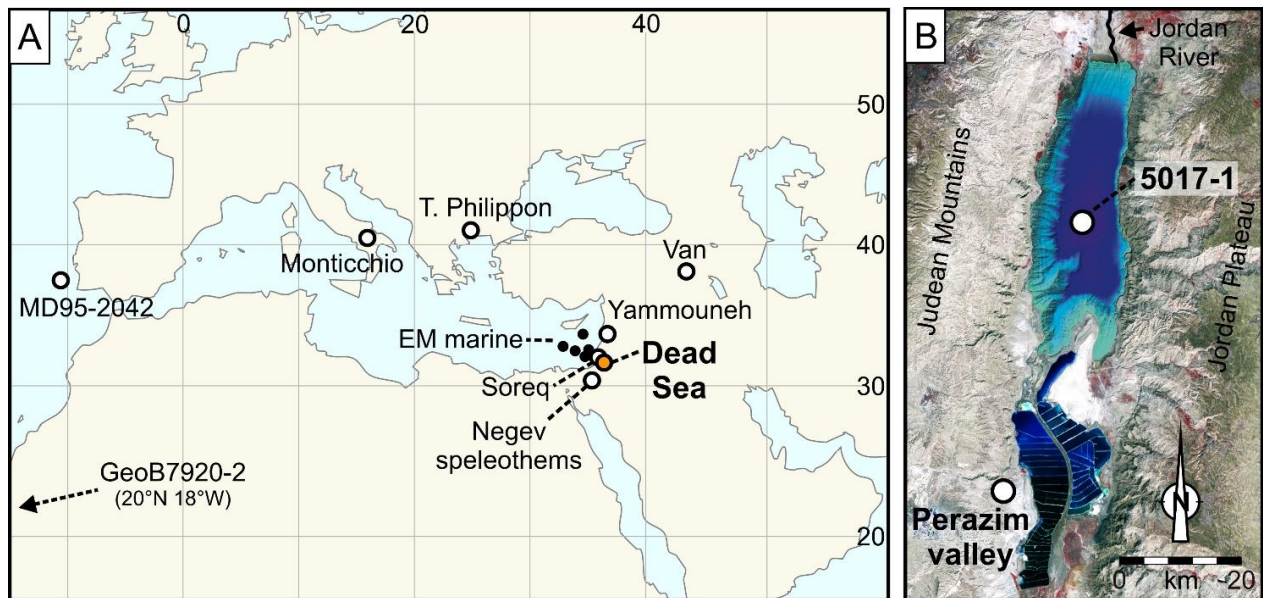
249 Yechieli, Y., Magaritz, M., Levy, Y., Weber, U., Kafri, U., Woelfli, W., and Bonani, G.: Late
250 Quaternary Geological History of the Dead Sea Area, Israel, Quaternary Research, 39, 59-67,
251 10.1006/qres.1993.1007, 1993.

252 Yechieli, Y., Gavrieli, I., Berkowitz, B., and Ronen, D.: Will the Dead Sea die?, Geology, 26, 755-
253 758, 10.1130/0091-7613(1998)026<0755:wtdsd>2.3.co;2, 1998.

254 Ziv, B., Dayan, U., Kushnir, Y., Roth, C., and Enzel, Y.: Regional and global atmospheric patterns
255 governing rainfall in the southern Levant, International Journal of Climatology, 26, 55-73,
256 10.1002/joc.1238, 2006.

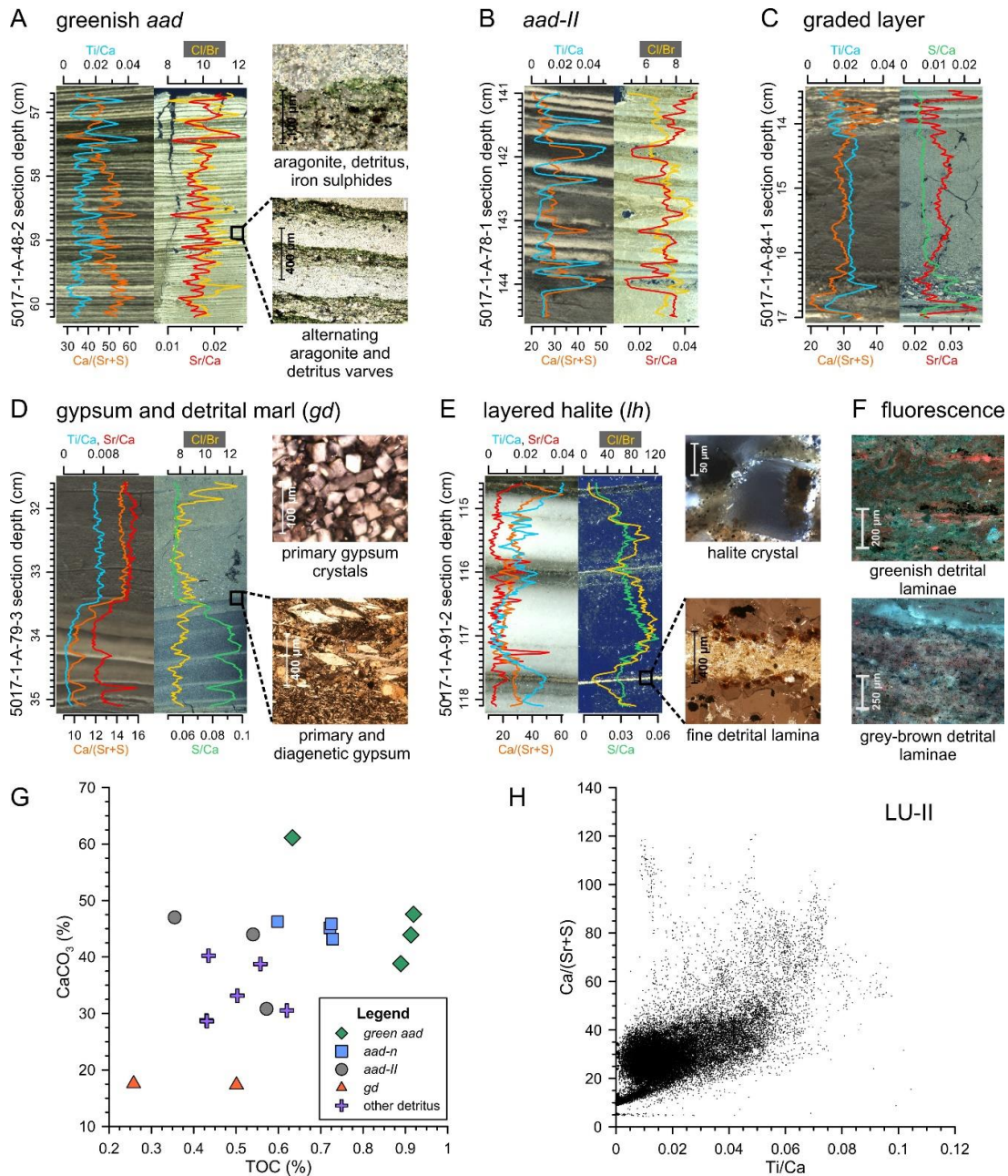
257

1 **Figures and figure captions**



2
3 Figure 1. (A) Location of Mediterranean records discussed in the text; EM marine – eastern
4 Mediterranean marine cores (Cheddadi and Rossignol-Strick, 1995; Almogi-Labin et al., 2009);
5 Negev speleothems – various caves in the northern, central and southern Negev (Vaks et al., 2010);
6 for references of the other records the reader is referred to the text. (B) Map of the Dead Sea (NASA
7 image by R. Simmon using Landsat data (2011) from USGS, www.visibleearth.nasa.gov/),
8 bathymetry of [the](#) northern Dead Sea basin from Sade et al. (2014), 5017-1 coring location, Perazim
9 valley Samra outcrop PZ-7 (Waldmann et al., 2009).

10

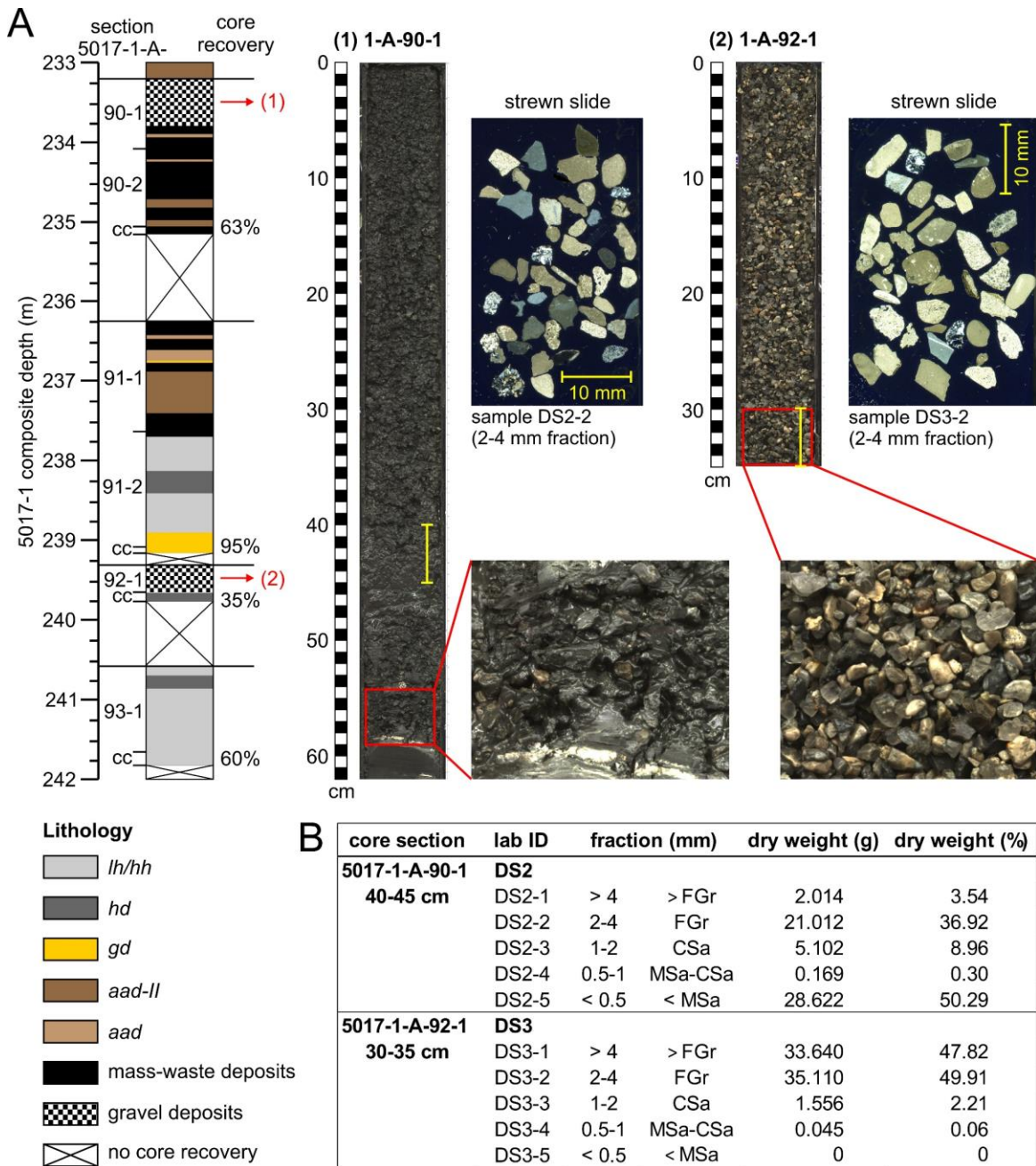


11

12 Figure 2. Micro-facies (core photos, polarised thin section scans and microscopic images with
 13 varying magnification and polarisation conditions) and μ XRF characteristics (element ratios): (A)
 14 green aad facies with peaks in Sr/Ca typical for aragonite layers and peaks in Ti/Ca and Ca/(Sr+S)
 15 indicating detrital layers; (B) aad-II facies containing greyish detritus and thicker aragonite layers
 16 than the green aad facies; (C) example of a mass-waste deposit: graded layer with high Ti/Ca ratio
 17 and increased S/Ca at the base due to diagenetic gypsum; (D) gd facies characterised by high S/Ca
 18 ratio; (E) lh facies with high Cl/Br and positively correlated S/Ca, but peaks of all other elements
 19 only in the thin detrital laminae; (F) fluorescence (violet light) microscope images of greenish

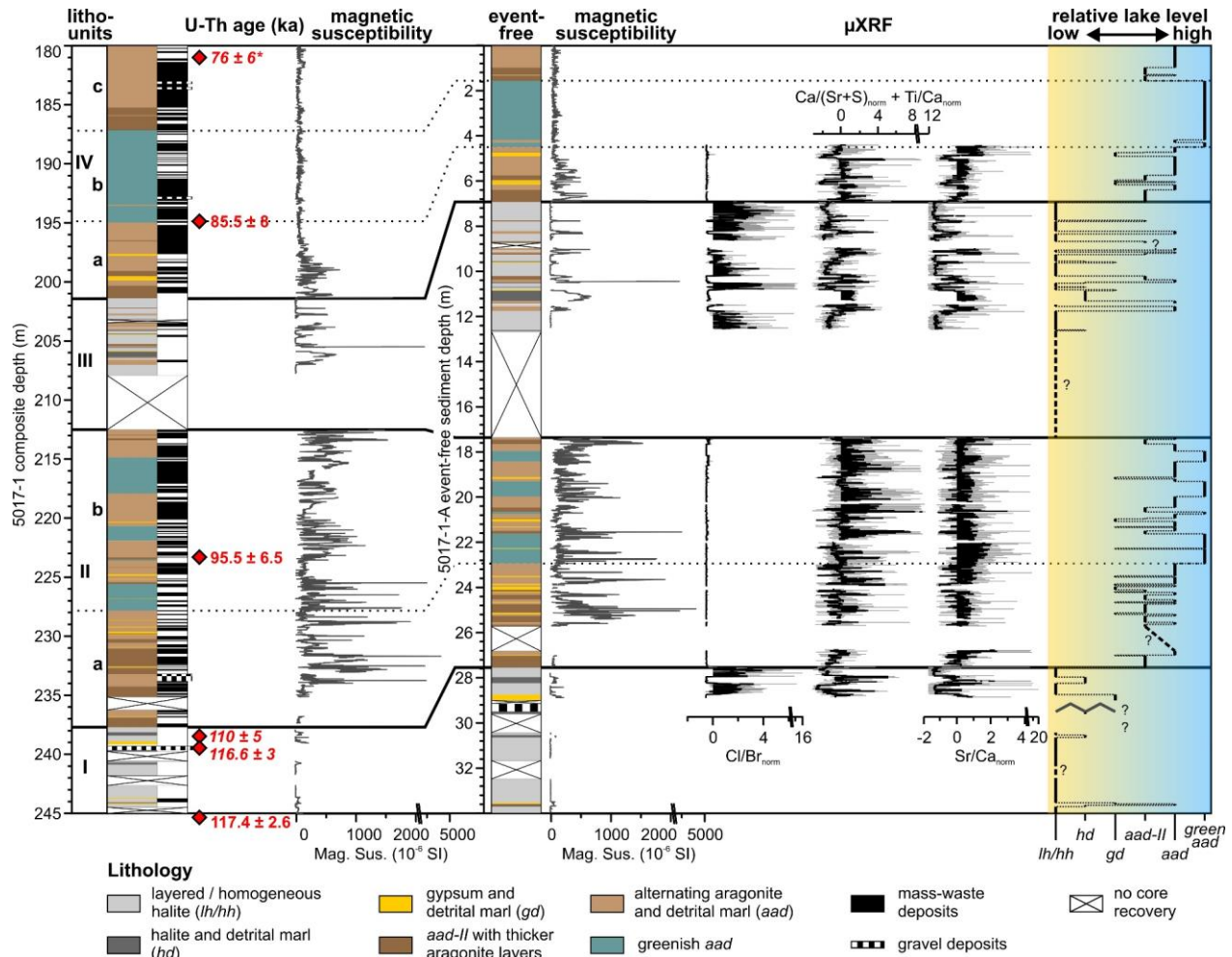
20 detrital laminae (upper photo, core section 5017-A-1-87-1, at ~72 cm) with very strong
21 fluorescence (red colour) and greyish-brownish detrital laminae (lower photo, core section 5017-
22 1-A-78-1, at ~140 cm) that are characterised by a weaker fluorescence; (G) correlation plot of TOC
23 against CaCO_3 contents of 19 samples distinguished for different micro-facies types; (H)
24 correlation plot of the two detrital fractions as derived from μXRF element scanning, exemplary
25 for lithological unit (LU) II: Ti/Ca as proxy for the siliciclastic detrital fraction and $\text{Ca}/(\text{Sr}+\text{S})$ as
26 proxy for the detrital carbonate fraction, $R^2 = 0.4$.

27



28

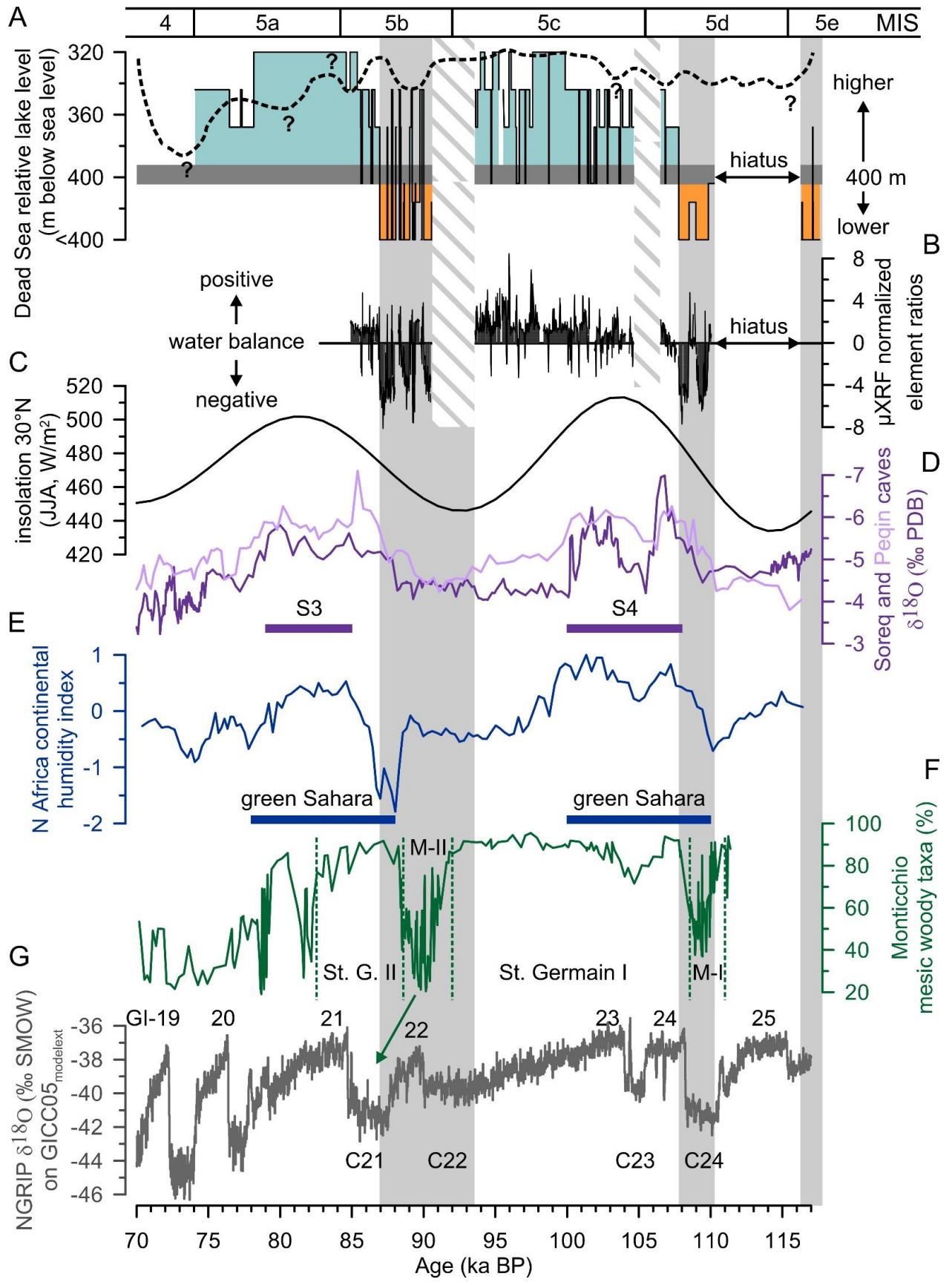
29 Figure 3. (A) Lithological profile from 233-242 m composite depth (cc – core catcher), two gravel
 30 deposits in core sections (1) 5017-1-A-90-1 (233.17 m composite depth) and (2) 5017-1-A-92-1
 31 (239.27 m composite depth) and strewn thin slide scans (polarised light) of the 2-4 mm grain
 32 fractions; yellow bars indicate sampling positions in the two core sections. (B) table of grain size
 33 fractions after sieving for one example of a mud-supported gravel occurrence and the pure gravel
 34 layer, both as shown in (A).



36

37 Figure 4. Lithology of the ~65 m long 5017-1 core section: lithostratigraphic units, U-Th ages (from
 38 Torfstein et al., 2015), with extrapolated ages in italic, * - interpolated age (see text for explanation),
 39 magnetic susceptibility (1 mm resolution, 10^{-6} SI); event-free lithology, μ XRF data (grey: 200 μ m
 40 steps, black: 101-steps running means of counts) and the relative lake level changes inferred from
 41 the changing micro-facies. All mass-waste deposits thicker than 1 cm were excluded from the
 42 event-free lithological profile and data, event-free sediment depth starts with zero at 180 m below
 43 lake floor. μ XRF data of normalized ratios: Cl/Br representing halite, Ca/(Sr+S) + Ti/Ca indicating
 44 the total carbonate and siliciclastic detritus, Sr/Ca indicating aragonite.

45



47 Figure 5. Comparison of the Dead Sea to other records: (A) the relative Dead Sea lake level curve
48 inferred from micro-facies analysis of the deep-basin core 5017-1 (this study; right y-axis) and
49 from site PZ-7 from the Perazim valley (dashed line; left y-axis, indicating maximum or minimum
50 relative lake levels) (Waldmann et al., 2009); (B) sum of normalized ratios of Ca/(Sr+S) and Ti/Ca
51 as proxies for carbonate and siliciclastic detritus, respectively, and of Sr/Ca, proxy for aragonite,
52 subtracted by the Cl/Br ratio, which is a proxy for halite, $[Ca/(Sr+S) + Ti/Ca + Sr/Ca - Cl/Br]$
53 indicating the water balance of the lake and agreeing well with the relative lake level curve; (C)
54 mean summer (JJA) insolation at 30°N (after Laskar et al., 2004); (D) $\delta^{18}O$ of Soreq and Peqin
55 speleothems, Israel (Bar-Matthews et al., 2003) and eastern Mediterranean sapropel events S3 and
56 S4 (according to Bar-Matthews et al., 2000); (E) humidity index of continental North Africa (core
57 GeoB7920-2) and “green Sahara” phases (Tjallingii et al., 2008); (F) Monticchio (southern Italy)
58 pollen record of mesic woody taxa and Mediterranean pollen zones Melisey (M) I and II, and St.
59 Germain I and II (Brauer et al., 2007; Martin-Puertas et al., 2014), note a possible chronological
60 shift of 3500 yr to the older for 92-76 ka according to Martin-Puertas et al. (2014); (G) Greenland
61 ice core $\delta^{18}O$ record on GICC05_{modelext} timescale (Wolff et al., 2010), indicated are also Greenland
62 interstadials (GI) after Rasmussen et al. (2014) and North Atlantic ice rafting events C21 to C24
63 (Chapman and Shackleton, 1999). Marine isotope stages are given according to Wright (2000).
64 Grey vertical bars indicate periods of negative water balance in the Dead Sea; obliquely banded
65 bars: no core recovery.